National Technical University of Athens
School of Naval Architecture and Marine Engineering
Division of Ship Design and Maritime Transport

Evaluating the impact of wind-assisted propulsion systems on ship energy efficiency

DIPLOMA THESIS

Dionysios Thalassinos

Supervisor:

Nikolaos Themelis,

Assistant Professor

ATHENS

October 24

Abstract

The maritime industry, responsible for approximately 2-3% of global carbon emissions, faces increasing regulatory pressures to adopt sustainable practices to meet the International Maritime Organization's (IMO) greenhouse gas (GHG) reduction goals. Among the various strategies to improve energy efficiency, wind-assisted propulsion (WASP) systems stand out as a promising solution, particularly through technologies such as the Flettner Rotor and eSAIL systems. This thesis aims to evaluate the impact of these WASP technologies on the fuel consumption and emissions reduction of commercial ships, with a specific focus on a bulk carrier case study.

The research develops a comprehensive theoretical model that incorporates wind forces, wave resistances, and side forces, alongside the effects of traditional propulsion methods. Using this model, the performance of the retrofitted vessel is assessed under varying environmental conditions. The case study vessel was analysed with both Flettner Rotor and eSAIL systems installed, and the results indicate that significant reductions in fuel consumption can be achieved, particularly when utilizing the eSAIL system. This study also evaluates the ship's compliance with IMO's Minimum Propulsion Power requirements, examining the vessel's manoeuvrability in adverse weather conditions.

A series of computational trials are conducted to predict the ship's speed and power curves, considering factors such as calm water resistance, wind resistance, and the additional propulsion provided by the WASP systems. The results highlight the potential of wind-assisted propulsion systems to reduce fuel consumption by up to 44% (when considering side forces) and 48% (when not considering side forces), depending on the environmental conditions and operational parameters. The study also addresses the challenges of side forces, which can impact the vessel's performance, necessitating the inclusion of drift and rudder-related resistances in the model.

In conclusion, this thesis demonstrates that wind-assisted propulsion systems, particularly the eSAIL, offer a viable path for the shipping industry to reduce its environmental impact. By achieving significant reductions in fuel consumption and emissions, these systems contribute to the decarbonization of maritime transport and provide a practical solution for compliance with evolving environmental regulations. The findings suggest that continued development and implementation of WASP technologies could play a crucial role in achieving future maritime sustainability goals.

Περίληψη

Η ναυτιλιακή βιομηχανία, η οποία ευθύνεται για περίπου 2-3% των παγκόσμιων εκπομπών άνθρακα, αντιμετωπίζει αυξανόμενες ρυθμιστικές πιέσεις για την υιοθέτηση βιώσιμων πρακτικών, ώστε να ανταποκριθεί στους στόχους μείωσης εκπομπών του Διεθνούς Ναυτιλιακού Οργανισμού (IMO). Ανάμεσα στις διάφορες στρατηγικές βελτίωσης της ενεργειακής αποδοτικότητας, τα συστήματα πρόωσης με τη βοήθεια του ανέμου (WASP) ξεχωρίζουν ως μια υποσχόμενη λύση, ειδικά μέσω τεχνολογιών όπως τα συστήματα Flettner Rotor και eSAIL. Η παρούσα διπλωματική εργασία στοχεύει στην αξιολόγηση της επίδρασης αυτών των τεχνολογιών WASP στην κατανάλωση καυσίμου και τη μείωση των εκπομπών των εμπορικών πλοίων, με ειδική έμφαση σε μια μελέτη περίπτωσης φορτηγού πλοίου.

Η έρευνα αναπτύσσει ένα ολοκληρωμένο θεωρητικό μοντέλο που ενσωματώνει τις δυνάμεις του ανέμου, τις αντιστάσεις των κυμάτων και τις πλευρικές δυνάμεις, σε συνδυασμό με τις παραδοσιακές μεθόδους πρόωσης. Με βάση αυτό το μοντέλο, αξιολογείται η απόδοση του πλοίου με τις εγκατεστημένες τεχνολογίες Flettner Rotor και eSAIL υπό διαφορετικές περιβαλλοντικές συνθήκες. Τα αποτελέσματα δείχνουν ότι μπορούν να επιτευχθούν σημαντικές μειώσεις στην κατανάλωση καυσίμου, ιδιαίτερα με τη χρήση του συστήματος eSAIL. Η μελέτη εξετάζει επίσης τη συμμόρφωση του πλοίου με τις ελάχιστες απαιτήσεις ισχύος πρόωσης του IMO, εξετάζοντας την ευελιξία του σε δυσμενείς καιρικές συνθήκες.

Πραγματοποιείται μια σειρά υπολογιστικών δοκιμών για την πρόβλεψη των καμπυλών ταχύτητας/ισχύος του πλοίου, λαμβάνοντας υπόψη παράγοντες όπως η αντίσταση σε ήρεμο νερό, η αντίσταση στον άνεμο και η πρόσθετη πρόωση που παρέχεται από τα συστήματα WASP. Τα αποτελέσματα υπογραμμίζουν το δυναμικό των συστημάτων πρόωσης με τη βοήθεια του ανέμου να μειώσουν την κατανάλωση καυσίμου έως και 44% (όταν λαμβάνονται υπόψη οι πλευρικές δυνάμεις) και 48% (όταν δεν λαμβάνονται υπόψη οι πλευρικές δυνάμεις), ανάλογα με τις περιβαλλοντικές συνθήκες και τις παραμέτρους λειτουργίας. Η μελέτη ασχολείται επίσης με τις προκλήσεις των πλευρικών δυνάμεων, οι οποίες μπορεί να επηρεάσουν την απόδοση του πλοίου, καθιστώντας απαραίτητη την ενσωμάτωση των αντιστάσεων από την πλαγιολίσθηση (drift) και το πηδάλιο στο μοντέλο.

Συμπερασματικά, η παρούσα διπλωματική εργασία δείχνει ότι τα συστήματα πρόωσης με τη βοήθεια του ανέμου, ειδικά το eSAIL, προσφέρουν μια βιώσιμη λύση για τη μείωση του περιβαλλοντικού αποτυπώματος της ναυτιλιακής βιομηχανίας. Με την επίτευξη σημαντικών μειώσεων στην κατανάλωση καυσίμου και τις εκπομπές, αυτά τα συστήματα συμβάλλουν στην απανθρακοποίηση των θαλάσσιων μεταφορών και παρέχουν μια πρακτική λύση για τη συμμόρφωση με τους εξελισσόμενους περιβαλλοντικούς κανονισμούς. Τα ευρήματα υποδεικνύουν ότι η συνεχής ανάπτυξη και εφαρμογή των τεχνολογιών WASP θα μπορούσε να διαδραματίσει κρίσιμο ρόλο στην επίτευξη των μελλοντικών στόχων βιωσιμότητας της ναυτιλίας.

Acknowledgments

I would like to express my deepest gratitude to my supervisor, Nikolaos Themelis, for his invaluable guidance, insightful feedback, and continuous support throughout the development and derivation of this thesis. His expertise and encouragement were instrumental in shaping the direction of this work.

I am also deeply thankful to my family for their unwavering support and understanding during this challenging yet rewarding journey. Their encouragement has been a constant source of motivation.

I extend my sincere thanks to bound4blue for generously providing the data and resources necessary for the analysis of the eSAIL system. This collaboration has been crucial in enabling the practical aspects of this research.

Table of Contents

List of Figures

List of Tables

List of Symbols

Symbol	Description
T_o	Propeller thrust
R_T	Total ship resistance
t	Thrust deduction factor
V_o	Advance speed
w	Wake fraction coefficient
V	Vessel speed
k_T	Thrust coefficient
J	Advance coefficient
ρ	Seawater density
n_o	Propeller rotational speed
D	Propeller diameter
Q_o	Propeller torque
η_r	Rotative efficiency
C_N	Propeller speed correction factor
C_P	Delivered power correction factor
n	Shaft speed
Q_D	Delivered torque
P_D	Delivered power
P_{ME}	Main engine power output
P_{MCR}	Main engine maximum continuous rating power
η_s	Shaft transmission efficiency
L_{pp}, L_{BP}	Length of ship between perpendiculars
L_{WL}	Length of waterline
h_s	Significant wave height
T_p	Peak wave period
V_w	Mean wind speed
V_{nav}	Minimum navigational speed
V_{ck}	Minimum course-keeping speed
$V_{ck,ref}$	Reference course-keeping speed
A_R	Rudder area
A_{FW}	Frontal windage area
A_{LW}	Lateral windage area
$A_{LS,cor}$	Ship's submerged lateral area corrected for the breadth effect
B_{wl}	Width of the water line
T_m	Draft of amidship
R_{cw}	Calm water resistance
R_{app}	Resistance of appendages
R_{air}	Added wind resistance
R_{aw}	Added wave resistance, for regular waves
$\overline{R}_{aw}$	Added wave resistance, for irregular waves
k	Form factor
C_F	Coefficient of frictional resistance
Re	Reynolds number
S	Wetted surface area of hull
V_s	Ship advance speed
v	Water kinematic viscosity
C_B	Hull block coefficient
R_{AA}	Added wave resistance

A_{XV}	Area of maximum transverse section exposed to wind
C_{DA}	Wind resistance coefficient
V_G	Measured ship's speed over ground
V_{WRref}	Relative wind speed at reference height
ρ_A	Mass density of air
ψ_{WRref}	Relative wind direction at reference height
R_{AWR}	Wave reflection added resistance
R_{AWM}	Ship motion added resistance
$S(\omega)$	Spectrum function
ω	Angular velocity
ζ_α	Wave amplitude
γ	Wind speed angle
V_t	True wind speed
R_{fr}	Radius of cylinder
N	Rotor revolutions per minute
V_a	Apparent wind speed
β	Apparent wind direction
V_{rat}	Velocity ratio
U_{rot}	Rotor rotational speed
μ_α	Dynamic viscosity of air
F_f	Resistance to the rotation of the cylinder
A_r	Rotor surface area
C_f	Coefficient of skin friction
P_{con}	Power needed to spin the rotor
L	Lift force
D	Drag force
C_L	Coefficient of lift
C_D	Coefficient of drag
A	Rotor cross-sectional affected surface
F_x	Horizontal effective force
F_y	Perpendicular effective force
P_s	System power in ship direction
P_{net}	System's net power output
η_s	System's efficiency
D_F	Horizontal effective force
H_F	Perpendicular effective force
M_{air}	Superstructure's aerodynamic moment
M_{sail}	Sail's moment
M_{hyd}	Hydrodynamic moment
N_H	Yaw moment
N_R	Rudder-induced moment
c_N	Aerodynamic moment coefficient
A_L	Lateral area of the hull and superstructure's overwater portion
x_S	Horizontal lever arm from the aerodynamic centre of pressure to midship
x_A	Centroid of the lateral area of the superstructure, including the hull part above the waterline
F_K	Heeling force
c_Y	Lateral aerodynamic force coefficient
x_R	Lever arm from the rudder's pressure point to midship
AR_h	Underwater portion of the hull's effective aspect ratio
Y'_u, Y''_u	Lateral force's hydrodynamic derivatives
v'	Drift dimensionless speed
β	Drift angle

v	y-direction ship velocity
u	x-direction ship velocity
c_{XD}	Drift-related non-dimensionalized additional resistance
X_D	Drift related additional resistance
N_H	Yaw moment
x_3	Span
A_r	Rudder area
c_{mean}	Mean chord
AR_r	Effective aspect ratio
v_r	Inflow speed to the rudder
F_{NY}	Lateral rudder force
a_r	Inflow angle
a_H	Ratio of the force on the hull caused by the rudder to the rudder force
δ	Rudder angle
F_{NX}	Rudder's additional resistance
$SFOC$	Specific fuel oil consumption of main engine

1 Introduction

1.1 Background

The global climate crisis has underscored the urgent need to reduce carbon dioxide (CO_2) emissions across all sectors. International shipping, which is responsible for approximately 2-3% of global CO_2 emissions, plays a significant role in this environmental challenge [1]. As global trade continues to expand, the shipping industry must adopt more sustainable practices to mitigate its environmental impact. Regulatory frameworks such as the International Maritime Organization's (IMO) strategy on reducing greenhouse gas emissions highlight the necessity for innovative solutions to decarbonize maritime transport.

In response to these challenges, a variety of strategies aimed at reducing emissions have been proposed, including the adoption of alternative fuels, energy-efficient technologies, and wind-assisted propulsion systems. Among these, wind propulsion stands out as a promising solution due to its potential to harness a renewable energy source—wind—thereby decreasing reliance on fossil fuels [2]. Wind-assisted propulsion systems are increasingly being integrated into modern vessels, contributing to significant fuel savings and emissions reduction, without compromising the efficiency of maritime operations.

One of the most well-known wind-assisted propulsion technologies is the Flettner Rotor, first developed in the 1920s by German engineer Anton Flettner [3]. The Flettner Rotor utilizes the Magnus effect, whereby rotating cylinders generate lift perpendicular to the wind direction, providing additional thrust to the vessel [4]. Though it showed promise in its early trials, such as on the ship *Buckau*, it was not widely adopted at the time due to low fuel costs and limited understanding of aerodynamic efficiency. However, the reemergence of environmental concerns has revived interest in this technology. Modern Flettner Rotors, made from advanced materials and optimized through computational fluid dynamics, are now installed on several commercial ships, significantly reducing fuel consumption by up to 10-30%, depending on wind conditions [5].

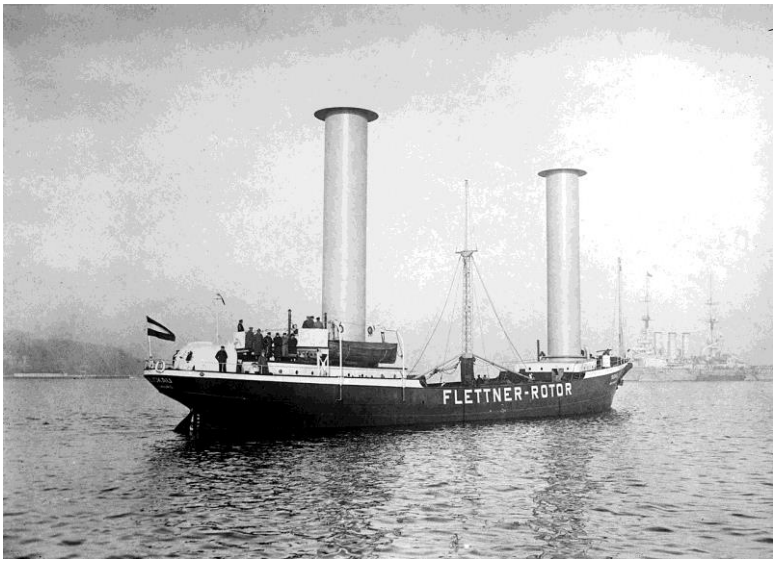

Figure 1: Ship Buckau with Flettner Rotor [6]

A notable advancement of the Flettner Rotor concept is the eSAIL system, an innovative air suction mechanism that enhances the performance of traditional wind propulsion. Developed by bound4blue [7], the eSAIL system integrates suction technology into the rotor, reducing drag and increasing the Magnus effect's efficiency. By improving aerodynamic performance, this system enables vessels to capture more energy from the wind, offering substantial fuel savings and emissions reductions, particularly for long-haul shipping routes. As maritime regulations continue to tighten, the eSAIL system presents a commercially viable solution that aligns with both environmental and operational goals.

Figure 2: eSAIL system fitted on tanker SANTIAGO I [8]

In addition to the Flettner Rotor and eSAIL system, several other wind-assisted propulsion technologies are currently being explored. Wing sails, for instance, operate on the same principles as aircraft wings and have been successfully used on commercial vessels, offering a highly efficient means of capturing wind energy [9]. Kite sails are another promising technology, where a large kite is deployed to harness high-altitude winds, significantly reducing fuel consumption [10]. Furthermore, DynaRigs—rigid sail systems—offer a modern take on traditional sailing, using automated control systems to adjust sail angles for optimal wind capture [11].

Figure 3: Wing sails on ship [12]

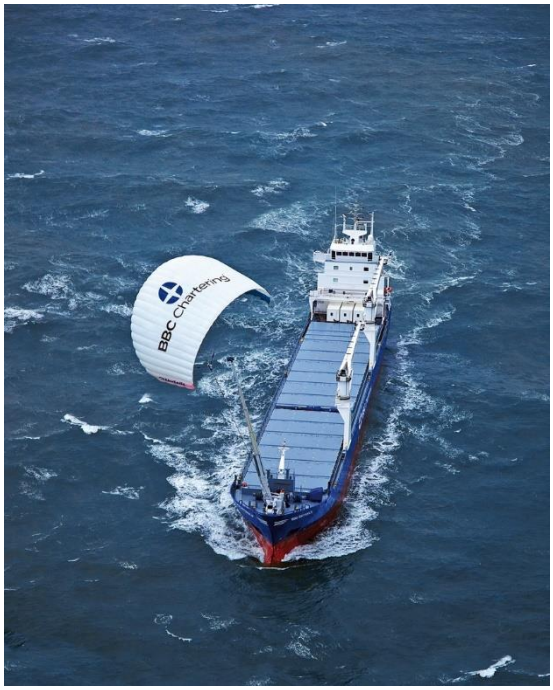

Figure 4: Kite sail on ship [13]

Figure 5: DynaRigs on ship [11]

The potential for wind-assisted propulsion to contribute to a greener maritime sector is clear. By leveraging these technologies, the shipping industry can make significant strides towards reducing its carbon footprint and meeting international emissions targets. The following chapters will delve deeper into the analysis of these systems, with a particular focus on the Flettner Rotor and eSAIL systems and their applications in commercial shipping.

1.2 Goal and thesis structure

The goal of this thesis is to evaluate the benefits of retrofitting a bulk carrier vessel with wind-assisted propulsion systems to reduce fuel consumption and, consequently, its emissions. The vessel's engine has been derated to lower the theoretical Energy Efficiency Existing Ship Index (EEXI) and ensure compliance with future emission regulations.

The steps, followed in this study include:

- Presentation of methodology for calculation of the vessel's speed/power trial prediction curves.
- Development of model which includes ship resistance along with added wind and wave resistances (Model 1[1]). This will be used for assessment of the vessel's compliance with the International Maritime Organization's (IMO) Minimum Propulsion Power requirement, considering the engine's derating.
- Development of models which include ship resistance along with added wind and wave resistance, as well as the utilization of wind energy through systems such as the Flettner Rotor and eSAIL (Model 2, Model 3[2]).
- Development of models which include ship resistance along with added wind and wave resistance as well as the utilization of wind energy through systems such as the Flettner Rotor and eSAIL and added resistances due to side forces generated by these systems (Model 1 modified, Model 2 modified, Model 3 modified[3]).
- Presentation of methodology for calculation of the vessel's fuel oil consumption.
- Presentation of results, that were produced, using the models mentioned above.

The study begins with the first chapter (Literature Review) which reviews wind-assisted propulsion technologies, including wing sails and Flettner Rotors, and compares their performance and efficiency. It highlights the increasing importance of these technologies in meeting emission regulations.

The third chapter (Theoretical Model for ship propulsion including wind-assisted propulsion) explores the theoretical models used to predict ship propulsion performance, including resistance calculations, propulsion efficiency and fuel consumption. This chapter establishes the technical basis for assessing wind-assisted technologies and coupling them with the main engine for the propulsion of the ship.

The fourth chapter (Case Study) applies the theoretical models to a specific bulk carrier retrofitted with eSAIL and Flettner Rotor systems. This chapter presents initial ship data, speed/power curves, and evaluates performance under various conditions, including adverse weather scenarios (IMO minimum power propulsion – Model 1). The implementation of WASP systems along with the added resistances due to the side forces caused by their use are calculated and new speed/power curves are generated. Finally, the fuel consumption for different operation profiles is calculated and compared.

[1] Reference to Different models examined in thesis
[2] Reference to Different models examined in thesis
[3] Reference to Different models examined in thesis

Fifth chapter (Conclusions), summarizes the main findings of the thesis, emphasizing the benefits of wind-assisted propulsion systems in reducing fuel consumption and emissions. It concludes with insights into the potential of these technologies in the maritime sector.

2 Literature Review

2.1 Wind-Assisted Propulsion

The shipping industry, a significant contributor to global greenhouse gas (GHG) emissions, has faced increasing pressure to reduce its carbon footprint. According to the Fourth IMO GHG Study (2020), shipping emissions account for about 2.89% of global anthropogenic emissions [14]. Despite a reduction in carbon intensity between 2012 and 2018, the rate of improvement has slowed, and projections for 2050 suggest that emissions could reach up to 130% of 2008 levels. This concerning trajectory has led to the adoption of stricter regulations, such as the Energy Efficiency Existing Ship Index (EEXI) and the Carbon Intensity Index (CII), introduced by the International Maritime Organization (IMO) [14].

In response to these regulations, wind-assisted propulsion technologies (WASP) have gained popularity due to their potential to reduce fuel consumption and CO2 emissions. By harnessing wind power, ships can reduce their reliance on traditional fossil fuels, which provides both environmental and economic benefits. WASP systems, such as wing sails and Flettner rotors, complement traditional propulsion systems [15]. This section reviews the key WASP technologies, including wing sails, Flettner rotors, and their comparative advantages in fuel savings and propulsion efficiency.

2.2 Wind-Assisted Propulsion Technologies

2.2.1 Wing Sails

Wing sails, a modern interpretation of traditional sails, offer a powerful solution for reducing fuel consumption by exploiting wind energy. These rigid sails, often shaped like airplane wings, generate thrust to assist the ship's conventional propulsion system. A novel method for evaluating the energy-saving potential of sail-assisted ships by analysing the wind resources available along specific routes was presented [16]. The research highlights the critical role that route-based wind analysis plays in optimizing the performance of wing sails.

The study constructed a three-degree-of-freedom motion model to assess the forces acting on wing sails under varying wind conditions, such as wind speed and direction. It was found that, on routes like China to the Middle East, sail-assisted ships could reduce energy consumption by 5.37% annually, and in optimal wind conditions, the reduction could reach as high as 9.54% [16]. These savings illustrate the significant potential of wing sails in improving the sustainability of long-haul shipping.

Furthermore, the effectiveness of wing sails depends not only on the wind but also on how the sails are controlled. Sails must be adjusted based on the wind’s relative angle to the ship, and factors such as rudder angle and ship stability need to be considered for maximizing energy savings [16]. Despite the challenges in wind variability, wing sails offer an attractive solution for reducing emissions in the global shipping industry.

2.2.2 Flettner Rotors

Flettner rotors, based on the Magnus effect, provide another promising wind-assisted propulsion technology. These rotating cylinders generate lift when exposed to wind, which is converted into thrust. Flettner rotors have gained popularity for their compact size, lightweight nature, and ease of integration into existing ships, particularly in retrofitting projects [14].

The work on Flettner rotors demonstrates their use in innovative applications beyond propulsion [15]. In a Marine Cloud Brightening (MCB) vessel, Flettner rotors were used to generate propulsion while facilitating solar radiation management through the release of seawater droplets [15]. The study showed that Flettner rotors could power an entire vessel, proving their versatility and efficiency when combined with alternative technologies such as hydrofoils, which provide additional power generation [15].

Figure 6: Fleet of Marine Cloud Brightening (MCV) vessels [15, Fig. 1]

One study, explored the potential of Flettner rotors when paired with diesel engines and controllable pitch propellers [14]. The research focused on optimizing the interaction between the rotor and conventional propulsion systems to minimize fuel consumption [14]. Using a 3000-ton Ro-Ro/Pax ferry as a case study, it was demonstrated that the integration of rotors can reduce fuel consumption by up to 22%, with a payback period of six years. Similar results were reported in other studies, with fuel savings ranging from 1% to 50%, depending on ship size, rotor configuration, and wind conditions [14]. Another study conducted a case study on a bulk carrier equipped with four Flettner rotors. The study highlighted the economic and environmental benefits of Flettner rotors, with NOx and CO2 emissions reduced by 154.3 tons and 5089 tons annually, respectively, on the longest route [17].

One of the primary advantages of Flettner rotors is their ability to function effectively in a wide range of wind conditions, including moderate to high wind speeds. Unlike wing sails, rotors are not as dependent on optimal wind direction, allowing for more consistent performance across varying sea conditions. Furthermore, Flettner rotors can be integrated into both new and existing vessels, offering flexibility for shipping companies looking to reduce their carbon footprint without extensive modifications to ship design [14]. Moreover, the 4-DOF simulation model emphasizes the importance of accounting for yaw and drift forces when analysing the performance of ships with wind-assisted propulsion [18]. The model showed that Flettner

rotors could deliver up to 20% fuel savings in rough sea conditions, although these savings vary depending on wind conditions and rotor configurations [18].

2.3 Comparison of Wind-Assisted Propulsion Technologies

Both wing sails and Flettner rotors have demonstrated significant potential in reducing fuel consumption and emissions. However, each technology presents unique advantages and challenges that must be considered when selecting the appropriate system for a given vessel.

Wing sails, while highly effective in certain conditions, require careful route planning and wind resource analysis to maximize their efficiency. They are more dependent on wind direction and speed, and their performance may be diminished in regions with variable or unfavourable wind patterns [16]. Additionally, their larger size and visibility concerns may limit their use on certain ship types, particularly those with space constraints on deck.

On the other hand, Flettner rotors offer more flexibility in terms of operational conditions. As a study highlights, rotors can produce consistent thrust even when wind conditions are less than ideal, making them suitable for a broader range of shipping routes [14]. Rotors are also easier to integrate into existing vessels and do not require extensive modifications to the ship's structure, making them an attractive option for retrofitting projects [14]. While the initial investment in Flettner rotors may be higher, studies indicate that the payback period for such systems ranges from 7 to 13 years, depending on the ship's route [17]. Additionally, another study highlighted the dual-functionality of Flettner rotors, which not only generate propulsion but also support energy-intensive processes such as marine cloud brightening [15]. This makes them particularly useful for multi-functional vessels that aim to address both propulsion and environmental challenges.

In terms of fuel savings, both technologies have shown impressive results. Studies on wing sails report fuel savings of 5% to 10%, depending on the route and wind conditions, while Flettner rotors have demonstrated savings ranging from 10% to 22% in favourable conditions [16] [14]. However, the higher initial investment costs associated with Flettner rotors may limit their widespread adoption, particularly for smaller vessels or those operating in less windy regions [14].

2.4 Energy Efficiency and Performance

The evaluation of energy efficiency for wind-assisted propulsion systems is critical in determining their viability for reducing emissions and improving fuel consumption. A study developed an energy-saving evaluation method based on wind resource analysis, which considers factors such as the ship's route, wind speed, and sail configuration [16]. The model emphasizes the importance of optimizing sail performance through careful control of the sails' attack angle and the ship's rudder, which can significantly impact fuel savings.

The combined use of Flettner rotors and hydrofoils, was explored, to enhance the energy output of a vessel. The research showed that the dual use of these technologies on a Marine Cloud Brightening vessel allowed the ship to achieve greater efficiency while performing complex tasks such as spraying seawater droplets to manage solar radiation [15]. The

hydrofoils provided pitch control and additional energy generation, demonstrating the benefits of integrating multiple green technologies to improve fuel efficiency [15].

For Flettner rotors, the 4-DOF simulation model provides a more accurate prediction of fuel consumption by accounting for environmental forces such as wind and waves. The model showed that ignoring yaw and drift forces can lead to an underestimation of fuel consumption, especially in ships equipped with wind-assisted propulsion [18]. This finding is particularly relevant for vessels operating in harsh weather conditions, where accurate predictions of fuel use are essential for operational efficiency.

Economic analysis of Flettner rotors revealed that the systems are most cost-effective on longer routes, with significant reductions in both fuel consumption and emissions. The study found that Flettner rotors can reduce fuel costs by up to 20%, depending on the route, and that the environmental benefits, such as reductions in NOx and CO2 emissions, make these systems highly attractive from both an economic and regulatory perspective [17].

Similarly, another study proposed a mathematical model for evaluating the interaction between Flettner rotors and conventional propulsion systems [14]. The model accounts for factors such as propeller pitch and rotor dimensions to assess the overall energy efficiency of the system. Results suggest that careful optimization of the rotor's operational parameters can lead to substantial reductions in fuel consumption and CO2 emissions.

Overall, studies highlight the importance of integrating wind-assisted technologies with existing propulsion systems to maximize energy efficiency. Whether through the use of advanced control systems for wing sails or the optimization of rotor performance, the key to achieving significant fuel savings lies in the effective management of the ship's propulsion system as a whole [16] [14].

2.5 Discussion on WASP technologies

Wind-assisted propulsion technologies, such as wing sails and Flettner rotors, offer significant potential for reducing fuel consumption and CO2 emissions in the shipping industry. While each technology presents unique challenges and advantages, both have demonstrated their effectiveness in real-world applications. Wing sails are more effective in regions with consistent wind patterns, Flettner rotors provide greater flexibility and can be integrated into a broader range of vessels. Research shows that these technologies can be combined with additional systems, such as hydrofoils, to maximize efficiency and achieve multiple environmental goals [15].

The successful implementation of these technologies requires careful consideration of the ship's route, wind conditions, and propulsion system. By optimizing the interaction between wind-assisted propulsion and traditional engines, shipping companies can significantly reduce their fuel consumption, leading to both economic and environmental benefits.

The successful implementation of these technologies will depend on continued advancements in control systems, route optimization, and integration with conventional propulsion systems. Future research should focus on improving the integration of these technologies with existing ship systems and exploring new ways to enhance their performance under varying operational conditions. With continued development, wind-assisted propulsion could play a key role in the decarbonization of the global shipping industry.

3 Theoretical Model for ship propulsion including wind-assisted propulsion

3.1 Different models examined in thesis

The models, mainly examined in thesis, are briefly described below and a synoptic flowchart diagram is provided.

1. **Model 1: Scantling draft with PSV, modified propeller, added wind and wave resistance** (used for the minimum power propulsion calculations and for reference when studying the other models)
2. **Model 2: Model 1 and Flettner Rotor horizontal effective force (thrust)**
3. **Model 3: Model 1 and eSAIL horizontal effective force (thrust)**
4. **Model 1 modified: Model 1 along with side forces**
5. **Model 2 modified: Model 2 along with side forces**
6. **Model 3 modified: Model 3 along with side forces**

In the current chapter, the theoretical background for analysing each different condition ‘s resistance is presented in detail. Additional calculations and theoretical components are provided in the appendices.

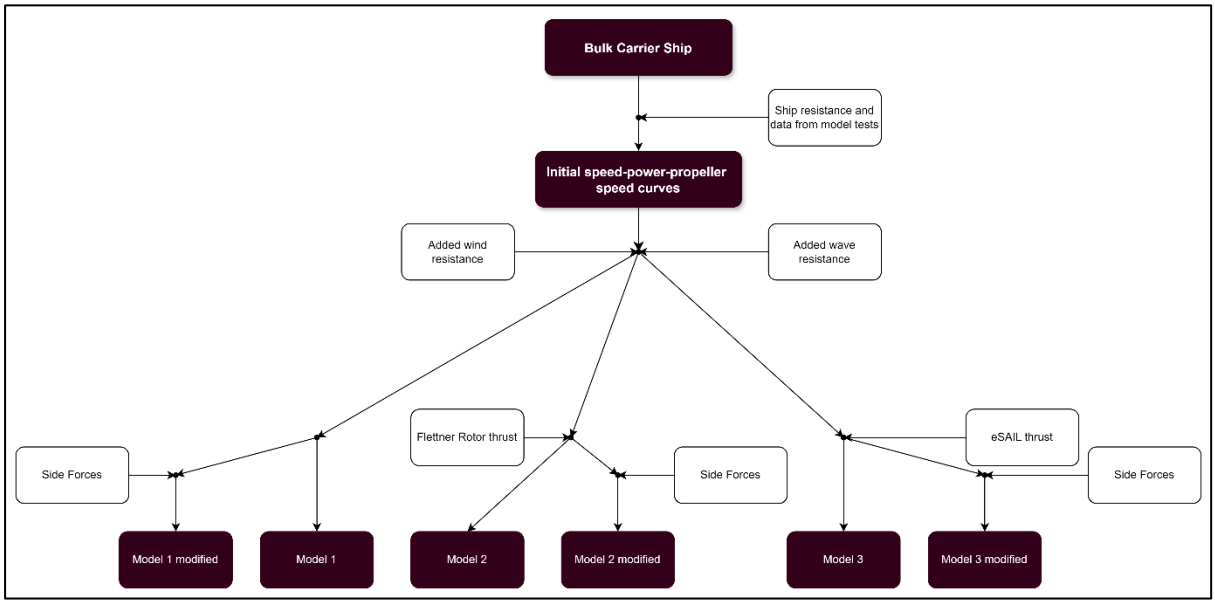

Figure 7: Flowchart diagram for the different models

3.2 Speed/Power trial prediction curves

In a fixed ship condition (specific draft, propeller and appendages) the speed/power trial prediction curves (with reference to propeller) result from following framework described in Propeller open water performance and Propeller performance when coupled with hull [19, Ch. 3–4] which is repeated for each different ship speed in the specified condition.

3.2.1 Propeller open water performance

For a specific ship speed V, propeller thrust T_0, advance speed V_0 are calculated:

$$T_0 = \frac{R_T}{1-t} \tag{3.1}$$

$$V_0 = (1-w)\cdot V \tag{3.2}$$

Constant number $c = \frac{k_T}{J^2} = \frac{\frac{T_0}{\rho \cdot n_0^2 \cdot D^4}}{\left(\frac{V_0}{n_0 \cdot D}\right)^2} = \frac{T_0}{\rho \cdot V_0^2 \cdot D^2}$ (3.3)[4] is utilized to create the $k_T = c \cdot J^2$ (3.4) curve. The previous curve is plotted in the same diagram with the $k_T = f(J)$ (3.5) curve of the propeller (from open water performance results) and the intersection of these two provides the working point of ship-propeller system. Using the propeller advance coefficient at the intersection, propeller speed n_0, efficiency η_0, torque Q_0 are estimated:

$$n_0 = \frac{V_0}{J \cdot D} \tag{3.6}$$

$$\eta_0 = f(J) \tag{3.7}$$

$$Q_0 = \frac{T_0 \cdot V_0}{2 \cdot \pi \cdot n_0 \cdot \eta_0} \tag{3.8}$$

3.2.2 Propeller performance when coupled with hull

To determine the performance of the propeller when coupled with hull, the rotative efficiency η_r, and correction factors[5] C_N, C_P are used. With these, (propeller) shaft speed n, delivered torque Q_D and power P_D at propeller are determined:

$$n = C_N \cdot n_0 \tag{3.9}$$

$$Q_D = \frac{Q_0}{\eta_r} \tag{3.10}$$

$$P_D = C_P \cdot 2 \cdot \pi \cdot n \cdot Q_D \tag{3.11}$$

[4] In this equation T_0 in N
[5] These correction factors are provided by the shipyard [20]

3.2.3 Extracting information using output power of main engine

If the power output of the main engine is known, as a percentage of the MCR, the ship speed and propeller shaft speed can be estimated. Assuming X is the power output of the engine, as percentage of MCR:

$$P_{ME} = \frac{X}{100} \cdot P_{MCR} \tag{3.12}$$

Delivered power to propeller is:

$$P_D = P_{ME} \cdot \eta_s \tag{3.13}$$

Using the points (V, n, P_D) created according to the previous sections:

$$n = f(P_D) \tag{3.14}$$

$$V = f(P_D) \tag{3.15}$$

3.3 IMO Minimum Propulsion Power – Assessment level 2

To reduce the EEDI value of a ship, one option is to reduce the MCR of the main engine. By this reduction, manoeuvrability in adverse weather conditions is directly impacted. The IMO has published interim guidelines [21] for ensuring that ships which comply with EEDI requirements possess installed propulsion power adequate for continuous manoeuvrability under adverse weather conditions. There are 2 assessment levels in these guidelines. The Assessment level 2 (simplified assessment) fundamental principle is that the ship shall be able to maintain course in waves and wind coming from any direction if it has enough installed power to travel at a specific advance speed in head waves and wind.

3.3.1 Adverse weather conditions

Adverse weather conditions depending on ship size are defined in the table below.

Table 1: Adverse weather conditions as a function of ship length [21, p. 2]

Ship length, m	Significant wave height h_s, m	Peak wave period T_P, s	Mean wind speed $V_w, m/s$
Less than 200	4	7 to 15	15.7
$200 \leq L_{pp} \leq 250$	Parameters linearly interpolated depending on ship's length		
More than $L_{pp} = 250$	5.5	7 to 15	19

3.3.2 Required ship speed

The required ship speed, under the influence of head wind and waves, is the maximum of:

- minimum navigational speed, V_{nav}
- minimum course-keeping speed, V_{ck}

3.3.2.1 Navigational speed

Navigational speed, V_{nav}, aids at reducing navigational danger and the possibility of excessive wave motion caused by an unfavourable heading relative to the wind and waves by enabling departure from the coastal area in enough time before the storm intensifies. For this speed the following value is used $V_{nav} = 4\ kn$

3.3.2.2 Course-keeping speed

Course-keeping speed, V_{ck}, is being chosen so that the ship can maintain its course in wind and waves coming from all directions. This speed is determined using two factors, an adjustment factor that accounts for the actual rudder area and the reference course-keeping speed $V_{ck,ref}$, which corresponds to ships with the rudder area A_R equal to 0.9% of the submerged lateral area corrected for width effect:

$$V_{ck} = V_{ck,ref} - 10 \cdot (A_{R\%} - 0.9), in\ kn \tag{3.16}$$

For bulk carriers, combination carriers and tankers $V_{ck,ref}$ is calculated based on the fraction A_{FW}/A_{LW} of frontal windage area (A_{FW}) and lateral windage area (A_{LW}):

$$V_{ck,ref} = \begin{cases} 4\,, & A_{FW}/A_{LW} \geq 0.4 \\ 9\,, & A_{FW}/A_{LW} \leq 0.1 \\ linear\ interpolation\ between\ 4\ and\ 9\ for\ 0.1 \leq A_{FW}/A_{LW} \leq 0.4 \end{cases} \tag{3.17}$$

Calculated as $A_{R\%} = A_R/A_{LS,cor} \cdot 100\%$ (3.18), the actual rudder area, A_R, is expressed as a percentage of the ship's submerged lateral area corrected for the breadth effect, $A_{LS,cor}$. The formula for the submerged lateral area corrected for the breadth effect is $A_{LS,cor} = L_{pp} \cdot T_m \cdot \left(1 + 25 \cdot \left(B_{wl}/L_{pp}\right)^2\right)$ (3.19), where B_{wl} is the width of the water line in meters, T_m is the draft of amidship in meters, and L_{pp} is the length between perpendiculars in meters.

3.3.3 Calculation of required power

The calculation of the required power to achieve the specified speed, from Required ship speed, shall be done according to the methodology described in Speed/Power trial prediction curves.

3.3.4 Calculation of Total Resistance R_T

The ship total resistance R_T is:

$$R_T = R_{cw} + R_{app} + R_{air} + R_{aw} \text{ (for regular waves)} \quad (3.20)$$

Or

$$R_T = R_{cw} + R_{app} + R_{air} + \bar{R}_{aw} \text{ (for irregular waves) (Model 1)} \quad (3.21)$$

Where:

- R_{cw}: is the calm water resistance
- R_{app}: is the resistance of appendages
- R_{air}: added wind resistance
- R_{aw}: added wave resistance, for regular waves
- $\bar{R}_{aw}$: added wave resistance, for irregular waves

Each resistance is described below.

3.3.5 Calm Water Resistance R_{cw}

For calculating the calm water resistance R_{cw} of the ship in a specified load condition and speed, the following formula has been proposed:

$$R_{cw} = (1 + k) \cdot C_F \cdot \frac{1}{2} \cdot \rho \cdot S \cdot V_s^2 \quad (3.22)$$

Where:

- k: form factor which should be acquired through model tests or else it can be calculated as $k = -0.095 + 25.6 \cdot \frac{C_B}{(L_{pp}/B_{wl})^2 \cdot \sqrt{B_{wl}/T_m}}$ (3.23)
- $C_F = \frac{0.075}{(\log_{10} Re - 2)^2}$ (3.24), coefficient of frictional resistance
- $Re = V_s \cdot L_{pp}/\nu$ (3.25)
- ρ: water density in $[kg/m^3]$
- S: wetted surface area of hull in $[m^2]$
- V_s: ship advance speed in $[m/s]$
- ν: water kinematic viscosity in $[m^2/s]$
- C_B: hull block coefficient
- L_{pp}: length between perpendiculars in $[m]$
- B_{wl}: breadth of waterline amidships in $[m]$
- T_m: draught amidships in $[m]$

3.3.6 Resistance of appendages R_{app}

The resistance of appendages can be approximately considered as the 2.5%[6] of the calm water resistance.

3.3.7 Added wind resistance R_{air}

Added wind resistance can be calculated using the following formula from ITTC [23, Eq. 7]:

$$R_{AA} = \frac{1}{2} \cdot \rho_A \cdot C_{DA} \cdot (\psi_{WRref}) \cdot A_{XV} \cdot V_{WRref}^2 - \frac{1}{2} \cdot \rho_A \cdot C_{DA}(0) \cdot A_{XV} \cdot V_G^2 \quad (3.26)$$

Where:

- A_{XV}: area of maximum transverse section exposed to wind $[m^2]$
- C_{DA}: wind resistance coefficient
- V_G: measured ship's speed over ground $[m/s]$
- V_{WRref}: relative wind speed $[m/s]$ at reference height
- ρ_A: mass density of air $[kg/m^3]$
- ψ_{WRref}: relative wind direction at reference height (0 means heading wind)

For specific true wind speed V_{WT} and true wind angle ψ_{WT} (where $\psi_{WT} = B_{WT} - Heading$ (3.27), see Figure 9) the relative wind speed V_{WRref} and relative wind angle ψ_{WRref} can be calculated from the equations:

$$V_{WRref} = \sqrt{V_{WT}^2 + V_G^2 - 2 \cdot V_{WT} \cdot V_G \cdot \cos(180 - \psi_{WT})} \quad (3.28)$$

$$\psi_{WR} = \tan^{-1}\left(\frac{V_{WRref}^2 + V_G^2 - V_{WT}^2}{2 \cdot V_{WR} \cdot V_G}\right) \quad (3.29)$$

The sign convention and sign convention for wind direction are depicted below.

[6] For cargo vessels, appendage resistance is between 2 to 3 percent [22, p. 13]

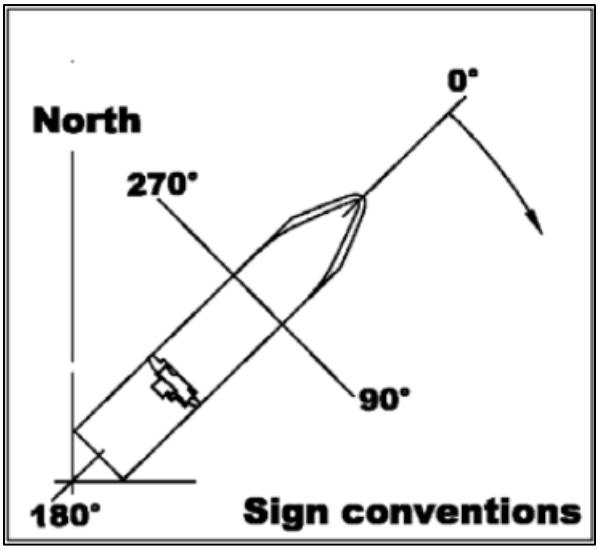

Figure 8: Sign convention [23, Fig. 3]

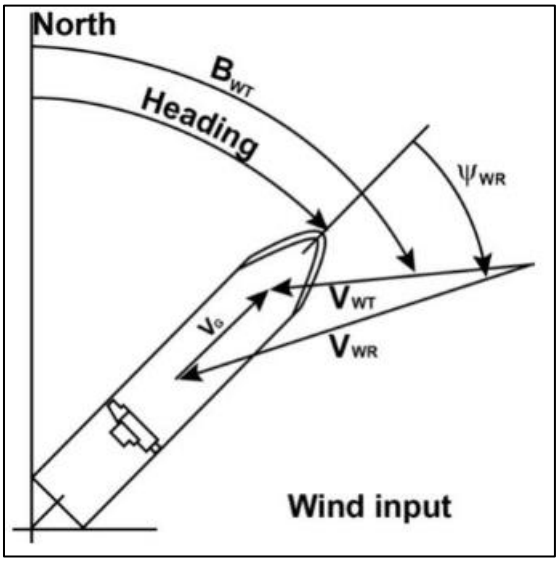

Figure 9: Sign convention for wind directions [23, Fig. 4]

3.3.7.1 Fujiwara regression formula

Refer to Appendix B: Added resistances, B.1.1 Added wind resistance.

3.3.8 Added wave resistance R_{aw} or $\overline{R}_{aw}$

To estimate added wave resistance, the Liu & Papanikolaou method [24] can be utilized. According to this method the total added wave resistance, in regular waves, is calculated:

$$R_{aw} = R_{AWR} + R_{AWM} \tag{3.30}$$

Where:

- R_{AWR}: wave reflection added resistance $[N]$
- R_{AWM}: ship motion added resistance $[N]$

For irregular waves:

$$\bar{R}_{aw} = 2\int_0^{\infty} S(\omega) \cdot \frac{R_{aw}(\omega)}{\zeta_a^2} \cdot d\omega \tag{3.31}$$

Where:

- S: spectrum function $[m^2/Hz]$
- ω: angular velocity $[rad/s]$
- ζ_a: wave amplitude $[m]$

Refer to Appendix B: Added resistances, B.1.2 Added wave resistance.

3.4 Wind Assisted Ship Propulsion (WASP) technologies and side forces

For propulsion, merchant vessels depend on the thrust produced by their main engine. These engines produce high levels of pollution emissions and fuel bills since they burn through copious amounts of fuel. By using the wind to provide clean forward propulsion, Wind-Assisted Propulsion Systems (WAPS) reduce the amount of engine thrust needed, which in turn reduces fuel consumption and emissions of pollutants. The implementation of these technologies, particularly the Flettner Rotor and the eSAIL is described below as well as in the Different models examined in thesis.

3.4.1 Rotor Sail - Flettner Rotor

Below is a brief introduction to the Flettner Rotor and then the theoretical background used to integrate the Flettner Rotor into the ship under study is presented. The theoretical background followed is the same as in [15].

3.4.1.1 Introduction to Flettner Rotor

A Flettner rotor is a cylindrical structure equipped with disc-shaped end plates, rotated along its lengthwise axis. When air flows perpendicular to it, the Magnus effect creates an aerodynamic force perpendicular to both the rotor's axis and the airflow direction as shown in Figure 10. This sail-type rotor is attributed to Anton Flettner, a German aircraft engineer and inventor, who initiated its design in the 1920s [3].

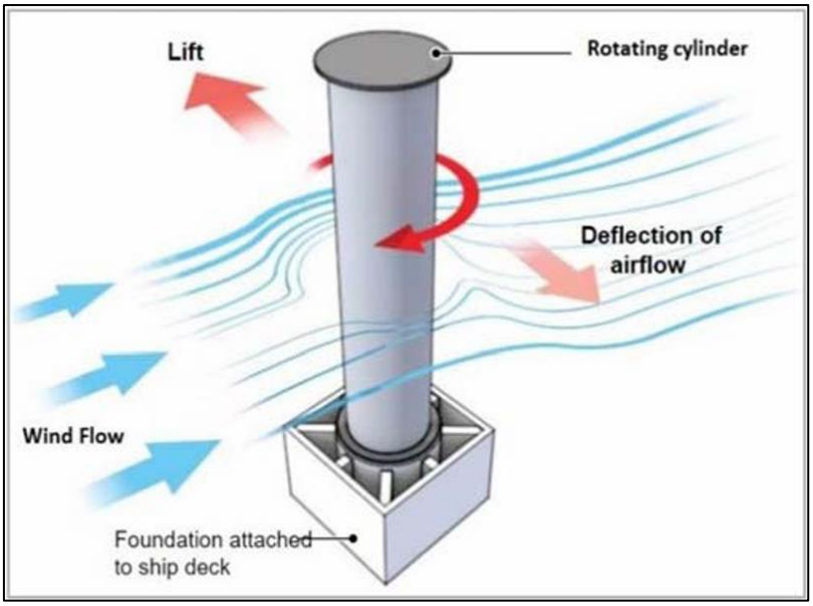

Figure 10: Flettner Rotor Lift force [25, Fig. 1b]

3.4.1.1.1 Magnus Effect

The fundamental idea guiding the operation of Flettner rotors is the Magnus effect. Gustav Magnus gave it its first definition in 1853 [4]. The effect is determined by the pressure and velocity of a rotating object traveling through a fluid or air, such as a cylinder or sphere. The pressure differential surrounding the rotating object can be used to explain the force that is produced. The moving fluid's velocity will decrease as the pressure surrounding the rotating object rises. The air will accelerate in one direction and retard in the other as the wind current flows toward a spinning cylinder. As a result, areas of high and low pressure will form around the rotating object. This phenomenon produces lift and drag forces perpendicular to and parallel to the direction of wind flow [25, p. 2].

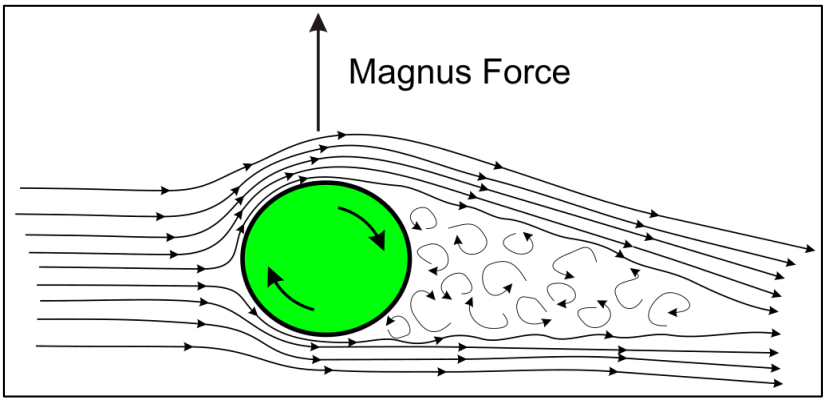

Figure 11: Magnus Effect [4]

3.4.1.2 Reference System

The reference system, with the basic quantities, used is depicted below.

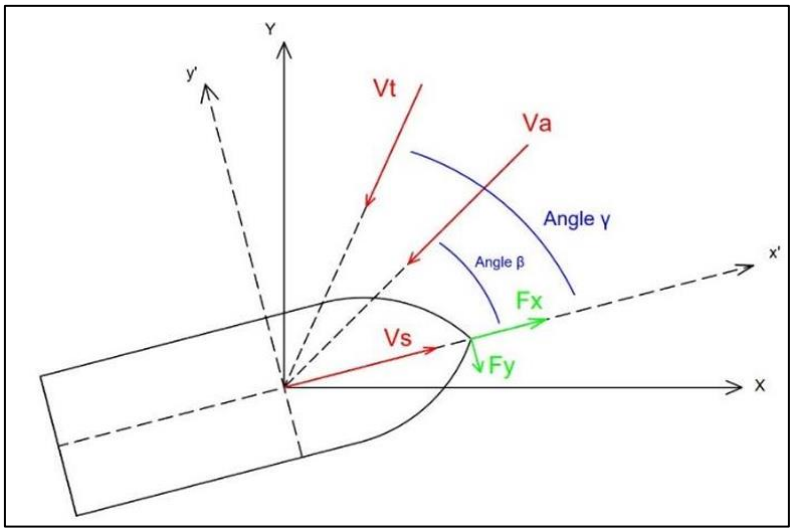

Figure 12: Vessel featuring a solitary Flettner rotor, depicting induced wind velocities, the velocity of the ship, angles of wind speed, and the aerodynamic forces generated by the system [15, Fig. 3]

3.4.1.3 Fundamental Equations

Using ship speed V_s, wind speed angle γ, true wind speed V_t, radius R_{fr} of cylinder, rotor revolutions per minute N (and therefore angle velocity $\omega = 2 \cdot \pi \cdot N/60$ (3.32)) the apparent wind speed V_a, apparent wind direction β, velocity ratio V_{rat}, rotor rotational speed U_{rot} and Reynold's number Re shall be calculated by the following equations [26, Eq. 3.4], [15, Eqs. 2–5]:

$$V_a = \sqrt{V_t^2 + V_s^2 - 2 \cdot V_t \cdot V_s \cdot \cos(\gamma + \pi)} \tag{3.33}$$

$$\beta = \cos^{-1} \frac{V_t^2 - V_s^2 - V_a^2}{-2 \cdot V_a \cdot V_s} \tag{3.34}$$

$$V_{rat} = \frac{\omega \cdot R_{fr}}{V_a} \tag{3.35}$$

$$U_{rot} = \omega \cdot R_{fr} \tag{3.36}$$

$$Re = \rho_A \cdot \omega \cdot R_{fr}^2 \cdot \frac{1}{\mu_\alpha} \tag{3.37}$$

Where:

- ρ: density of air (taken $1.225\ kg/m^3$ for air temperature of 15°C)
- μ_a: dynamic viscosity of air (taken $1.81 \cdot 10^{-5}\ kg/(m \cdot s)$ for air temperature of 15°C)

The resistance to the rotation of the cylinder F_f caused by frictional force from the air is estimated [15, Eq. (6),(8)]:

$$F_f = \frac{1}{2} \cdot C_f \cdot \rho_A \cdot U_{rot}^2 \cdot A_r \tag{3.38}$$

Where:

- A_r: rotor surface area
- $C_f = \left(0.0576/Re^{\frac{1}{5}}\right)$ (3.39): coefficient of skin friction

The power P_{con} [15, Eq. 9] needed to spin the rotor does not include endplate and bearing friction [15, p. 5].

$$P_{con} = F_f \cdot U_{rot} \tag{3.40}$$

As stated in Magnus Effect, lift and drag forces are created due to the Magnus effect. Drag force acts parallel to the apparent wind and perpendicular to lift force. These are calculated [15, Eq. (10),(11)]:

$$L = \frac{1}{2} \cdot \rho_A \cdot V_a^2 \cdot A \cdot C_L \tag{3.41}$$

$$D = \frac{1}{2} \cdot \rho_A \cdot V_a^2 \cdot A \cdot C_D \tag{3.42}$$

Where:

- C_L: coefficient of lift (dependent on velocity ratio)
- C_D: coefficient of drag (dependent on velocity ratio)
- A: rotor cross-sectional affected surface

The horizontal and perpendicular effective forces F_x and F_y [15, Eq. (12),(13)] acting on the ship's motion are:

$$F_x = L \cdot \sin\beta - D \cdot \cos\beta \tag{3.43}$$

$$F_y = L \cdot \cos\beta + D \cdot \sin\beta \tag{3.44}$$

The horizontal force F_x times the ship speed V_s yields the system power in ship direction [15, Eq. 14], which can be calculated:

$$P_s = F_x \cdot V_s \tag{3.45}$$

The difference between the power provided by the rotors and the power required to overcome air friction is the system's net power output, or P_{net} [15, Eq. 15]:

$$P_{net} = (P_s - P_{con}) \cdot \eta_s \tag{3.46}$$

Where:

- η_s: system's efficiency [15, p. 7]

The decision for the activation or deactivation of the rotor is determined based on the net power output P_{net}. If the output is positive the system is activated because the propulsion power offered by the rotor is greater than the power needed for operation, whereas in other cases the system is deactivated. When the system is not in use, additional resistance is created due to the rotor acting as appendage (as a superstructure because it is located above main deck). In such cases the additional horizontal effective force is calculated [27, Eq. 6]:

$$F_x = -\frac{1}{2} \cdot K \cdot \rho_A \cdot V_a^2 \cdot A \cdot \cos\beta \tag{3.47}$$

Where:

- K: is dependent on the rotor aspect ratio, 0.8 was considered to be the value [27, p. 6]

Based on the equation above, when the system is not in use, the perpendicular effective force is calculated:

$$F_y = -\frac{1}{2} \cdot K \cdot \rho_A \cdot V_a^2 \cdot A \cdot \sin\beta \tag{3.48}$$

To integrate the effect of the Flettner rotor in the ship propulsion, the horizontal effective force F_x must be included to the total resistance (and therefore thrust) that the propeller should compensate for the ship to develop a specific speed. The analytical expression, that incorporates the previous, is written below. When the F_x is positive the rotor helps in propelling the ship. If the F_x is negative, then the rotor increases the total resistance of the ship and ultimately the power needed for propulsion.

Total resistance being:

$$\boldsymbol{R_T = R_{mt} + R_{air} + \bar{R}_{aw} - Number\ of\ Flettner\ Rotors} \cdot \boldsymbol{F_x}\ (Model\ 2) \tag{3.49}$$

Where:

- R_T: total ship resistance
- R_{mt}: ship resistance from model tests
- R_{air}: added wind resistance
- $\bar{R}_{aw}$: added wave resistance (in irregular waves)
- F_x: horizontal effective force (thrust) of Flettner Rotor

3.4.2 Suction Sail – eSAIL

Suction wings are wing sails with a built-in mechanical air suction mechanism and a particularly thick profile. A boundary layer suction is used to control the airflow around the "thick" foil shape. Therefore, one or more ventilators must be installed inside the suction wing profile. The airflow is accelerated at the leading edge, or the "nose" of the egg-shaped cross section, which causes extremely low pressure to occur throughout the suction-side and on the top-left side of the profile. It is a manufactured method of lowering the wing profile's drag coefficient while maintaining a high lift coefficient—up to 7-8 depending on the angle of attack and suction efficiency [28].

When the sail is inactive, drag is created due to its presence in incoming wind as shown below.

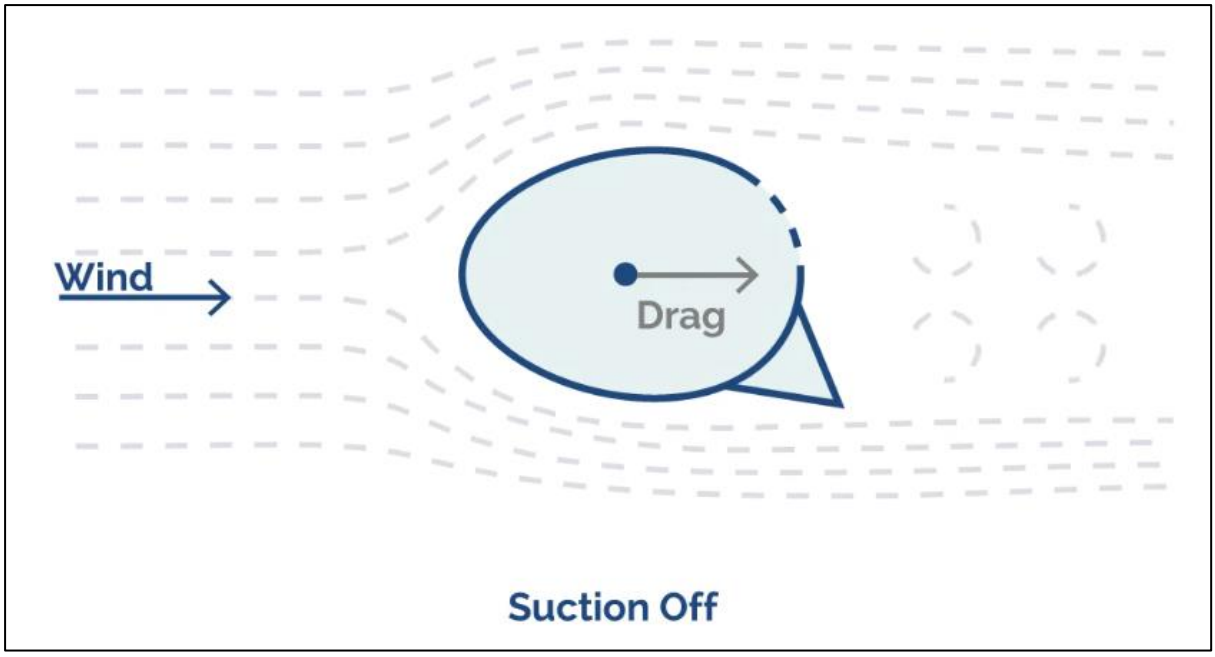

Figure 13: Suction sail inactive [7]

After activation, lift is generated, and drag is reduced.

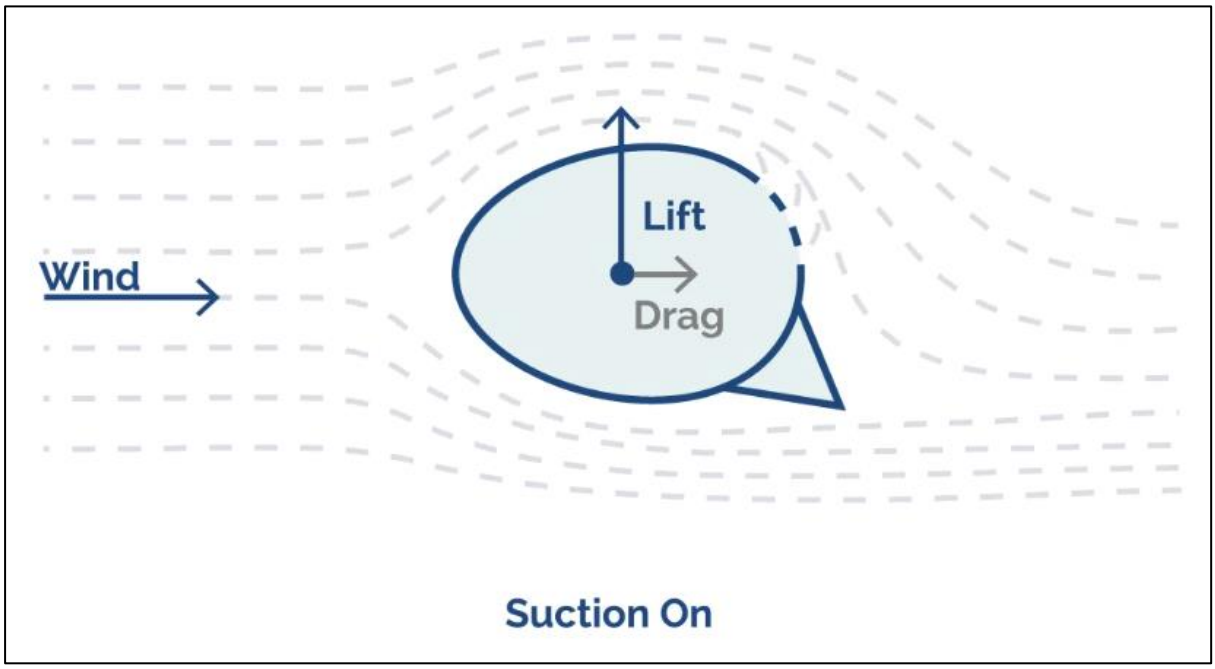

Figure 14: Suction sail active [7]

With appropriate rotation the lift can be further increased while minimal increase in drag is induced.

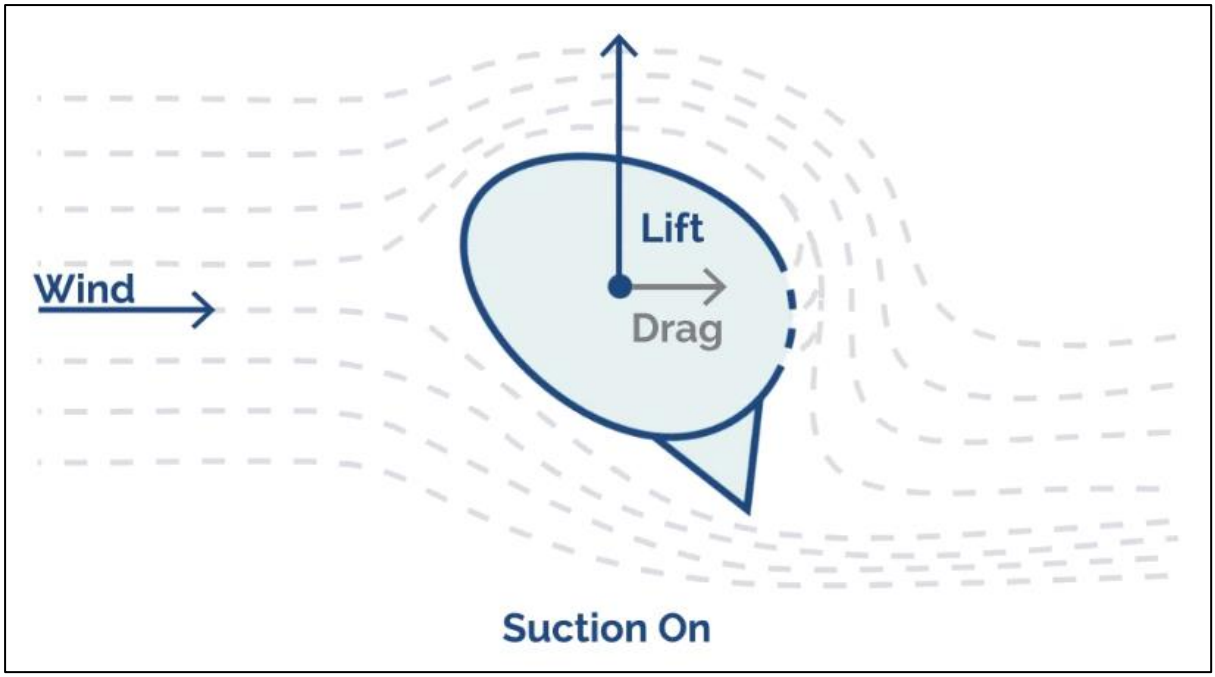

Figure 15: Suction sail active with appropriate rotation [7]

A photograph of the eSAIL is found below:

Figure 16: eSAIL [7]

To integrate the effect of the eSAIL in the ship propulsion, the horizontal effective force must be included to the total resistance (and therefore thrust) that the propeller should compensate for the ship to develop a specific speed. The analytical expression, that incorporates the previous, is written below. When the effective force is positive the rotor helps in propelling the ship. If it is negative, then the rotor increases the total resistance of the ship and ultimately the power needed for propulsion.

Total resistance being:

$$\boldsymbol{R_T = R_{mt} + R_{air} + \bar{R}_{aw} - Number\ of\ eSAILs \cdot D_F}\ (Model\ 3) \tag{3.50}$$

Where:

- R_T: total ship resistance
- R_{mt}: ship resistance from model tests
- R_{air}: added wind resistance
- $\bar{R}_{aw}$: added wave resistance (in irregular waves)
- D_F: horizontal effective force (thrust) of eSAIL

3.4.3 Side Forces

To estimate velocity and construct a ship with a sailing system, it is crucial to take significant rudder angles and the induced resistance, caused by drift, into account. Increased hull and rudder resistances during drift were found in a study conducted [29] on the operational performance of wind-assisted ships. Another study [30] conducted a comparison between a 1-DOF model (pure added resistance) and a 4-DOF model (surge, sway, heel, and yaw). The results indicated that the 1-DOF model, which did not account for the influences of drift and the rudder, overvalued the reduction in fuel consumption by 7% and the propulsion power of the sailing systems by 40%. From the above, it is obvious that a method should be used to estimate the rudder and drift angle as well as the corresponding resistance. For this goal, the Skogman's method from was used [31]. For ease, the centre of gravity is located at the midship section. The formulations are based on the equilibrium of moments that can arise, around it, under steady-state conditions. As seen in Figure 17, the y direction of the coordinate system is positive to starboard and the x-direction is positive in the forward ship direction. When the superstructure's aerodynamic moment (M_{air}), the sails' moment (M_{sail}), and the hydrodynamic moment (M_{hyd}) are all in balance:

$$M_{air} + M_{sail} + M_{hyd} = 0 \tag{3.51}$$

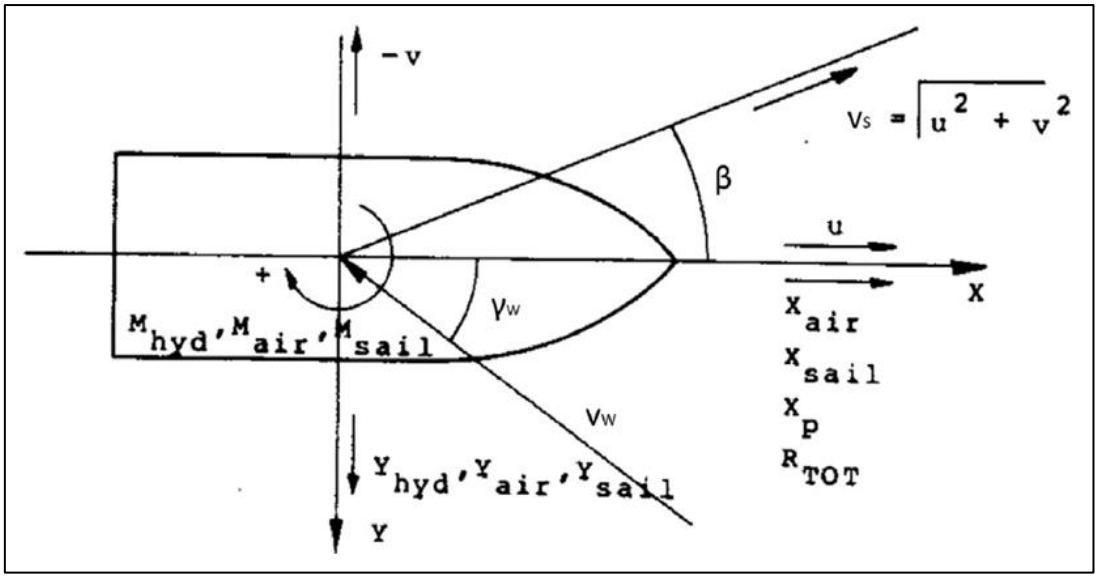

Figure 17: System of coordinates for the Skogman method [31, Fig. 4]

The yaw moment N_H and the rudder-induced moment N_R make up the hydrodynamic moment M_{hyd}. The formulas for M_{air} and M_{sail} are as follows:

$$M_{air} = -0.5 \cdot \rho_A \cdot A_L \cdot V_{WR}^2 \cdot c_N \cdot x_A \tag{3.52}$$

$$M_{sail} = F_K \cdot x_S \tag{3.53}$$

In which, the aerodynamic moment coefficient is c_N, lateral area of the hull and superstructure's overwater portion is represented by A_L, the horizontal lever arm from the aerodynamic centre of pressure to midship is represented by x_S, and the centroid of the lateral area of the superstructure, including the hull part above the waterline, is represented by x_A. The heeling force F_K must be interpreted as negative for the wind force from starboard.The lateral force of aerodynamics is:

$$F_{air} = -0.5 \cdot \rho_A \cdot A_L \cdot V_{WR}^2 \cdot c_Y \tag{3.54}$$

As in a study [32], the aerodynamic moment coefficient c_N and the lateral aerodynamic force coefficient c_Y are both assumed to be 1.25. After that, an auxiliary factor is computed using x_R as the lever arm from the rudder's pressure point to midship:

$$Y_{m0} = \frac{1}{0.5 \cdot \rho \cdot T \cdot L_{WL} \cdot V_s^2} \cdot \left(F_{air} + F_K - \frac{1}{x_R} \cdot (M_{air} + M_{sail}) \right) \tag{3.55}$$

The underwater portion of the hull's effective aspect ratio, or AR_h, is:

$$AR_h = \frac{2 \cdot T}{L_{WL}} \tag{3.56}$$

The lateral force's hydrodynamic derivatives, Y_v' and Y_v'', are as follows:

$$Y_v' = -0.5 \cdot \pi \cdot AR_h - 1.4 \cdot C_B \cdot \frac{B_{WL}}{L_{WL}} \tag{3.57}$$

$$Y_v'' = -6.6 \cdot (1 - C_B) \cdot \frac{T}{B_{WL}} + 0.08 \tag{3.58}$$

Drift dimensionless speed v' is calculated:

$$v' = \frac{\left(Y'_v + \frac{AR_h \cdot L_{WL}}{x_R}\right) + \sqrt{\left(Y'_v + \frac{AR_h \cdot L_{WL}}{x_R}\right)^2 + 4 \cdot Y'_{vv} \cdot Y_{m0}}}{Y'_{vv}} \tag{3.59}$$

Drift angle β is:

$$\beta = arc\sin v' \tag{3.60}$$

y-direction ship velocity is:

$$v = v' \cdot V_S \tag{3.61}$$

x-direction ship velocity is:

$$u = \sqrt{V_s^2 - v^2} \tag{3.62}$$

The drift-related non-dimensionalized additional resistance is:

$$c_{XD} = 0.0833 \cdot \beta - 0.1 \cdot \beta^2 + 0.0041667 \cdot \beta^3 \tag{3.63}$$

Drift-related additional resistance is then:

$$X_D = c_{XD} \cdot 0.5 \cdot \rho \cdot u^2 \cdot L_{WL} \cdot T \cdot 10^{-3} \tag{3.64}$$

Yaw moment is:

$$N_H = 0.5 \cdot \rho \cdot L_{WL}^2 \cdot T \cdot V_s^2 \cdot (-AR_h \cdot v') \tag{3.65}$$

The span x_3 (see Figure 18) across the rudder area A_r and mean chord line c_{mean} are used to compute the effective aspect ratio, or AR_r, before calculating the rudder angle:

$$AR_r = 2 \cdot AR_{geometric} = 2 \cdot \frac{x_3}{c_{mean}} \tag{3.66}$$

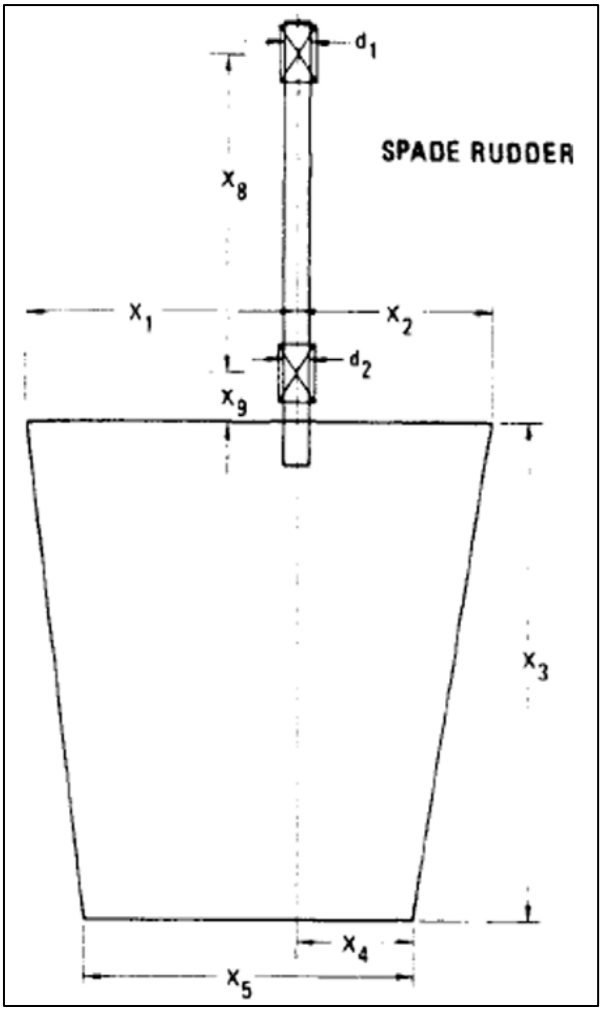

Figure 18: Spare rudder dimensions [31, Fig. 5]

The wake decreases the inflow speed v_r to the rudder:

$$v_r = V_s \cdot (1 - w) \tag{3.67}$$

In the beginning, the lateral rudder force F_{NY} needs to be calculated using an arbitrary inflow angle α_r, such as $-5°$:

$$F_{NY} = 0.5 \cdot \rho \cdot \frac{6.13 \cdot AR_r}{2.25 + AR_r} \cdot A_r \cdot v_r^2 \cdot \sin(\alpha_r) \tag{3.68}$$

The term "hydrodynamic force" refers to the force that the rudder action exerts on the ship's hull. Using regression analysis based on model testing α_H, which is the ratio of the force on the hull caused by the rudder to the rudder force, is calculated [33]:

$$\alpha_H = 0.64 \cdot C_B - 0.154 \tag{3.69}$$

To find the rudder angle δ, the following formula is used:

$$\delta = 0.5 \cdot arcsin\left(\frac{2}{-(1 + \alpha_H) \cdot x_R \cdot \frac{F_{NY}}{\sin(\alpha_r)}} \cdot (0.5 \cdot \rho \cdot AR_h \cdot L_{WL}^2 \cdot T \cdot V_s^2 \cdot v' - M_{air} - M_{sail}) \right) \tag{3.70}$$

The rudder force F_{NY} needs to be calculated again using the new inflow angle. The rudder's additional resistance is:

$$F_{NX} = -F_{NY} \cdot \sin\delta \tag{3.71}$$

Finally, rudder moment is:

$$N_R = -(1 + \alpha_H) \cdot x_R \cdot F_{NY} \cdot \cos\delta \tag{3.72}$$

For the side forces to be considered, the rudder force F_{NY} and drift-related additional resistance X_D must be included to the total resistance (and therefore thrust) that the propeller should compensate for the ship to develop a specific speed. The analytical expressions, that incorporate the previous, are written below.

It should also be mentioned that the heeling force F_K, for a specific system, is the product between the number of WASP systems and the perpendicular effective force produced by each one of the systems.

Total resistance being $\boldsymbol{R_T = R_{mt} + R_{air} + \bar{R}_{aw} + (X_D + F_{NX})}$ (3.73) (Model 1 modified), $\boldsymbol{R_T = R_{mt} + R_{air} + \bar{R}_{aw} - Number\ of\ Flettner\ Rotors \cdot F_x + (X_D + F_{NX})}$ (3.74) for Flettner Rotor (Model 2 modified) and $\boldsymbol{R_T = R_{mt} + R_{air} + \bar{R}_{aw} - Number\ of\ eSAILs \cdot D_F + (X_D + F_{NX})}$ (3.75) for eSAIL (Model 3 modified)

Where:

- R_T: total ship resistance
- R_{mt}: ship resistance from model tests
- R_{air}: added wind resistance
- $\bar{R}_{aw}$: added wave resistance (in irregular waves)
- F_x: horizontal effective force (thrust) of Flettner Rotor
- D_F: horizontal effective force (thrust) of eSAIL
- X_D: added resistance due to ship drift
- F_{NX}: added resistance due to the rudder

3.5 Fuel Oil Consumption Calculation

For the calculation of the daily fuel consumption the equation below is used:

$$Daily\ fuel\ consumption = SFOC \cdot P_{ME} \cdot 24 \cdot 10^{-6} \tag{3.76}$$

Where:

- $Daily\ fuel\ consumption$: $[tn]$

- $SFOC$: specific fuel oil consumption of main engine $[g/kWh]$
- P_{ME}: power output of the engine $[kW]$ equal to $\frac{P_D}{\eta_s}$ (η_s: transmission efficiency)

4 Case Study

4.1 Ship initial data

The ship utilized in this study is a Bulk Carrier with principal particulars shown in Table 2.

Table 2: Ship principal particulars

PRINCIPAL PARTICULARS	
LENGTH O.A.	229 m
LENGTH B.P.	225.5 m
BREADTH (MLD.)	32.26 m
DEPTH (MLD.)	20.05 m
DESIGNED DRAFT	12.20 m
C_B @ DESIGNED DRAFT	0.8624
DEADWEIGHT (DESIGNED DRAFT)	64911.79 t
SCANTLING DRAFT	14.45 m
C_B @ SCANTLING DRAFT	0.8772
DEADWEIGHT (SCANTLING DRAFT)	80996.09 t
LIGHTSHIP WEIGHT	13800.11 t
MAIN ENGINE	MAN B&W 6S60ME-C8.5-TII
TRANSMISSION EFFICIENCY η_s	0.99
P_{MCR}	9930 kW
$P_{MCR\_ME,lim}$	8230 kW
n_{MCR}	90.4 rpm
P_{AE}	496.5 kW
TYPE OF FUEL (ME & AE)	DIESEL/GAS OIL

Information regarding ship towing tank tests is also available. Therefore, open water performance characteristics[7] of modified[8] propeller, effective power curve[9] (which includes resistance due to the presence wind) at scantling draft (with PSV), self-propulsion factors[10] at scantling draft (with PSV) are known. These data can be found at Appendix A: Ship data from towing tank test report. The initial condition used in the current thesis is **Scantling draft with modified propeller and PSV**.

[7] Referring to J, k_T, k_Q, η_0

[8] For this ship two different propellers are investigated, the original propeller of ship and a modified one. The modified propeller is a hypothetical propeller that resulted through the reverse engineering of the sea trial results. Thus, the open water characteristics for the modified propeller are more accurate for the propeller of the ship.

[9] Referring to total resistance for each speed

[10] Referring to t, w, η_r, C_P, C_N

4.2 Speed/Power trial prediction curves of ship

Using a MATLAB script which applies the computational framework described in Speed/Power trial prediction curves to the above data, the speed/power trial prediction curves are obtained for each different condition.

4.2.1 Main engine load diagram with trial prediction curves

Ship trial prediction curves can also be plotted along the main engine load diagram. For the calculation of load diagram points, CEAS [34] calculation tool was used for the model of the engine.

4.3 IMO Minimum Propulsion – Assessment level 2

In this section, the theoretical framework developed in IMO Minimum Propulsion Power – Assessment level 2, is applied. The scantling condition with PSV and modified propeller will be verified through the guideline.

4.3.1 Adverse weather conditions

Using linear interpolation for $L_{pp} = 225.5\ m$, adverse weather conditions can be specified.

Table 3: Adverse weather conditions for ship under study

Ship length, m	Singificant wave height h_s, m	Peak wave period T_p, s	Mean wind speed V_w m/s
225.5	4.765	7 to 15	17.383

4.3.2 Required ship speed and peak wave period

To calculate the required ship speed, we use the data tables:

Table 4: V_{ck} calculation

A_{FW} [m^2]	574		A_R [m^2]	52

A_{LW} [m^2]	1615		$A_{LS,cor}$ [m^2]	4925.7
$V_{ck,ref}$ [kn]	4.743		$A_{R\%}$ [-]	1.06
V_{ck} [kn]			**3.186**	

Table 5: V_{nav}

V_{nav} [kn]	**4**

The required speed is $V_s = \max(V_{ck}, V_{nav}) \Rightarrow \boldsymbol{V_s = 4\ kn}$

4.3.3 Calculation of required power

Because towing tank results (water resistance $R_{cw} + R_{app}$, wake fraction coefficient w, thrust deduction factor t, rotative efficiency η_R,power correction factor C_P and propeller revolution correction factor C_N) for speeds as low as $4kn$ are not available, the theory (developed in the Theoretical) to estimate the resistance will be used. Regarding the rest factors, the following assumption will be made: these factors, for the speed of $4kn$, are assumed the same as those for the lowest speed available from towing tank test results.

Table 6: Factors for speed of 4kn

w [-]	0.37
t [-]	0.215
η_R [-]	0.99
C_P [-]	0.99
C_N [-]	1

4.3.4 Calm Water Resistance R_{cw}

The calm water resistance is calculated using the table:

Table 7: Calm water resistance calculation at scantling draft for ship speed of 4kn

k [-]	0.2126
C_F [-]	0.0017
Re [-]	$4.4189*10^8$
ρ [kg/m^3]	1025
S [m^2]	12468.4
v [m^2/s]	$1.05*10^{-6}$
B_{wl} [m]	32.26

T_{wl}	14.45
R_{cw} [N]	**55715**

4.3.5 Resistance of appendages R_{app}

As stated in the respective section in the Theoretical the resistance of appendages is approximately $2.5\% \cdot R_{cw}$.

Table 8: Appendages resistance at scantling draft for ship speed of 4kn

R_{app} [N]	**1393**

4.3.6 Added wind resistance R_{air}

For the added wind resistance, the head wind resistance should be calculated. The data required for the calculations (at scantling condition) are the following:

Table 9: Required data for scantling draft

Required Data		
L_{BP}	225.5	m
B	32.26	m
A_{OD}	705	m^2
A_{XV}	637	m^2
A_{YV}	2034	m^2
C_{MC}	-7.51	m
h_{BR}	28.7	m
h_C	5.7	m
μ	10	deg

Table 10: C_{LF}, C_{XLI}, C_{ALF} for scantling draft

$0<\psi_{WR}<90$	
C_{LF}	0.818941
C_{XLI}	0.113509
C_{ALF}	0.435656
$90<\psi_{WR}<180$	
C_{LF}	0.698735
C_{XLI}	-0.20487
C_{ALF}	0.701161

Table 11: Wind resistance coefficient C_{DA} for different angles

C_{DA} for Angle of Wind Attack $0<\psi_{WR}<\pi$		
Angle of Attack [deg]	**Angle of Attack [rad]**	**Wind Res. Coef. (C_{DA})**
0	0.0000	0.819
10	0.1745	0.880
20	0.3490	0.900
30	0.5236	0.866
40	0.6981	0.779
50	0.8726	0.649
60	1.0471	0.494
70	1.2216	0.329
80	1.3962	0.163
90	1.5707	0.000
100	1.7452	-0.091
110	1.9197	-0.207
120	2.0942	-0.358
130	2.2688	-0.530
140	2.4433	-0.692
150	2.6178	-0.805
160	2.7923	-0.843
170	2.9668	-0.801
180	3.1414	-0.699
C_{DA} for Angle of Wind Attack $-\pi<\psi_{WR}<0$		
Angle of Attack [deg]	**Angle of Attack [rad]**	**Wind Res. Coef. (C_{DA})**
0	0.0000	0.819
-10	-0.1745	0.880
-20	-0.3490	0.900
-30	-0.5236	0.866
-40	-0.6981	0.779
-50	-0.8726	0.649
-60	-1.0471	0.494
-70	-1.2216	0.329
-80	-1.3962	0.163
-90	-1.5707	0.000
-100	-1.7452	-0.091
-110	-1.9197	-0.207

-120	-2.0942	-0.358
-130	-2.2688	-0.530
-140	-2.4433	-0.692
-150	-2.6178	-0.805
-160	-2.7923	-0.843
-170	-2.9668	-0.801
-180	-3.1414	-0.699

The respective plots of wind resistance coefficient versus the wind angle are depicted in the figures:

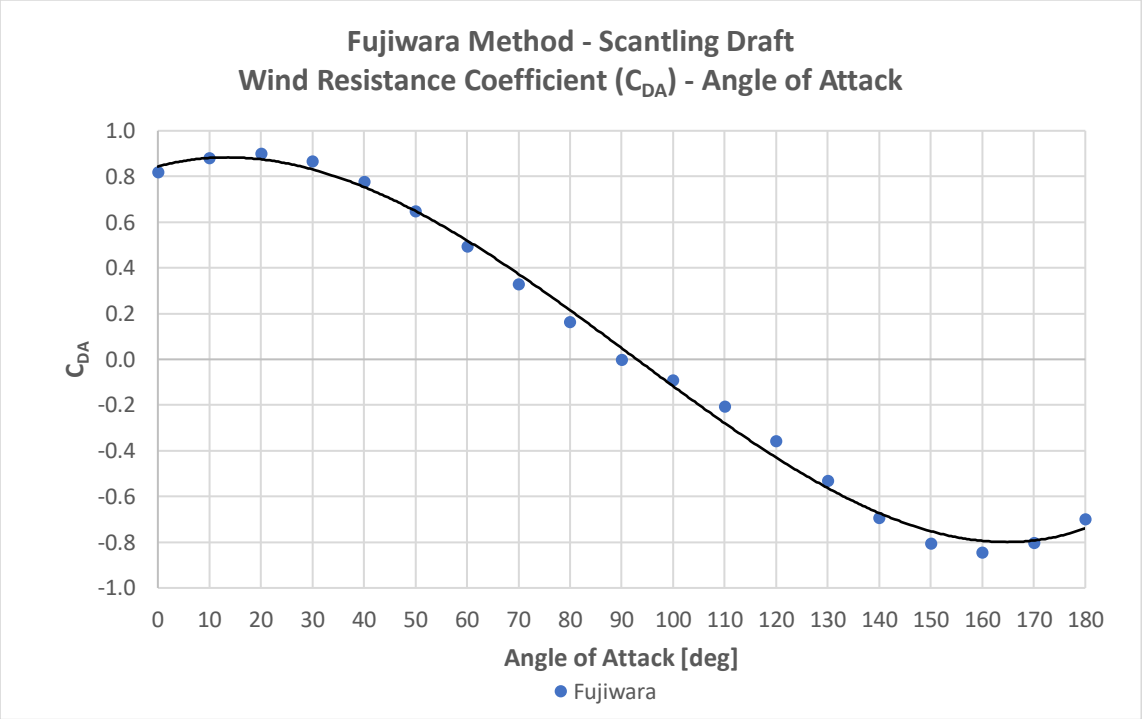

Figure 19: Wind Resistance Coefficient C_{DA} versus the Angle of Attack

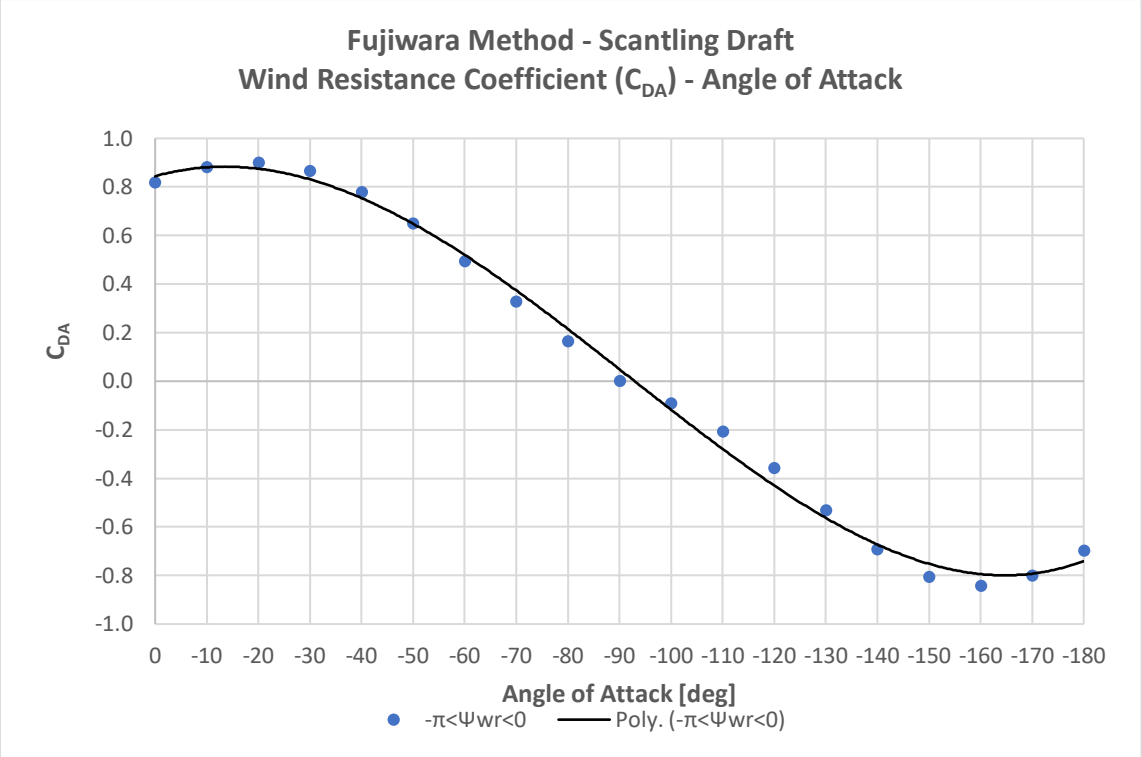

Figure 20: Wind Resistance Coefficient C_{DA} versus the Angle of Attack

Using the wind resistance coefficient $C_{DA} = 0.819$ for 0 degrees and that air density is approximately $\rho_A = 1.2466\ kg/m^3$ it is calculated:

Table 12: Added wind resistance for head winds at scantling draft and ship speed of 4kn

R_{air} [N]	96875

4.3.7 Added wave resistance R_{aw} or $\bar{R}_{aw}$

For the added wave resistance, the head wave resistance should be calculated. The data required for the calculations (at scantling condition) are the following:

Table 13: Required data for scantling draft and sea state

L_{BP}	225.5	[m]
T_a	14.45	[m]
T_f	14.45	[m]
L_{E1}	35.5	[m]
L_R	30	[m]
g	9.81	[m/s^2]
k_{yy}	0.22	[-]
E_1	0.4265	[rad]
E_2	0.4933	[rad]

4.3.7.1 Added wave resistance R_{aw} in regular waves

Using MATLAB code developed for the theory of added wave resistance described in Theoretical, the added wave (non-dimensional) resistances R_{AWR}, R_{AWM}, R_{aw} for bow waves are computed versus the wave length λ divided by length between perpendiculars L_{BP} for vessel speed of $4\ kn$ in regular waves.

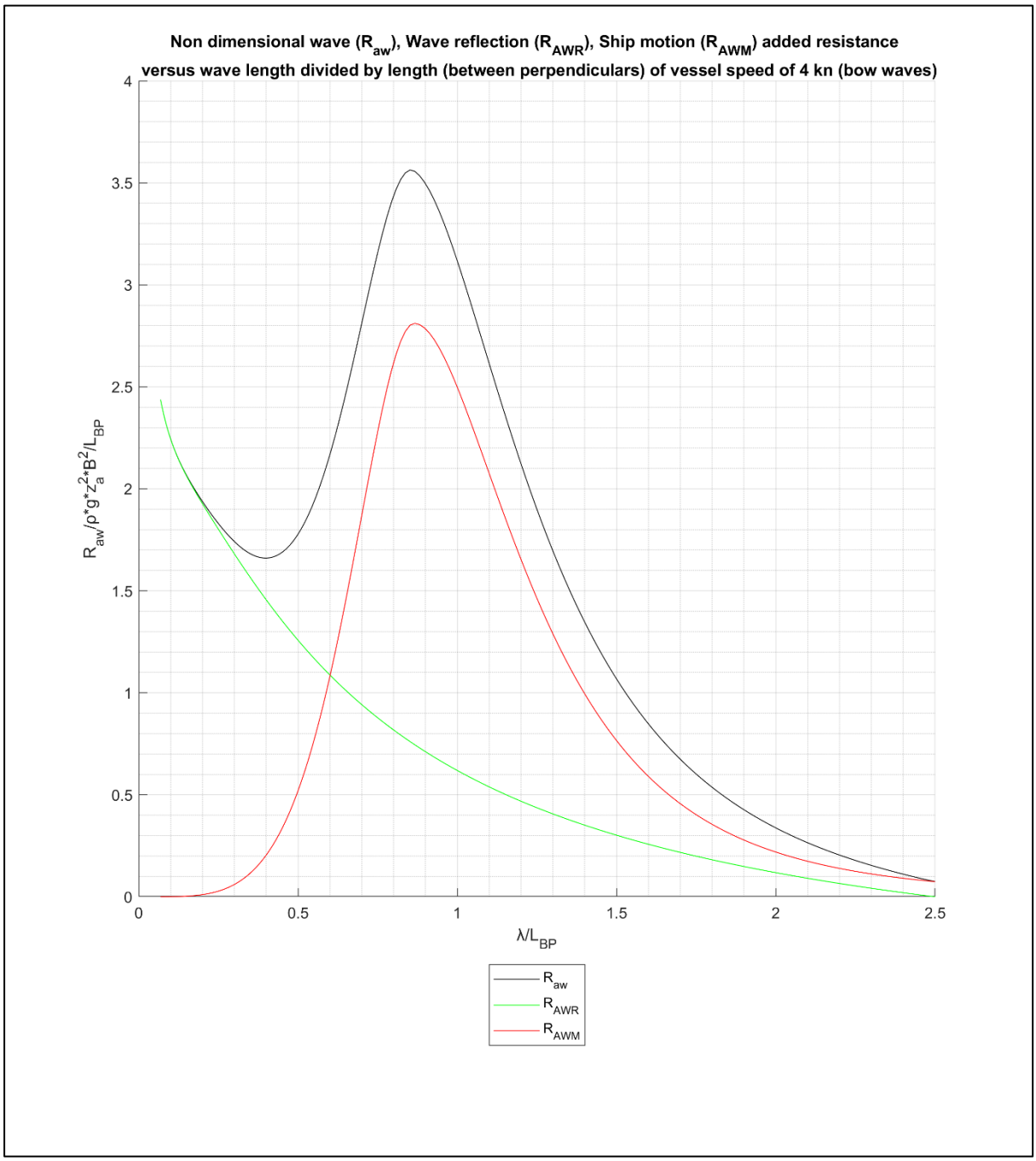

Figure 21: Added wave (non-dimensional) resistances R_{AWR}, R_{AWM}, R_{aw} for bow waves versus peak wave angular velocity for vessel speed of $4\ kn$

4.3.7.1 Added wave resistance $\overline{R}_{aw}$ in irregular waves

A real sea state can be described by a sum of regular waves which can be achieved through a spectrum function. In the present work, the JOHNSWAP spectrum [24, Tbl. 2] was used.

$$S(H_s, T_p, \gamma) = \frac{\alpha^* \cdot H_s^2 \cdot \omega^{-5}}{\omega_p^{-4}} \cdot exp\left[-\frac{5}{4} \cdot \left(\frac{\omega}{\omega_p}\right)^{-4}\right] \cdot \gamma^{exp\left[\frac{-(\omega-\omega_p)^2}{2\cdot\sigma^2\cdot\omega_p}\right]} \quad (4.1)$$

Where:

- $\alpha^* = \frac{0.0624\cdot(1.9+\gamma)}{0.23+0.0336\cdot\gamma-0.185}$ (4.2)
- H_S: significant wave height $[m]$
- ω_p: peak angular velocity $[rad/s]$
- $\gamma = 3.3$
- $\sigma = \begin{cases} 0.07, \omega < \omega_p \\ 0.09, \omega > \omega_p \end{cases}$ (4.3)

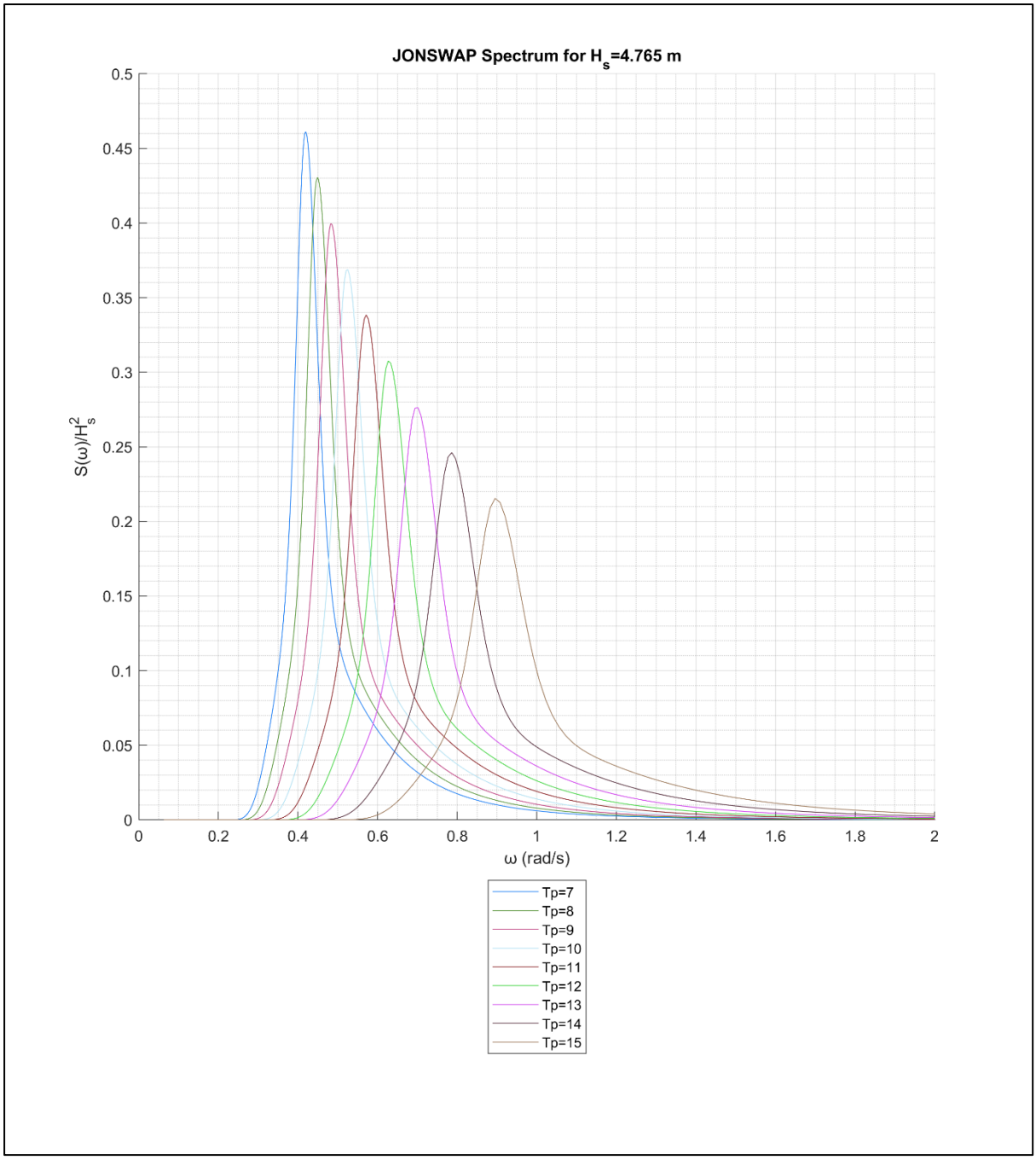

Figure 22: JOHNSWAP spectrum for Hs=4.765m

By utilizing the equation below, the resistance in irregular waves is calculated.

$$\bar{R}_{aw} = 2\int_0^{\infty} S(\omega) \cdot \frac{R_{aw}(\omega)}{\zeta_{\alpha}^2} \cdot d\omega \tag{4.4}$$

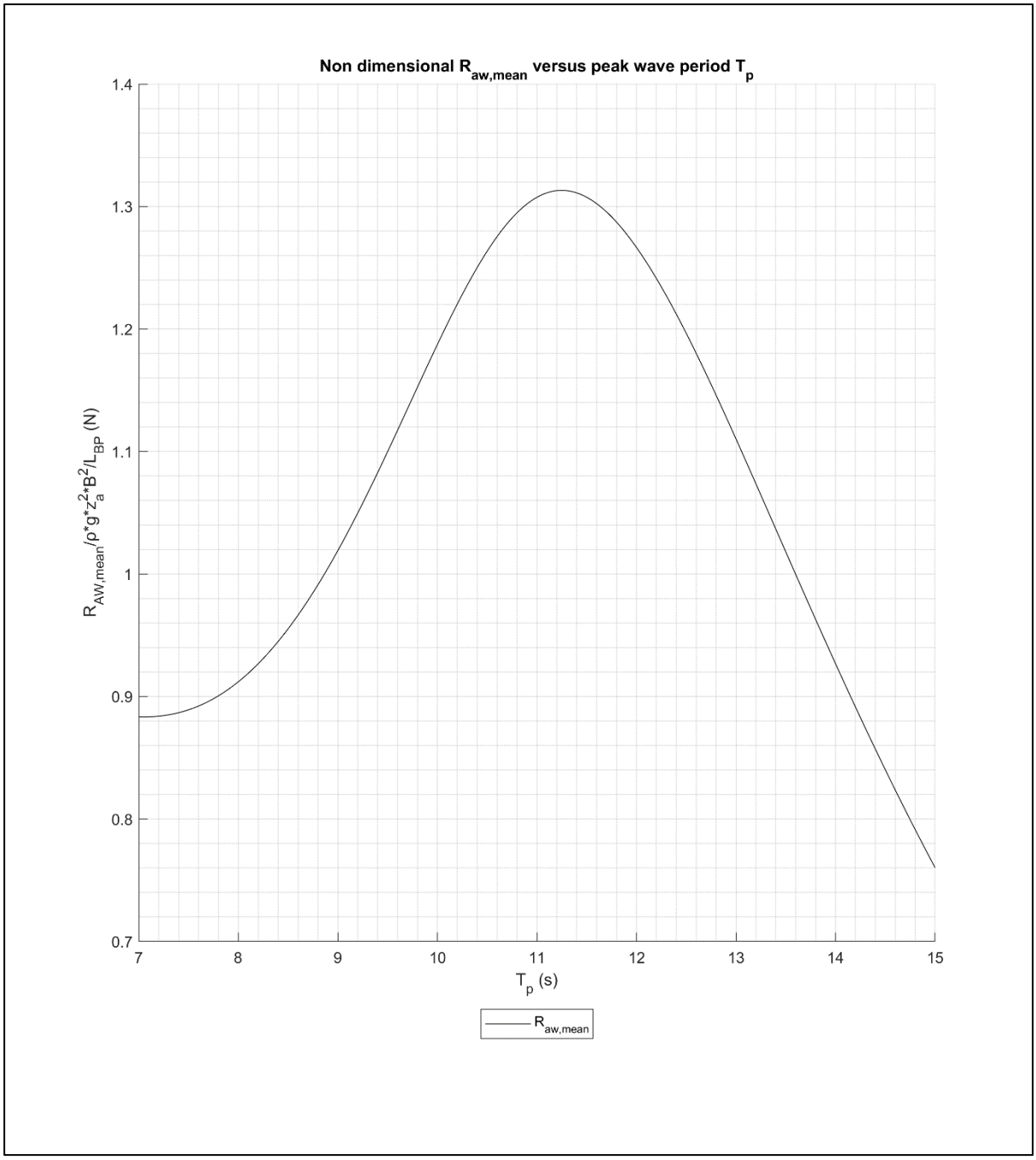

Figure 23: Non-dimensional $\bar{R}_{aw}$ versus peak wave period

The peak wave period that maximized $\bar{R}_{aw}$ is $\boldsymbol{T_p = 11.25s}$.

Table 14: Added wave resistance for head waves at scantling draft and ship speed of 4kn

$R_{aw,mean}$ [N]	345907

4.3.8 P-V-n curves

Utilizing the code mentioned in Speed/Power trial prediction curves, the P-V-n curves can be created for scantling draft with PSV and modified propeller. Below, the respective figures are depicted.

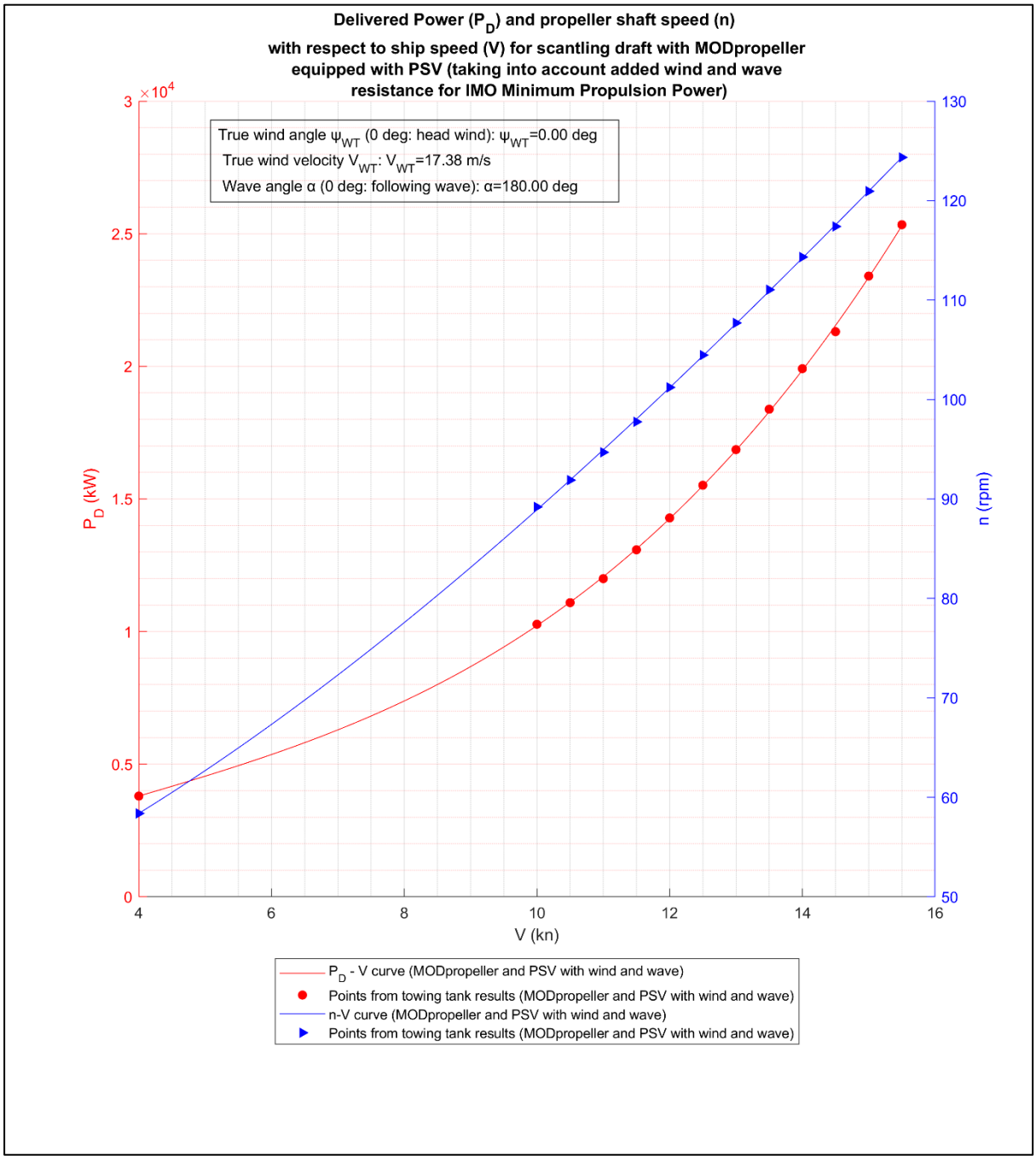

Figure 24: P-V-n curve for scantling draft with PSV (taking into account added wind and wave resistance) and modified propeller

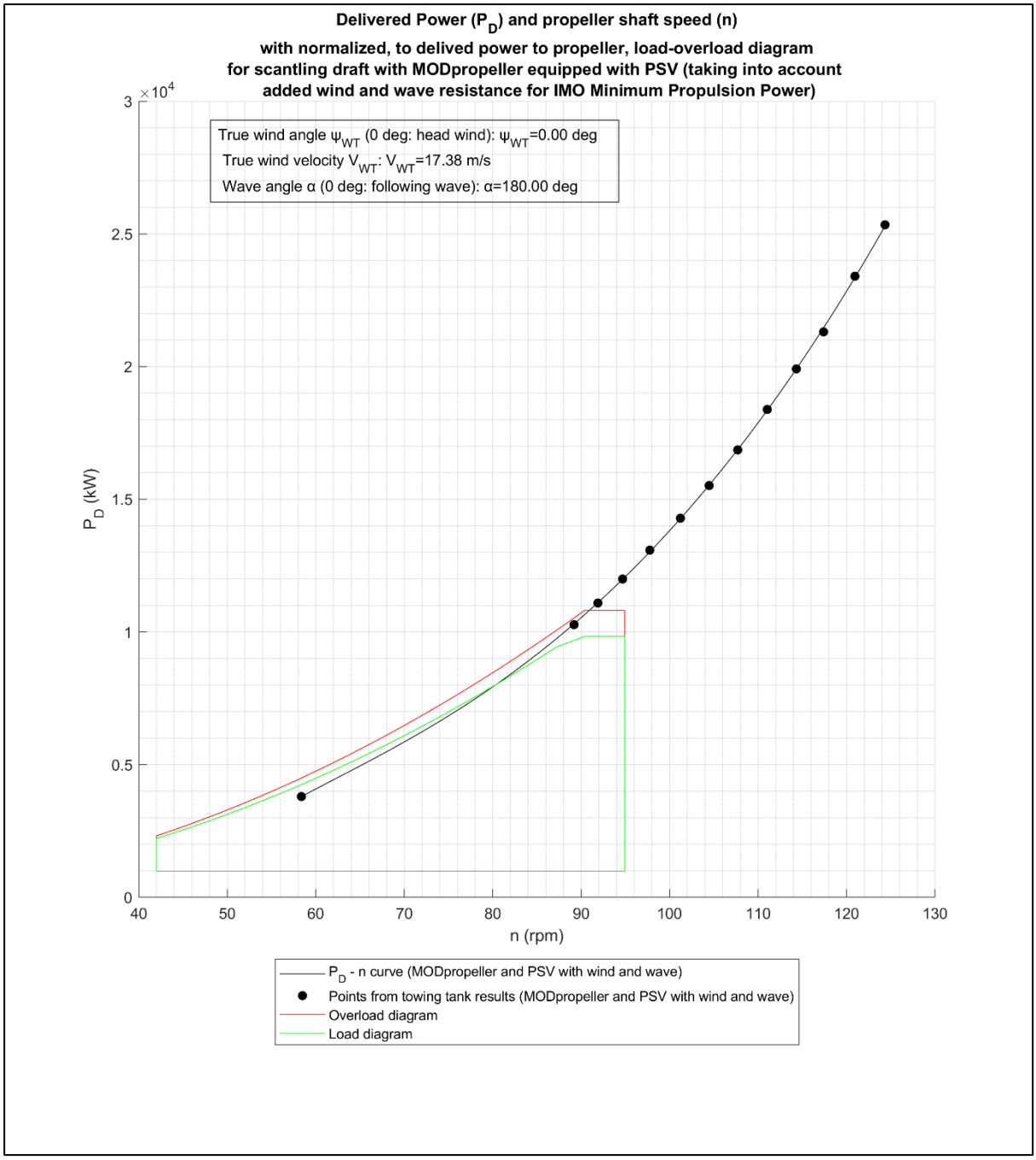

Figure 25: P-n curve for scantling draft with PSV (taking into account added wind and wave resistance) and modified propeller with load-overload diagram of engine (without MCR limitation)

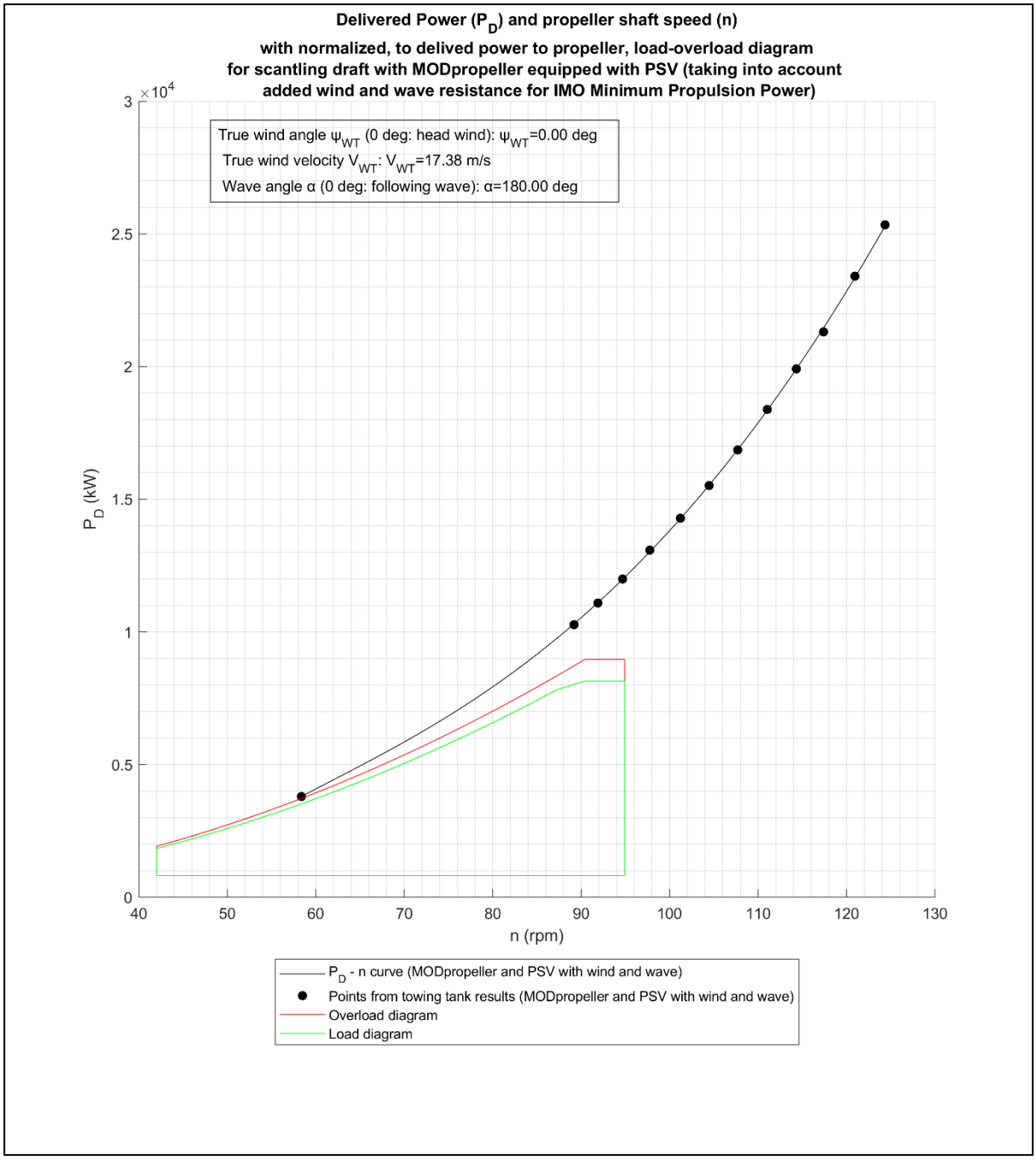

Figure 26: P-n curve for scantling draft with PSV (taking into account added wind and wave resistance) and modified propeller with load-overload diagram of engine (with MCR limitation)

It is calculated that for the ship to movie with 4kn under the influence of head wind and waves (adverse weather conditions) the required:

- Delivered power to propeller is $\boldsymbol{P_D = 3797.17\ kW}$
- Revolutions of propeller are $\boldsymbol{n = 58.38\ rpm}$

This point lies within the main engine load diagram when MCR limitation is not considered. But when MCR limitation is considered, the point lies above the engine overload limit which means that the ship cannot operate at this point without causing serious damage to the engine. It is concluded that the ship **does comply** with the IMO Minimum Power Propulsion Guideline, as expressed through the assessment level 2, without Maximum Continuous Rating limitation

which has been applied to the main engine for reducing the EEDI value of the ship. But for the case of MCR limitation the ship **does not comply** with the IMO Minimum Power Propulsion Guideline.

4.4 Seagoing scenarios with added wind, wave resistance, wind assisted ship propulsion (Flettner Rotor and eSAIL) and side forces

In this section, actual seagoing scenarios are examined. For that reason, the added wind, wave resistances, the thrust of Flettner Rotor and eSAIL are considered along with the side forces produced by these systems. Moreover, the vessel is to be equipped with four Flettner Rotor and four eSAIL systems. For each scenario, the six models mentioned in Seagoing scenarios with added wind, wave resistance, wind assisted ship propulsion (Flettner Rotor and eSAIL) and side forces are considered:

- Model 1
- Model 2
- Model 3
- Model 1 modified
- Model 2 modified
- Model 3 modified

4.4.1 Added wind resistance

The theoretical framework for the added wind resistance is the same as in Added wind resistance $\boldsymbol{R_{air}}$. The parameters used are the same as in Added wind resistance $\boldsymbol{R_{air}}$.

4.4.2 Added wave resistance

The theoretical framework for the added wave resistance is the same as in Added wave resistance $\boldsymbol{R_{aw}}$ or $\boldsymbol{\overline{R}_{aw}}$ but with some minor changes that are obvious in the below text. The parameters used are the same as in Added wave resistance $\boldsymbol{R_{aw}}$ or $\boldsymbol{\overline{R}_{aw}}$.

In the real sea environment, the significant wave height h_s is dependent on the wind speed. For this study, not fully developed severe sea states are considered. Therefore the following relationship is utilized [35, Eq. 11]:

$$h_s = 0.115 \cdot V_{WT}^{1.41} \tag{4.5}$$

Where:

- h_s: significant wave height in $[m]$
- V_{WT}: true wind speed in $[m/s]$

For the calculation of added wave resistance in irregular waves $\bar{R}_{aw}$, for each different speed, the following procedure is executed:

- Calculate the significant wave height h_s based on true wind speed V_{WT}
- Calculate the added wave resistance $\bar{R}_{aw}$ for each different wave peak period T_p (T_p between 7 and 15 s) using the JOHNSWAP spectrum [24, Tbl. 2]
- For the specific speed the added wave resistance $\bar{R}_{aw}$ is the mean value of the added wave resistances $\bar{R}_{aw}$ for peak period T_p between 7 and 15 s.

4.4.3 Position of Flettner Rotor and eSAIL on ship deck

The number of Flettner Rotors and eSAILs to be installed, in each case, was chosen to be 4. The position of those, on ship main deck, is depicted in the drawing below.

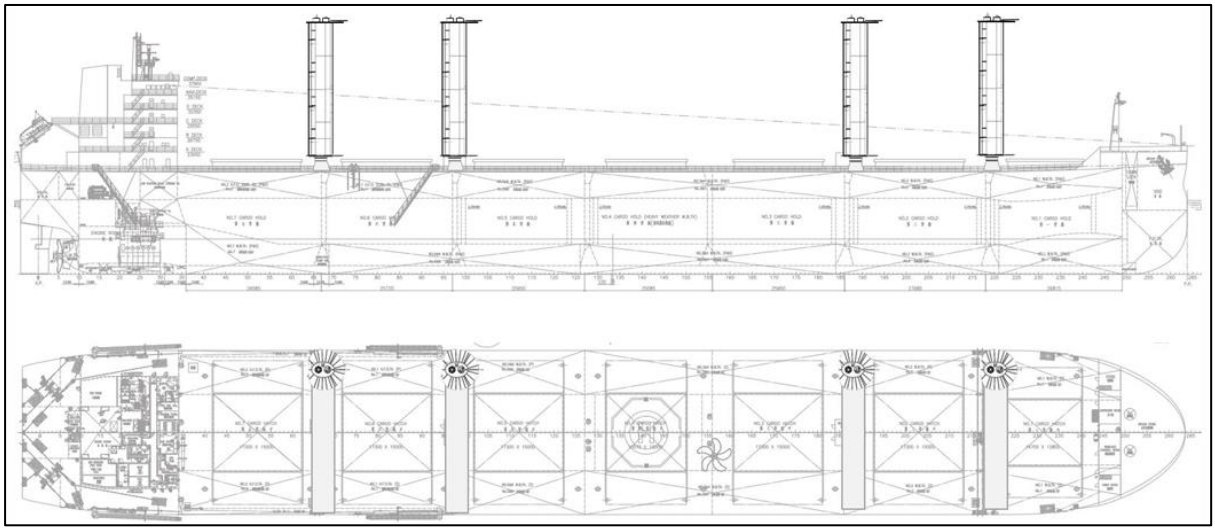

Figure 27: Position of eSAILs and Flettner Rotor, in each case, on ship main deck

4.4.4 Rotor Sail - Flettner Rotor

The Flettner Rotor Sail used in this study is one with endplate and dimensions of $h = 20\ m$ and $R_{fr} = 1.2\ m$ [15, p. 4].

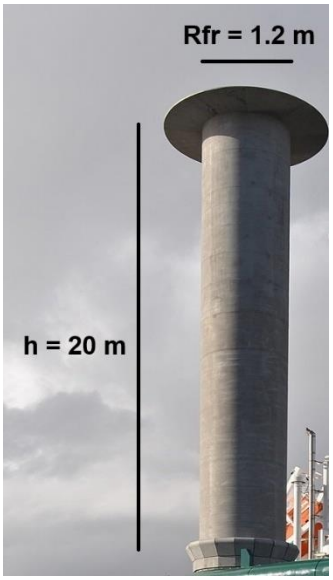

Figure 28: Flettner Rotor sail with end plate and dimensions (original picture from [6])

4.4.4.1 Lift and Drag Coefficients (C_L, C_D)

Coefficients of lift C_L and drag C_D used to calculate the lift and drag forces, of Flettner Rotors with endplates, correspondingly are exported from Seifert's article [36].

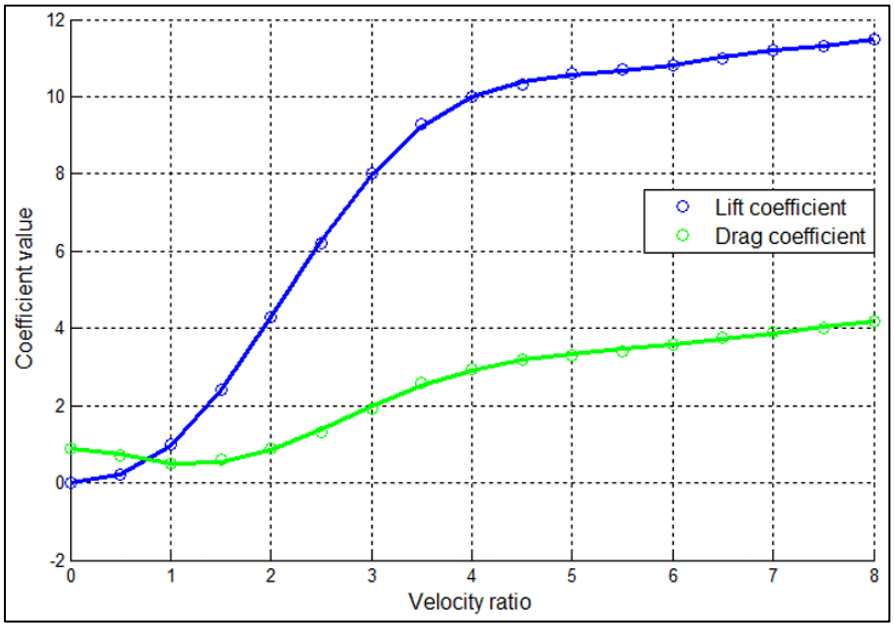

Figure 29: Lift and Drag Coefficients with respect to Velocity ratio

Something worth noting is that both coefficients are functions of the velocity ratio.

4.4.4.2 Selection of Flettner Rotor revolutions per minute (RPM)

One crucial parameter that must be defined for the Flettner Rotor system is the revolutions per minute (RPM). This parameter is crucial to determine the lift and drag forces as well as the consumed power of the system. A usual range for the system is between 0 and 1000 RPM [15, Fig. 7]. Due to the size of the ship under study along with the size of the rotor system, speeds above 400 RPM were deemed excessive and therefore not included. To determine the appropriate RPM for each different wind speed and angle pair, the following procedure was followed. The calculation of net power output was conducted for speeds between 0 and 400 RPM and the speed which corresponds to the greatest net power output was chosen. Of course, all the above are true when the net power output is positive. In different case, the system remains inactive, and resistance is increased due to the presence of the system's surface in free incoming wind as described in Fundamental Equations. A typical diagram of net power output for different true wind angles along with rotor speed as parameter and specific true wind and ship speed is given below.

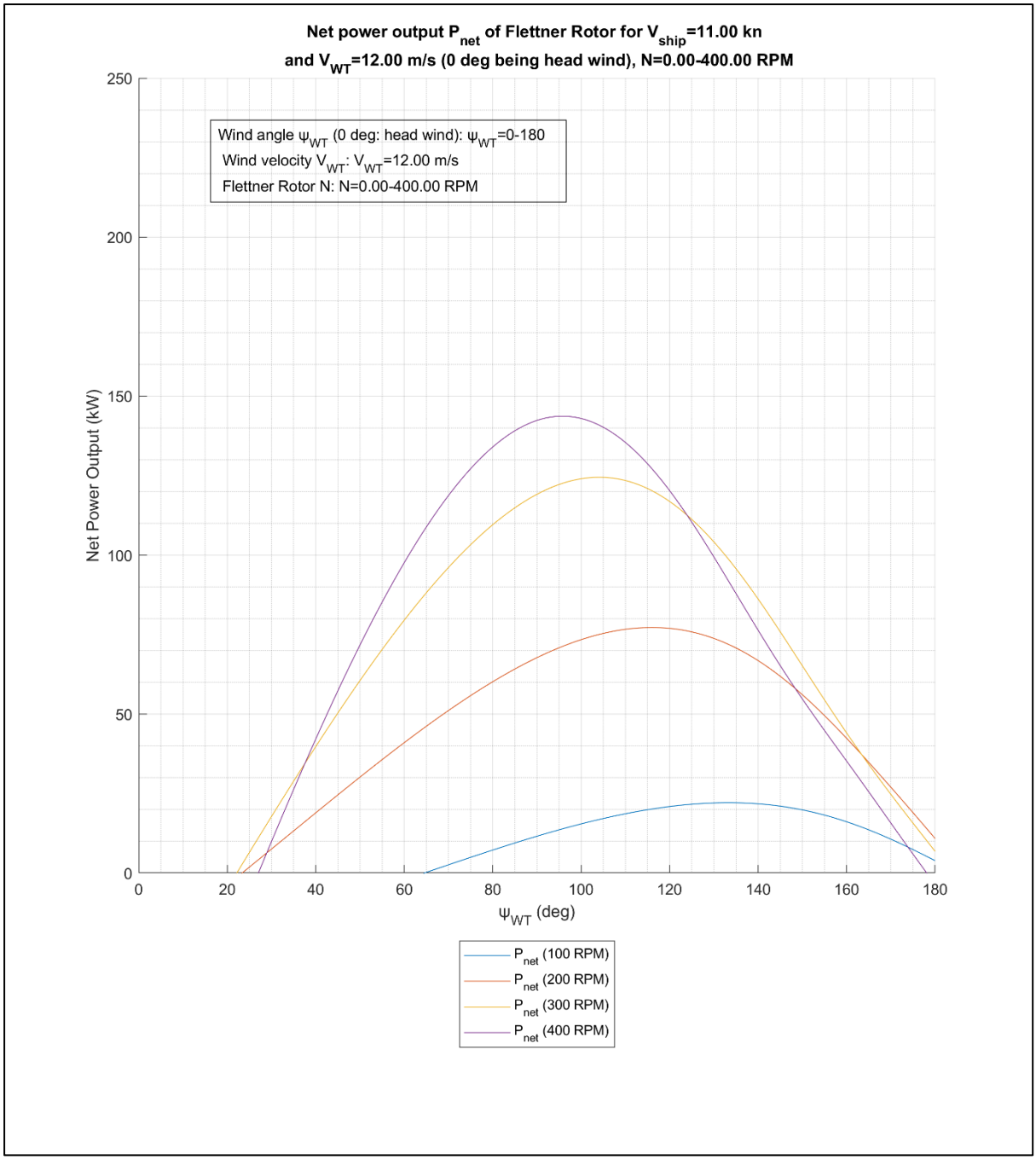

Figure 30: Net power output P_{net} of Flettner Rotor for $V_{ship} = 11\ kn$ and $V_{WT} = 12\ m/s$ (0 deg being head wind), $N = 0 - 400\ RPM$

4.4.4.3 Lift, Drag, Horizontal and Perpendicular Flettner Rotor effective forces for typical scenario

Below the resultants lift, drag, horizontal F_x and perpendicular F_y effective forces of a single Flettner Rotor are demonstrated for ship speed $V_{ship} = 11\ kn$, true wind speed $V_{WT} = 10\&12\ m/s$ and revolutions per minute between $0 - 400$ according to above paragraph.

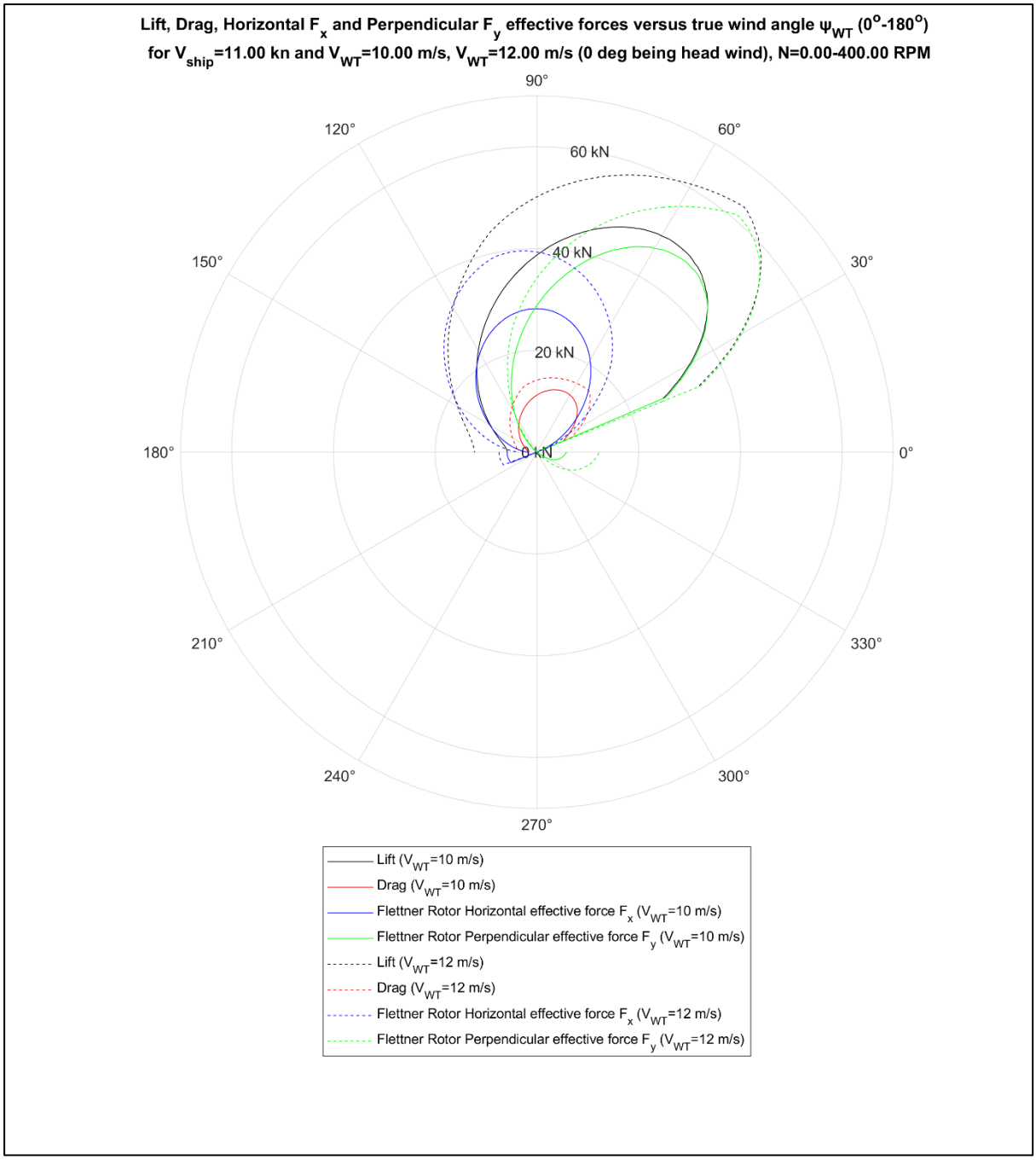

Figure 31: Lift, Drag, Horizontal and Perpendicular effective forces for $V_{ship} = 11\ kn$ and $V_{WT} = 10\ m/s$, $V_{WT} = 12\ m/s$ (0 deg being head wind), $N = 0 - 400\ RPM$

4.4.5 Suction Sail – eSAIL

According to bound4blue [7] there are 3 different eSAIL models. These are eSAIL model 1, 2, and 3. According to their page and after contacting the company, the use of model 2 was suggested for the ship under study.

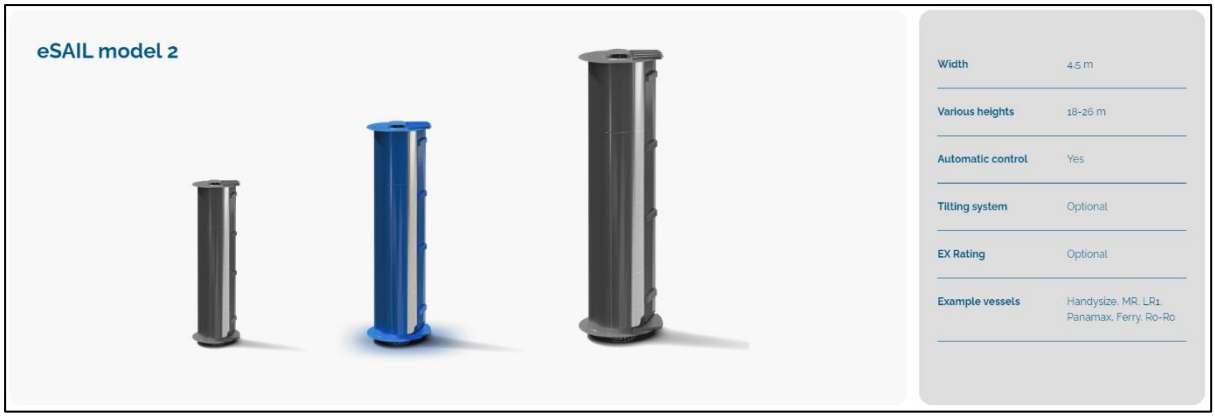

Figure 32: eSAIL model 2 [7]

Since there are no available analytical expressions for eSAIL calculations, measurements from test were provided by the company. In particular, an EXCEL sheet was provided, in which the horizontal D_F and perpendicular H_F effective forces (horizontal and perpendicular being the parallel to x and y axis forces respectively, see Figure 12) along with the consumed power P_{cons} were available for a specific apparent wind speed V_a and apparent wind direction β. The consumed power P_{cons} is the required power for controlling the eSAIL (for example, rotating) and powering the air suction system. When no thrust can be produced by the system (D_F is negative), due to not favourable wind speed and angle, power is not fed and therefore it remains shut off. When powered off, the system creates additional resistance due to its presence in moving wind. This added resistance is considered in the calculations through the addition of the horizontal effective force in the total resistance of the ship.

4.4.5.1 Horizontal and perpendicular effective eSAIL forces for typical scenario

Below the resultants horizontal D_F and perpendicular H_F effective forces of a single eSAIL are demonstrated for ship speed $V_{ship} = 11\ kn$, true wind speed $V_{WT} = 10\&12\ m/s$ and revolutions per minute between $0 - 400$ according to above paragraph.

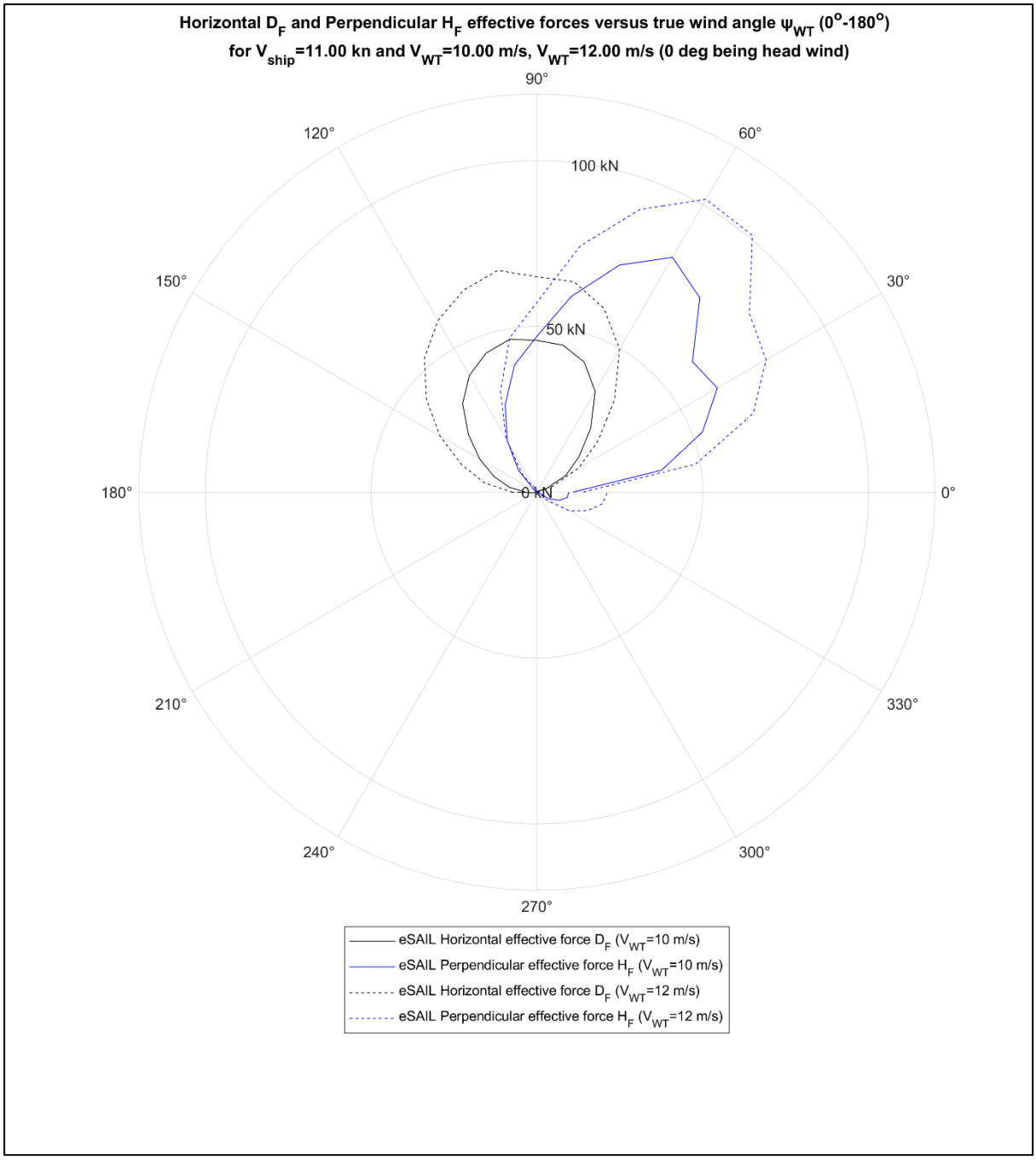

Figure 33: Horizontal D_F and Perpendicular H_F effective forces for $V_{ship} = 11\ kn$ and $V_{WT} = 10\ m/s$, $V_{WT} = 12\ m/s$ (0 deg being head wind)

4.4.6 Side Forces

The parameters used for the calculation of side forces are presented below.

Table 15: Parameters for calculation of side forces

A_L [m^2]	1749
c_N [-]	1.25

x_A [m]	-12.53
x_S [m]	-4.75
c_Y [-]	1.25
L_{WL} [m]	229
x_R [m]	112.75
x_3 [m]	9.639

Using a range of heeling force F_K between -160kN and 160kN, the following diagrams are produced.

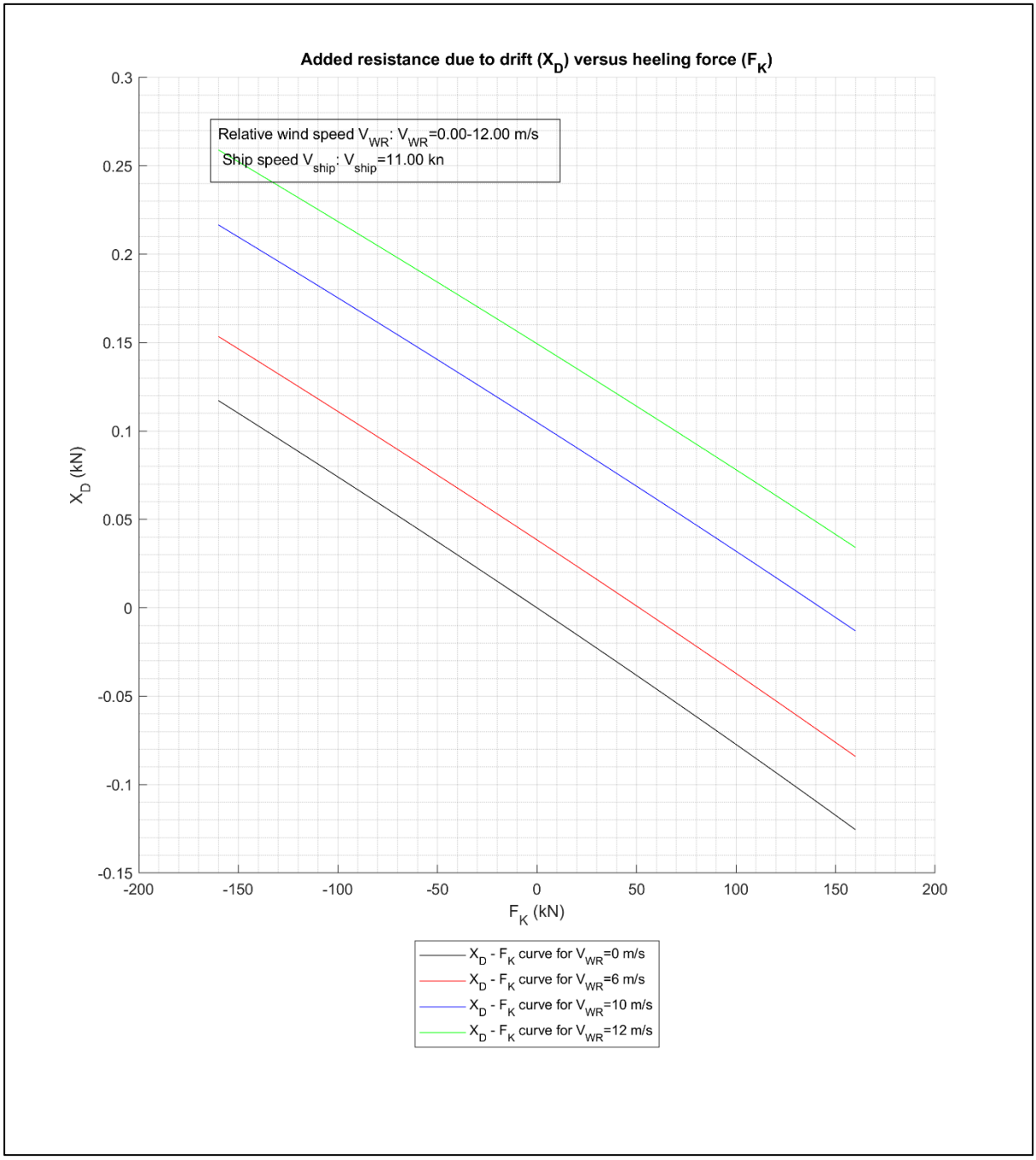

Figure 34: Added resistance due to drift (X_D) versus heeling force (F_K)

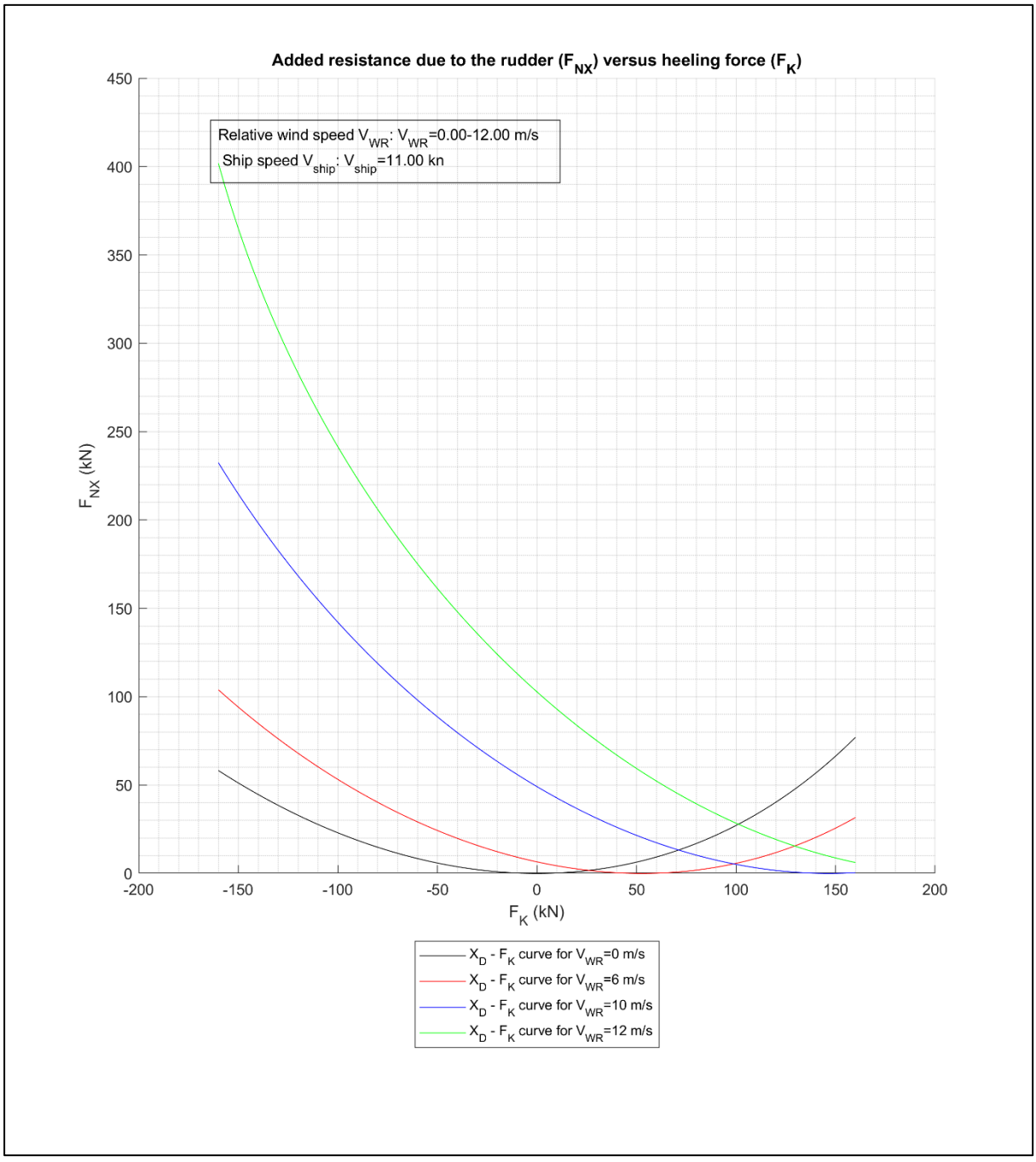

Figure 35: Added resistance due to the rudder (F_{NX}) versus heeling force (F_K)

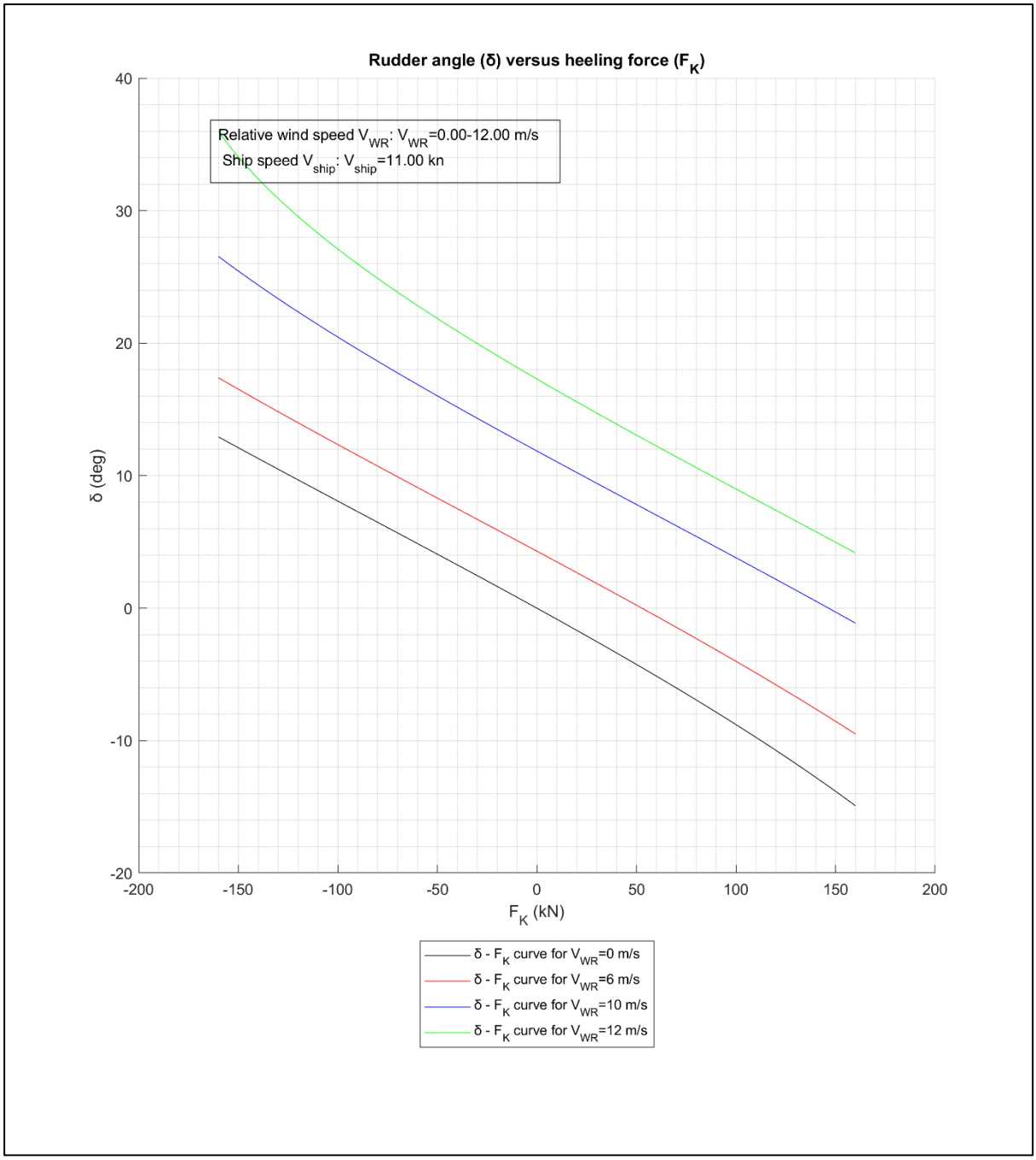

Figure 36: Rudder angle (δ) versus heeling force (F_K)

Additional diagrams can be found at Appendix C: Side forces.

4.4.7 Fuel Oil Consumption Calculation

The specific fuel oil consumption curve of the main engine was acquired from the main engine ‘s shop test results document [37]. Relative information is found below

Table 16: Specific Fuel Oil Consumption versus engine load

Engine Load (%)	SFOC (g/kWh)

25	175.85
35	172.75
50	167.68
71.6	165.96
75	167.65
100	172.6
110	174.94

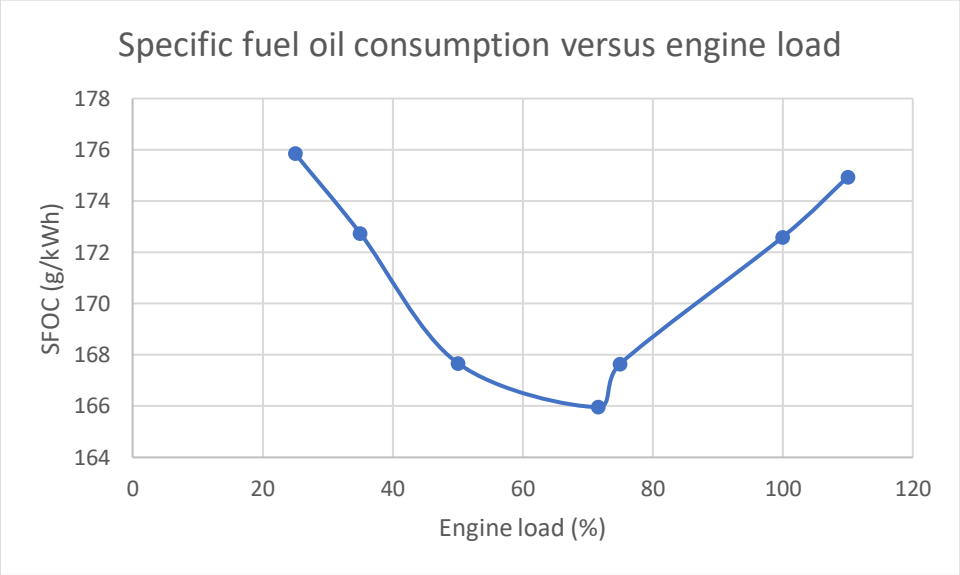

Figure 37: Curve of specific fuel oil consumption versus engine load

4.4.8 Results

The results for the different models mentioned in Different models examined in thesis are presented below. For the first scenario, delivered power, propeller speed curves along with the engine load diagram, forces analysis and fuel oil consumption for different vessel speeds, constant wind/wave angles. For the second scenario, delivered power, forces analysis and fuel oil consumption for constant vessel speed and different wind/wave angles are presented. Both scenarios have constant true wind velocity. In that way, the first scenario covers different vessel speeds but with constant wind/wave angles while the second scenario covers constant speeds with different wind/wave angles.

4.4.8.1 First scenario (different vessel speeds, constant wind/wave angles)

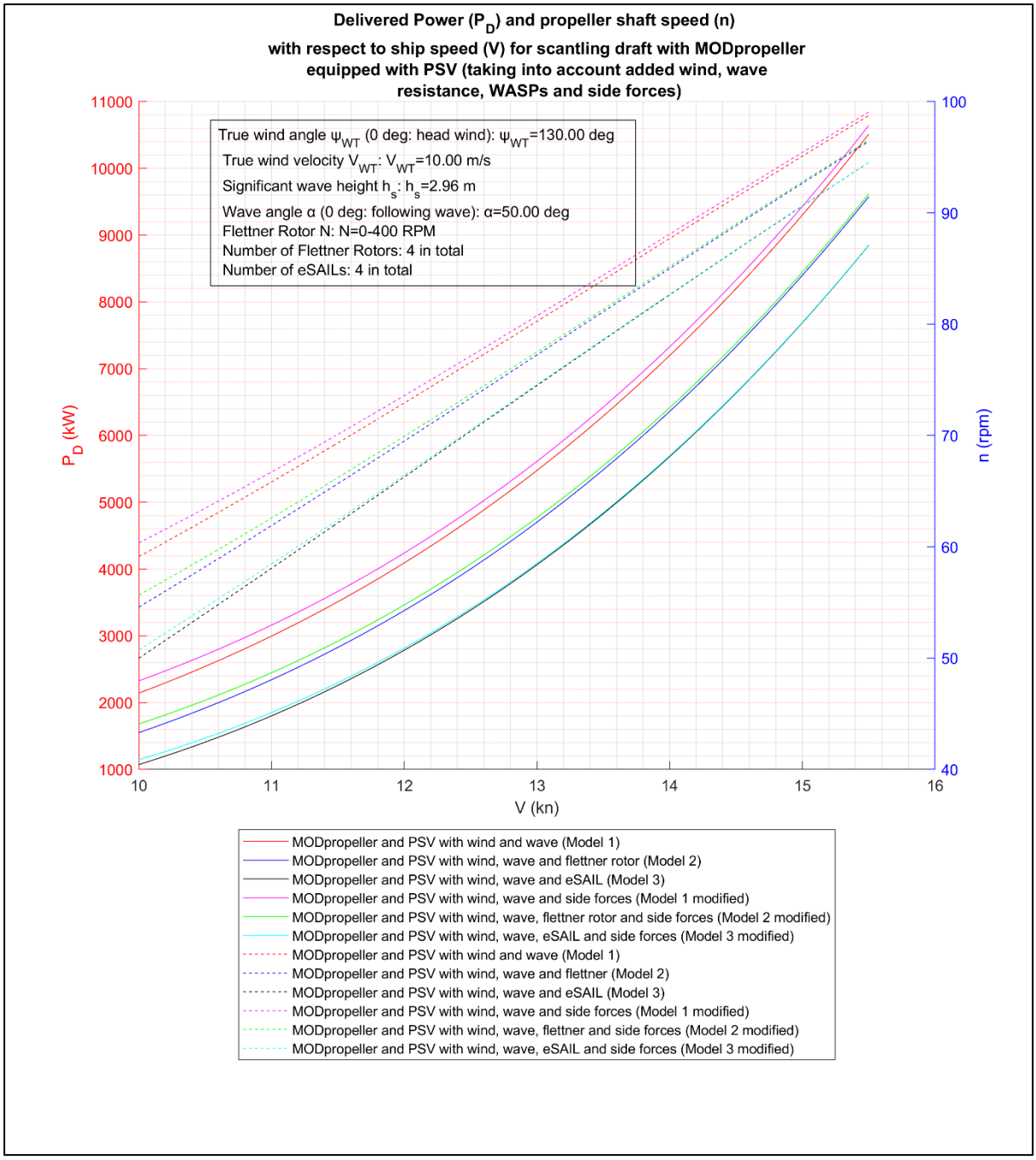

Figure 38: Delivered Power (P_D) and propeller shaft speed (n) with respect to ship speed (V) for scantling draft with MODpropeller equipped with PSV (taking into account added win, wave resistance, WASPs and side forces)

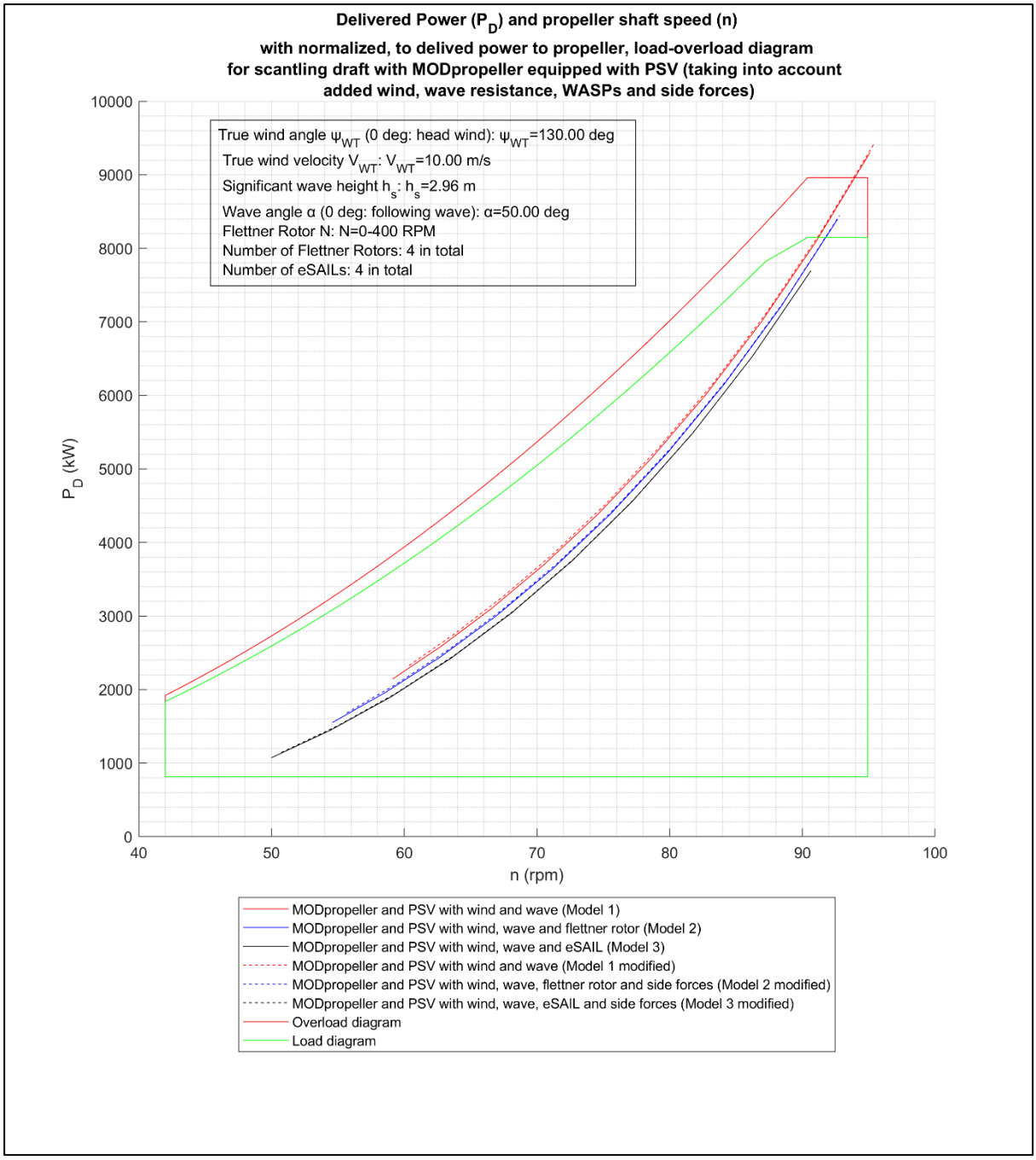

Figure 39: Delivered Power (P_D) and propeller shaft speed (n) with normalized, to delivered power to propeller, load-overload diagram for scantling draft with MODpropeller equipped with PSV (taking into account added wind, wave resistance, WASPs and side forces)

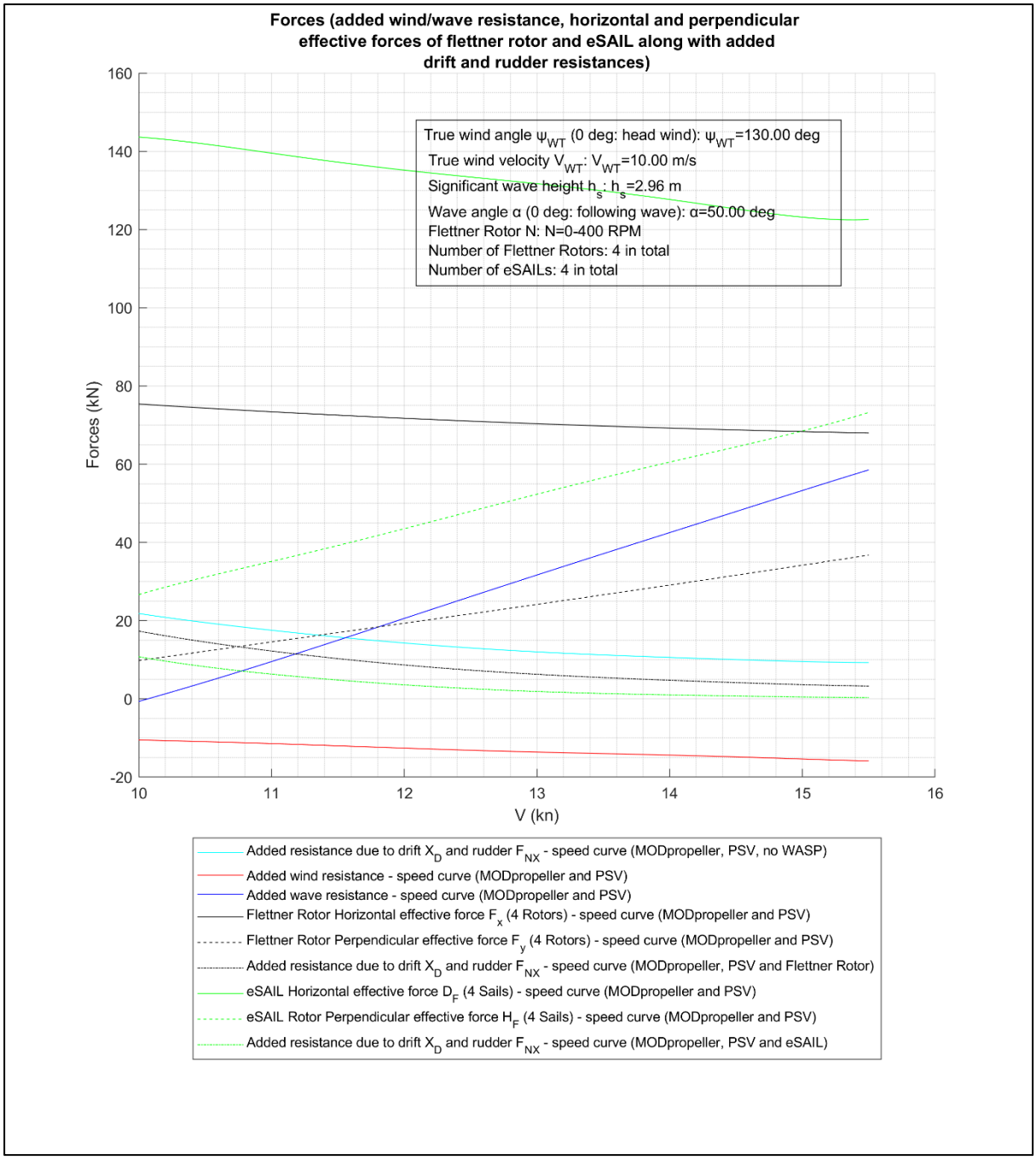

Figure 40: Forces (added wind/wave resistance, horizontal and perpendicular effective forces of flettner rotor and eSAIL along with added dirft and rudder resistances)

For facilitation of reading, a table with the values of forces is provided. The numbers ([1],[2] etc.) are the corresponding numbers of forces when reading the Figure 40 legend from top to bottom.

Table 17: Values of forces for different vessel speeds

V (kn)	[1]	[2]	[3]	[4]	[5]	[6]	[7]	[8]	[9]
10	21.82	-10.49	-0.65	75.41	9.81	17.33	143.63	26.66	10.79
11	17.55	-11.43	9.53	73.4	14.56	12.24	139.53	35.14	6.33
12	14.29	-12.59	20.57	71.74	19.34	8.67	135.19	43.5	3.59
13	12.02	-13.6	31.67	70.35	24.16	6.28	131.73	52.33	1.89

14	10.6	-14.38	42.51	69.23	29.1	4.76	127.69	60.53	1.02
15	9.55	-15.37	53.27	68.34	34.17	3.64	123.16	68.34	0.49

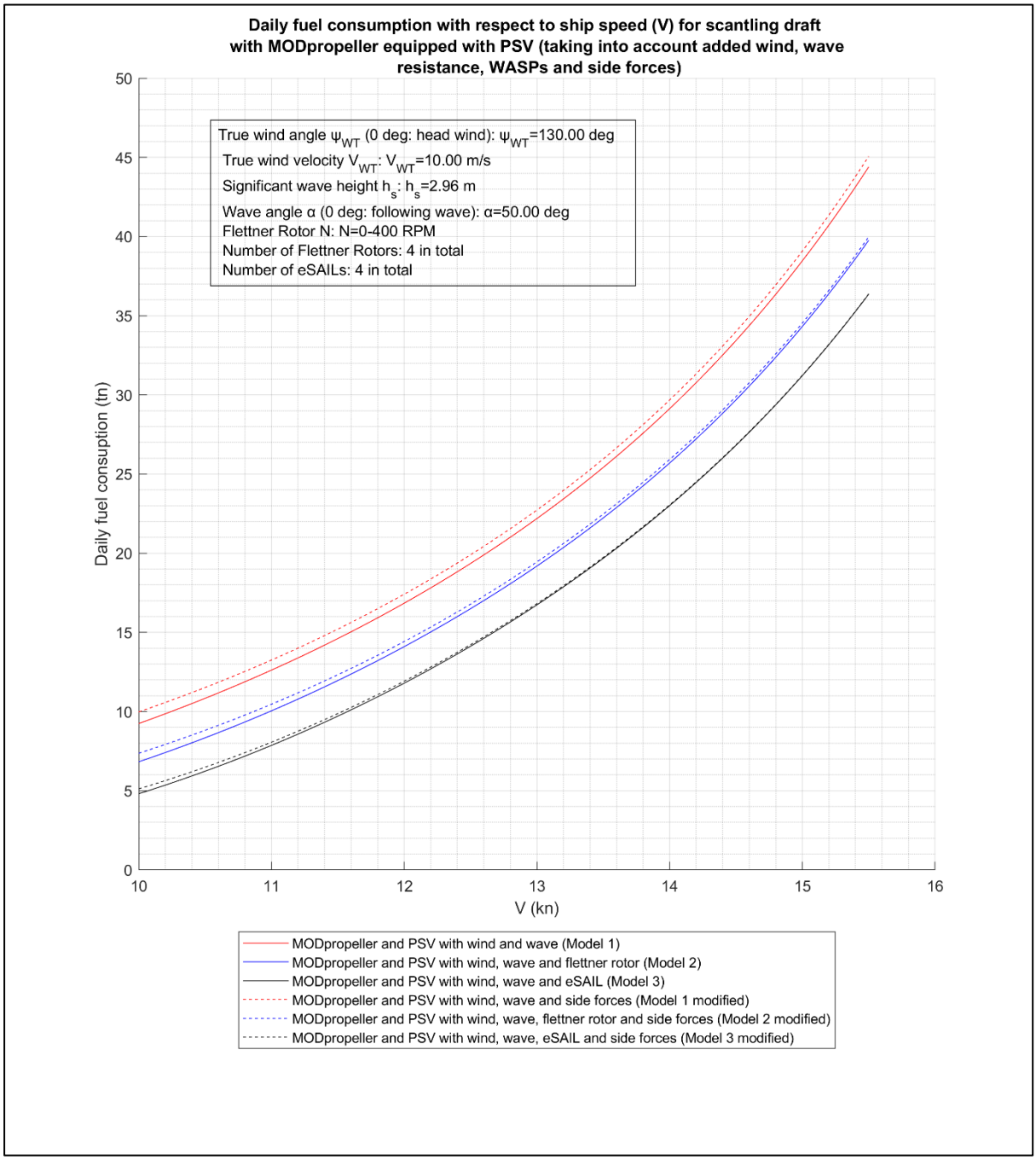

Figure 41: Daily fuel consumption with respect to ship speed (V) for scantling draft with MODpropeller equipped with PSV (taking into account added wind, wave resistance, WASPs and side forces

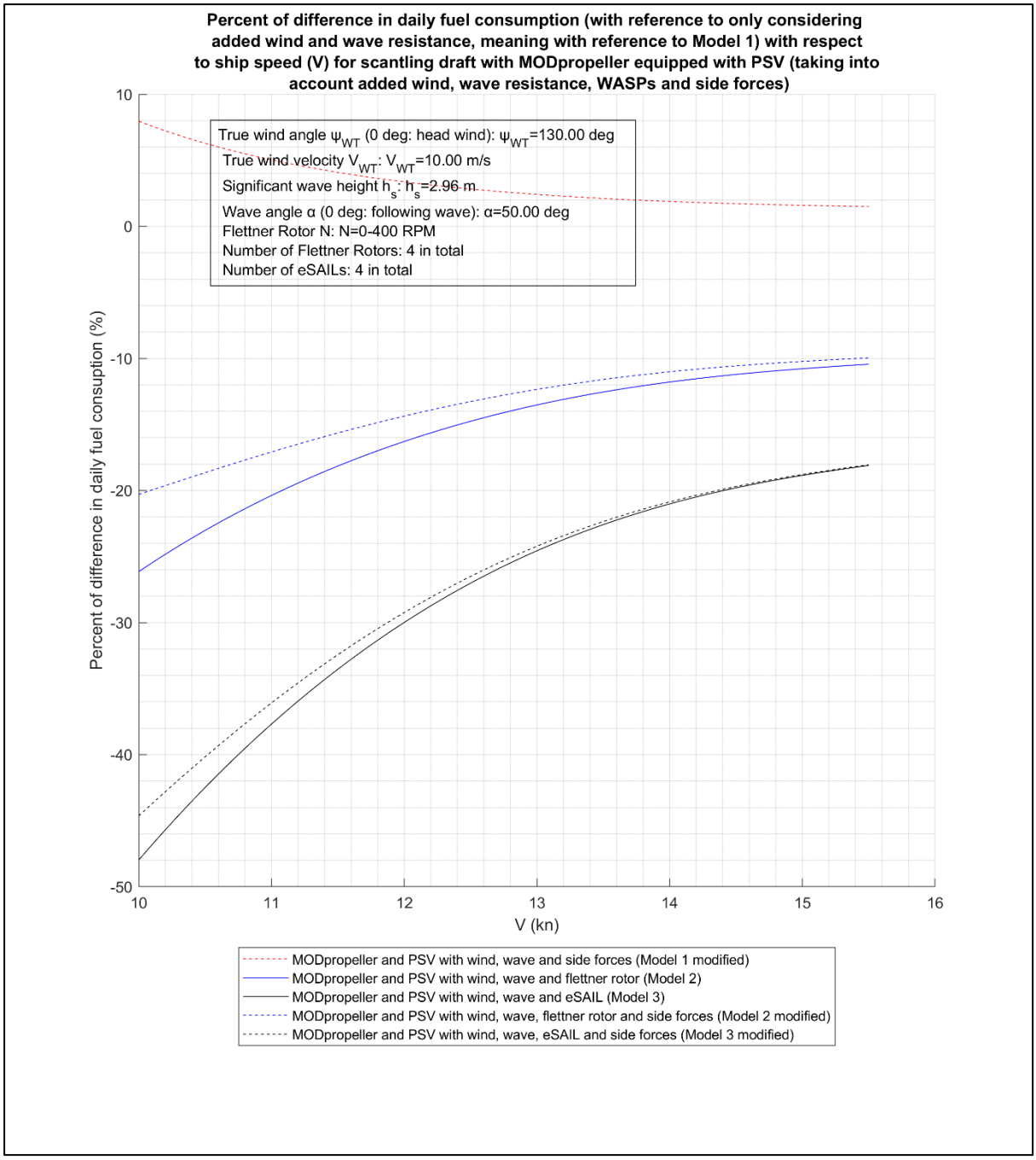

Figure 42: Percent of difference in daily fuel consumption (with reference to only considering added wind and wave resistance, meaning with reference to Model 1) with respect to ship speed (V) for scantling draft with MODpropeller equipped with PSV (taking into account added wind, wave resistance, WASPs and side forces)

4.4.8.2 Second scenario (constant vessel speed, different wind/wave angles)

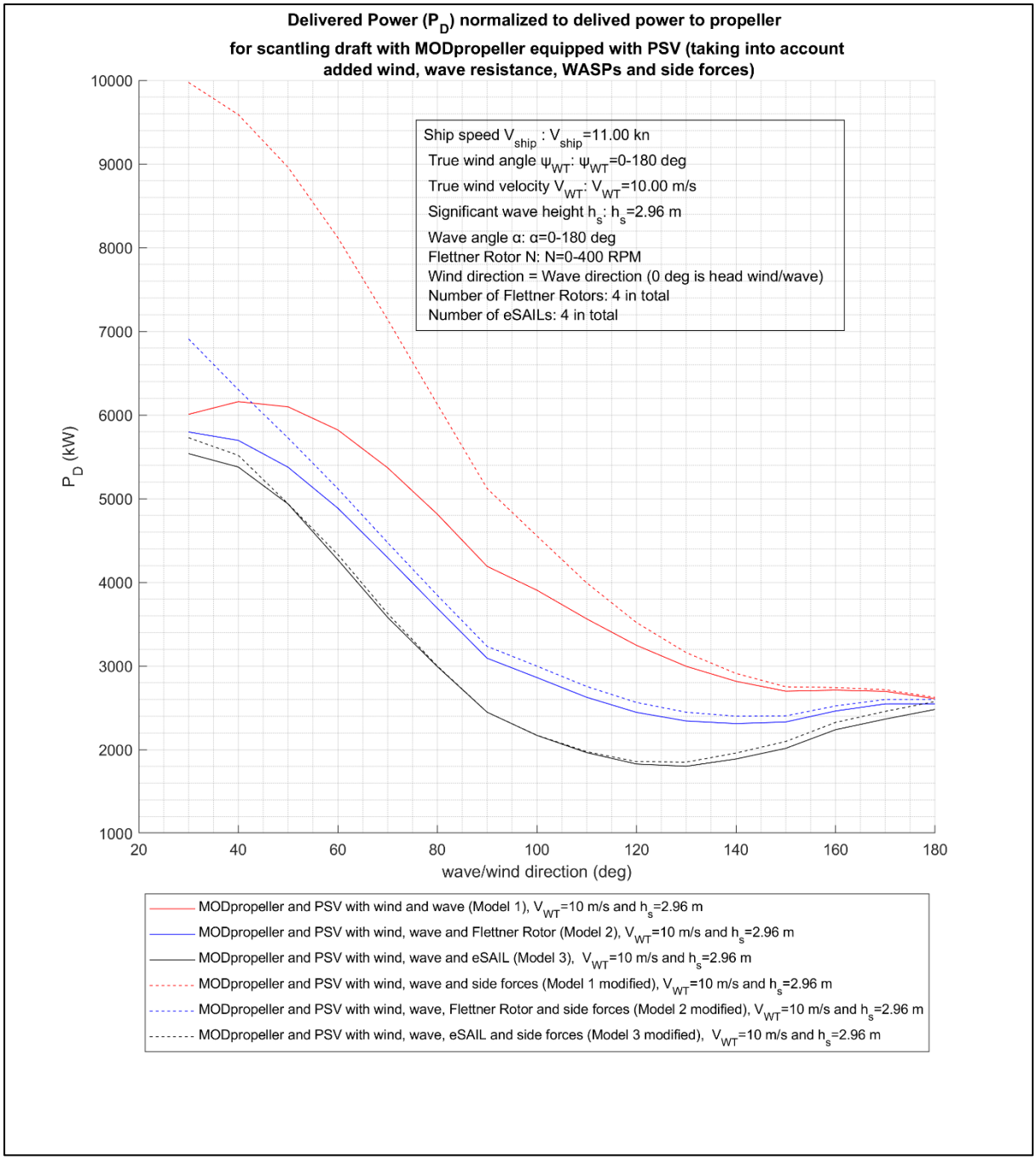

Figure 43: Delivered Power (P_D) normalized to delivered power to propeller for scantling draft with MODpropeller equipped with PSV (taking into account added wind, wave resistance, WASPs and side forces)

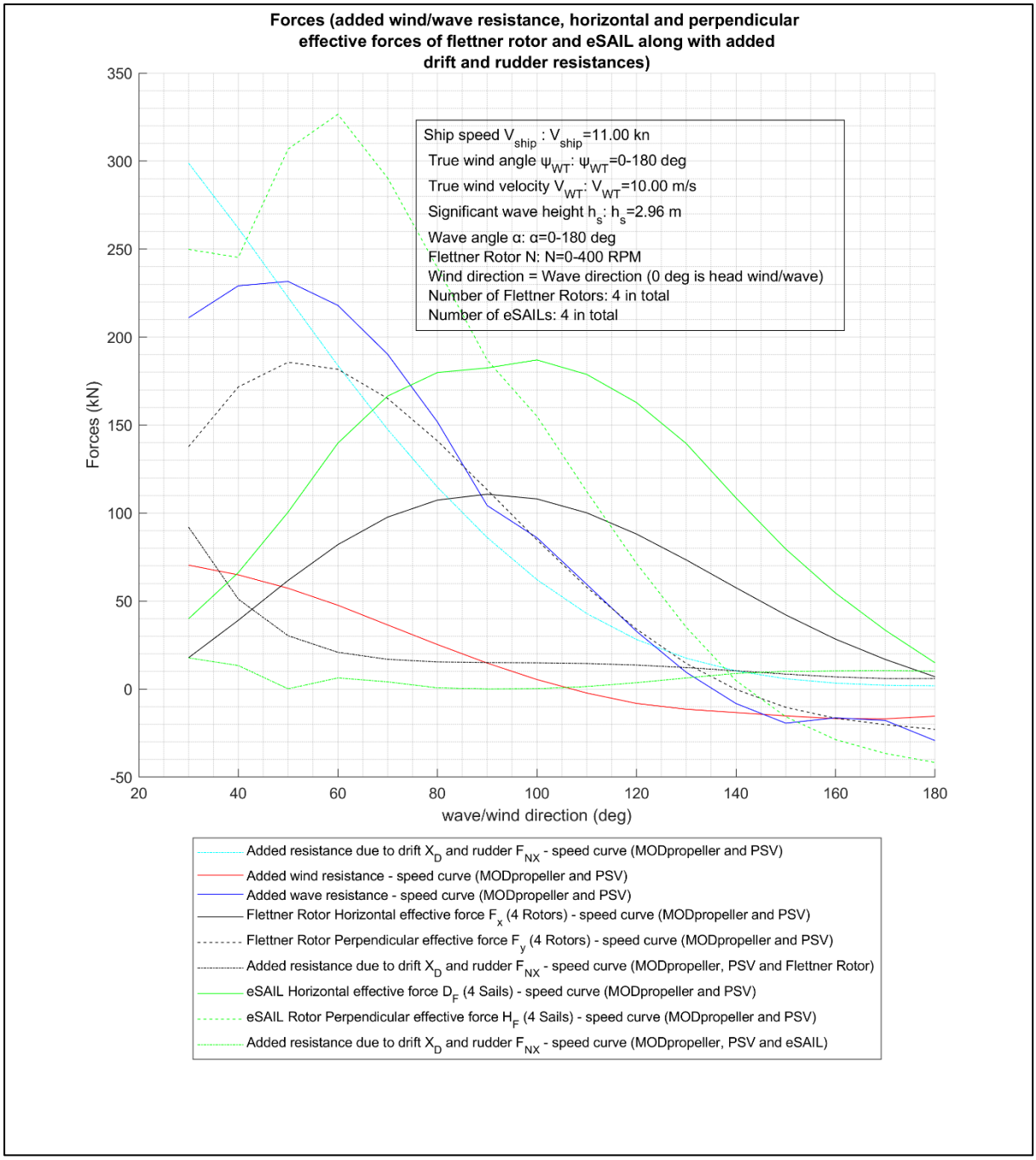

Figure 44: Forces (added wind/wave resistance, horizontal and perpendicular effective forces of flettner rotor and eSAIL along with added drift and rudder resistances)

For facilitation of reading, a table with the values of forces is provided. The numbers ([1],[2] etc.) are the corresponding numbers of forces when reading the Figure 44 legend from top to bottom.

Table 18: Values of forces for different wind/wave angles

wave/wind direction (kn)	[1]	[2]	[3]	[4]	[5]	[6]	[7]	[8]	[9]
30	298.86	70.42	210.95	17.83	137.74	92.04	39.98	249.83	17.75
40	261.8	64.91	229.16	39.12	171.69	51.1	66.21	245.26	13.39
50	222.52	57.3	231.6	61.74	185.72	30.33	100.56	306.85	0.16

60	183.85	47.66	218.02	82.08	181.72	20.92	139.73	326.58	6.37
70	147.53	36.46	190.26	97.72	165.14	16.92	166.48	290.4	4.12
80	114.72	25.33	151.84	107.39	141.03	15.45	179.86	239.41	0.72
90	86.14	14.79	104.31	110.74	113.24	15.06	182.48	187	0.09
100	62.19	5.43	86.03	108.05	84.76	14.93	187.02	155.02	0.22
110	42.94	-2.24	59.53	100.16	57.88	14.54	178.81	112.3	1.45
120	28.2	-8.14	32.86	88.12	34.09	13.67	162.83	71.51	3.64
130	17.55	-11.43	9.53	73.4	14.56	12.24	139.53	35.14	6.33
140	10.35	-13.33	-8.19	57.61	-0.2	10.41	108.61	4.84	8.92
150	5.89	-15.21	-19.36	42.16	-10.34	8.52	79.57	-15.68	10.08
160	3.38	-16.77	-16.33	28.39	-16.57	6.93	54.58	-28.7	10.33
170	2.18	-16.91	-17.82	16.86	-20.23	6	33.45	-36.55	10.44
180	1.84	-15.37	-29.26	7	-22.85	6.03	14.93	-41.69	10.24

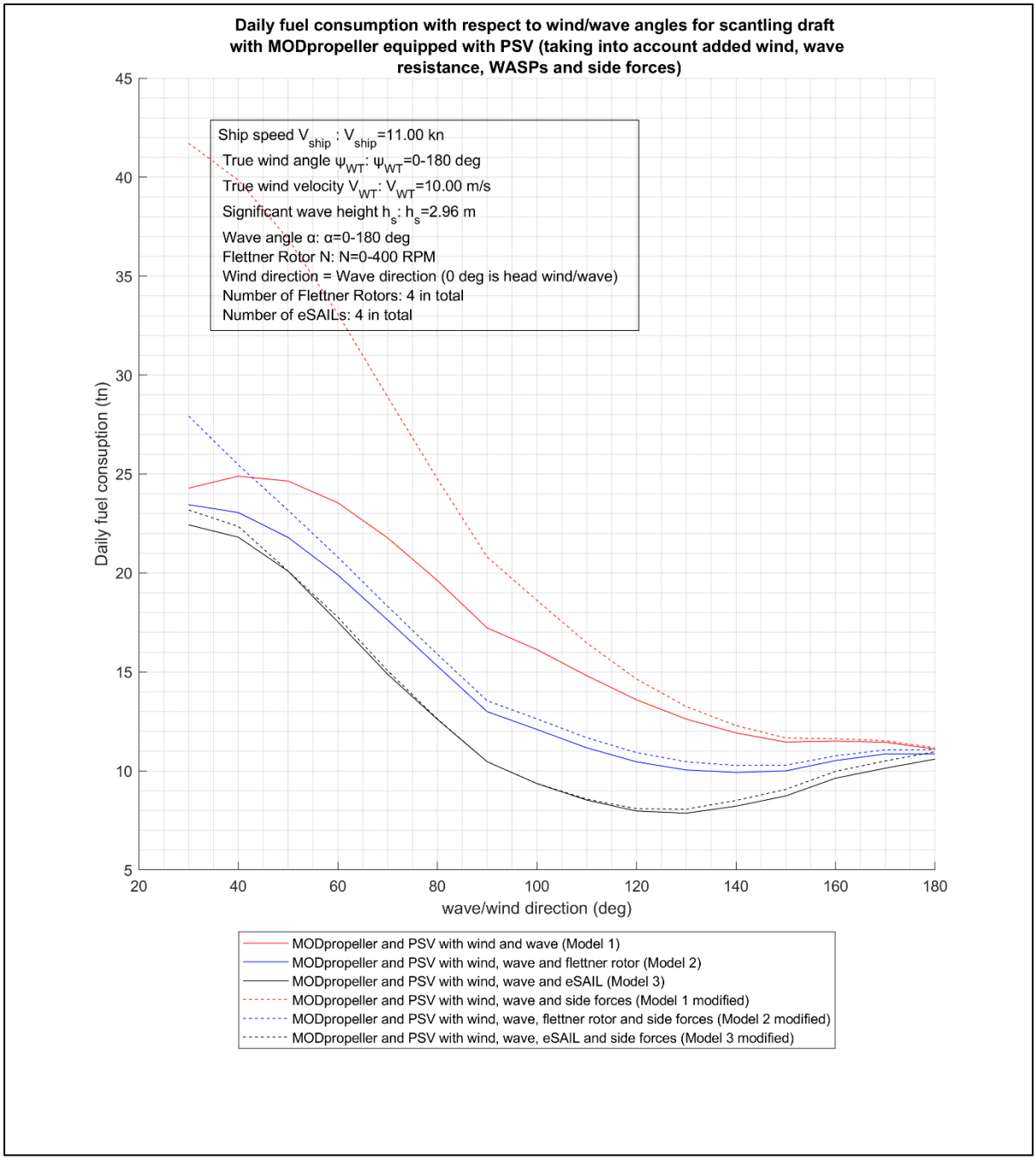

Figure 45: Daily fuel consumption with respect to different wind/wave angles for scantling draft with MODpropeller equipped with PSV (taking into account added wind, wave, resistance, WASPs and side forces)

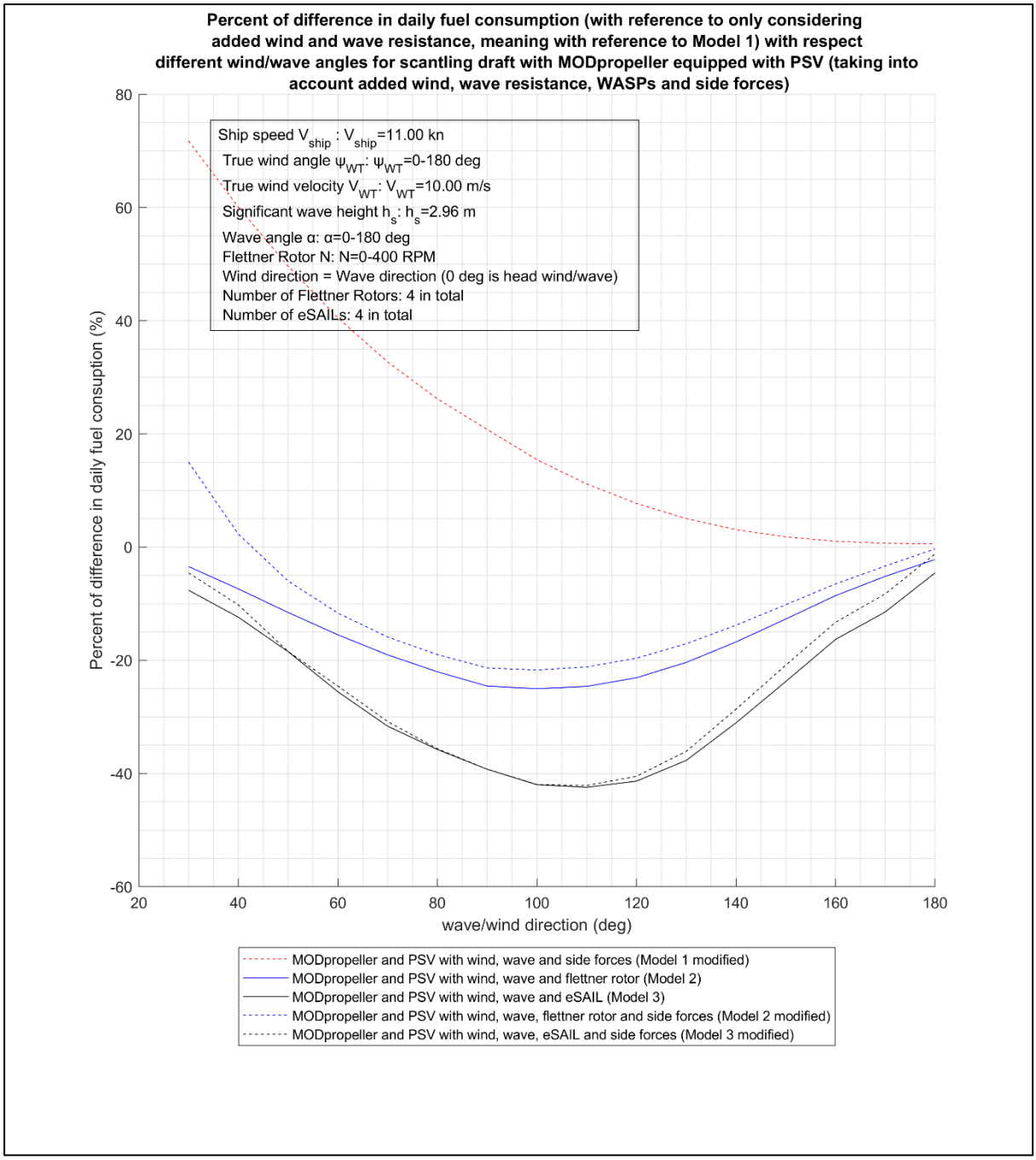

Figure 46: Percent of difference in daily fuel consumption (with reference to only considering added wind and wave resistance, meaning with reference to Model 1) with respect to different wind/wave angles for scantling draft with MODpropeller equipped with PSV (taking into account added wind, wave resistance, WASPs and side forces)

4.4.8.3 Comments on results

Comments regarding the results above are made.

4.4.8.3.1 First scenario

Based on the images from the first scenario, it is evident that under given wind and wave conditions and for different ship speeds, the use of the Flettner Rotor and the eSAIL proves beneficial, as both systems lead to reduced power demand and, consequently, lower fuel consumption for all examined ship speeds. This remains true even when side forces are considered. Additionally, we observe that the inclusion of side forces is significant, as they noticeably increase the required power and, therefore, the fuel consumption across all examined ship speeds in each model (model 1, model 2, model 3). However, even when side forces are included, the use of the Flettner Rotor and the eSAIL remains a beneficial option.

Another point worth highlighting, based on Figure 40, is that although the eSAIL seems to generate a higher perpendicular effective force than the Flettner Rotor, it results in lower added resistance due to side forces. This is expected, as shown in Figure 34 and Figure 35, which reveal a declining behaviour of added resistance as a function of heeling force. It is also noteworthy that the eSAIL achieves a greater horizontal effective force compared to the Flettner Rotor.

Finally, it should be mentioned that the use of the Flettner Rotor and eSAIL systems can lead to a reduction in fuel consumption of up to 20% in the case of the Flettner Rotor and 44% in the case of the eSAIL (e.g., at a speed of 10 knots) when side forces are taken into consideration. These figures increase to 26% and 48%, respectively, when side forces are not considered.

4.4.8.3.2 Second scenario

The observations made for the first scenario also apply to the second scenario (except for the consumption values mentioned at the end of the first scenario). However, the second scenario reveals some additional noteworthy conclusions. Initially, it is observed that the impact of side forces becomes significant for wind/wave angles approaching the bow. Specifically, when no system such as the Flettner Rotor or eSAIL is used (model 1 modified), the increase in required power and, consequently, in fuel consumption is substantial. This implies that the use of the Flettner Rotor and eSAIL has a stabilizing effect and helps prevent significant added resistance due to side forces. It is worth mentioning that in the case of the Flettner Rotor, when side forces were considered (Model 2 modified), there was no fuel saving but additional fuel consumption when compared to the scenario of not implementing Flettner Rotor to the ship (Model 1) but that was true only for a narrow range of angles, primarily around 30 degrees

Moreover, based on the consumption charts, we observe that under favourable wind/wave conditions, a fuel consumption reduction of 20% and 41% is achieved for the Flettner Rotor and eSAIL, respectively, when side forces are considered. When side forces are not considered, savings of 22% and 41%, respectively, are achieved.

5 Conclusions

This thesis explored the potential of wind-assisted propulsion (WASP) technologies, specifically the Flettner Rotor and eSAIL systems, to enhance the fuel efficiency and environmental performance of a bulk carrier vessel. The study aimed to assess the impact of retrofitting these technologies on reducing fuel consumption and emissions, thereby aligning with international regulatory frameworks such as the International Maritime Organization's (IMO) strategy on reducing greenhouse gas emissions.

The findings of this thesis underscore the significant potential of wind-assisted propulsion technologies, specifically the Flettner Rotor and eSAIL systems, in reducing fuel consumption and emissions for bulk carrier vessels. By integrating these systems, the shipping industry can make substantial progress towards achieving sustainability goals, complying with international environmental regulations, and reducing operational costs.

The analysis demonstrated that both Flettner Rotors and eSAIL systems effectively harness wind energy to provide auxiliary thrust, thereby reducing the load on the main engine. This reduction in engine load translates directly into lower fuel consumption and decreased greenhouse gas emissions, aligning with the IMO's strategy for reducing CO_2 emissions from shipping. The eSAIL system showcased enhanced aerodynamic efficiency due to its innovative air suction mechanism, which increases lift while minimizing drag, further improving the system's overall performance.

Key findings from the case study include:

- **Theoretical Modeling**: Theoretical models developed during the thesis, including Model 1 (baseline with wind and wave resistance) and the modified models incorporating the Flettner Rotor and eSAIL, provided a robust framework for evaluating ship propulsion performance. The models accounted for various resistance factors, including calm water resistance, added wind and wave resistance, WASP systems thrust, and the effects of side forces generated by these systems. The incorporation of these factors into the models allowed for precise predictions of fuel consumption, ship speed, and propulsion power under different operating conditions.
- **IMO Minimum Propulsion Power Compliance**: The retrofitted vessel (without the implementation of WASP systems) was assessed against the IMO Minimum Propulsion Power requirements. While compliance was achieved under specific conditions without Maximum Continuous Rating (MCR) limitations, the analysis highlighted potential challenges when MCR limitations are imposed, underscoring the need for consideration of compliance with requirements, imposed by authorities, when applying modifications (like the MCR limitation).
- **Performance under Different Scenarios**: The performance of the bulk carrier equipped with WASP systems (Flettner Rotor and eSAIL) was evaluated under various operational scenarios. The study modelled conditions such as adverse weather, varying wind and wave angles, and different ship speeds. It was found that both technologies improved propulsion efficiency and contributed to fuel savings, especially in scenarios with favourable wind conditions. For instance, during headwind scenarios, both systems showed a reduction in resistance, which allowed for more efficient propulsion. The results indicated that the systems remain effective under a wide range of conditions, making them versatile options for retrofitting existing vessels or equipping new builds.

- **Technical Challenges and Optimization**: The thesis also highlighted some technical challenges, such as the need to optimize the interaction between traditional propulsion systems and wind-assisted devices. The rotor speed, system efficiency, and operational parameters must be carefully managed to maximize net power output and minimize resistance when the systems are not active. The study provided insights into optimal settings for rotor RPM and the configuration of the eSAIL system, which are critical for achieving the best performance.
- **Impact of Side Forces and Added Resistances**: The study accounted for added wind and wave resistances, WASP thrust (horizontal effective forces), as well as the influence of side forces generated by the WASP systems. The integration of these factors into the propulsion model revealed that side forces, particularly from the rudder and drift effects, can influence overall vessel performance, necessitating careful consideration in real-world applications. It was illustrated that the addition of wind-assisted propulsion devices alters the total resistance encountered by the vessel. The inclusion of side forces generated by these systems, along with the added resistances due to wind and waves, requires careful consideration of the ship's manoeuvrability and overall performance. The use of advanced models, such as those accounting for yaw and drift forces, ensures a more accurate prediction of fuel consumption and system efficiency. This is particularly obvious in Figure 42 and Figure 46, in which, reduction in fuel consumption (with reference to Model 1) was observed when implementing WASP systems without considering side forces (Model 2 and Model 3). However, when the side forces were considered, fuel saving was reduced (Model 2 modified and Model 3 modified) with reference to Model 1. In the case of Model 1 modified, additional fuel consumption was observed with reference to Model 1. It is worth mentioning that in the case of the Flettner Rotor, when side forces were considered (Model 2 modified), there was no fuel saving but additional fuel consumption when compared to the scenario of not implementing Flettner Rotor to the ship (Model 1) but that was true only for a narrow range of angles, primarily around 30 degrees. In other words when not accounting for side forces (Model 2 and Model 3), it was demonstrated that the use of Flettner Rotor and eSAIL systems reduced the fuel consumption (reference to Model 1) but when the side forces were also accounted for (Model 2 modified and Model 3 modified), the fuel saving was reduced.
- **Fuel Efficiency and Emissions Reduction**: The deployment of WASP systems showed potential fuel savings of up to 48% when not accounting for side forces (Model 2 and Model 3) and up to 44% when accounting for side forces (Model 2 modified and Model 3 modified), depending on wind conditions and the operational setup of the vessel. The savings are most pronounced in favourable wind conditions, where the systems can provide substantial thrust without the need for engine power. This translates into significant reductions in CO_2 and NOx emissions, aligning with the goals of the IMO's decarbonization strategy.
- **Comparative Analysis of WASP Systems**: The comparative analysis between the Flettner Rotor and eSAIL systems revealed distinct advantages and challenges for each. The Flettner Rotor offered lower horizontal and perpendicular effective force while the eSAIL system, with its innovative air suction mechanism, developed increased horizontal and perpendicular effective forces. Overall, the eSAIL offered larger decrease in power needed and therefore consumption.

The deployment of wind-assisted propulsion systems is expected to grow as the industry seeks cost-effective and sustainable solutions to reduce its carbon footprint. Continued research and development into these technologies will likely yield further improvements in system efficiency and integration, making them even more attractive to ship operators.

Moreover, advancements in control algorithms, materials, and aerodynamic designs could enhance the performance of these systems, leading to wider adoption across various vessel types.

To fully realize the benefits of wind-assisted propulsion, future studies should focus on the following:

- Refining models to account for complex interactions between propulsion systems and environmental forces.
- Exploring hybrid systems that combine multiple green technologies, such as solar panels and hydrofoils, to further reduce dependency on fossil fuels.
- Conducting long-term trials and data collection on operational vessels to validate theoretical models and optimize system performance.

In conclusion, the integration of Flettner Rotors and eSAIL systems presents a viable pathway toward a more sustainable maritime industry. By leveraging the natural power of the wind, these technologies not only reduce operational costs and emissions but also contribute to the broader goal of decarbonizing global shipping. As the industry continues to innovate, wind-assisted propulsion will play a crucial role in shaping the future of marine transport.

6 References

[1] 'Fourth Greenhouse Gas Study 2020'. Accessed: Sep. 16, 2024. [Online]. Available: https://www.imo.org/en/ourwork/Environment/Pages/Fourth-IMO-Greenhouse-Gas-Study-2020.aspx

[2] L. Khan, J. Macklin, B. Peck, O. Morton, and J.-B. R. G. Souppez, 'A Review Of Wind-Assisted Ship Propulsion For Sustainable Commercial Shipping: Latest Developments And Future Stakes: Wind Propulsion Conference', *Proc. Wind Propuls. Conf. 2021*, Sep. 2021, Accessed: Sep. 16, 2024. [Online]. Available: https://www.rina.org.uk/Wind_Propulsion_2021.html

[3] 'Flettner rotor', *Wikipedia*. Jan. 22, 2024. Accessed: Apr. 03, 2024. [Online]. Available: https://en.wikipedia.org/w/index.php?title=Flettner_rotor&oldid=1197825958

[4] 'Magnus effect', *Wikipedia*. Mar. 09, 2024. Accessed: Apr. 03, 2024. [Online]. Available: https://en.wikipedia.org/w/index.php?title=Magnus_effect&oldid=1212837977

[5] I. S. Seddiek and N. R. Ammar, 'Harnessing wind energy on merchant ships: case study Flettner rotors onboard bulk carriers', *Environ. Sci. Pollut. Res.*, vol. 28, no. 25, pp. 32695–32707, Jul. 2021, doi: 10.1007/s11356-021-12791-3.

[6] 'Rotor ship', *Wikipedia*. Mar. 13, 2024. Accessed: Apr. 16, 2024. [Online]. Available: https://en.wikipedia.org/w/index.php?title=Rotor_ship&oldid=1213527024

[7] 'Wind-Assisted Propulsion Systems for vessels | bound4blue'. Accessed: May 09, 2024. [Online]. Available: https://bound4blue.com/esail/

[8] 'Marflet Marine Partners with Bound4blue for Cutting-Edge Wind Propulsion', MarineTraffic.com. Accessed: Sep. 16, 2024. [Online]. Available: https://www.marinetraffic.com/en/maritime-news/22/ship-building and technology/2024/11246/marflet-marine-partners-with-bound4blue-for-cutting-edge-win

[9] 'Wingsail', *Wikipedia*. Sep. 28, 2023. Accessed: Sep. 16, 2024. [Online]. Available: https://en.wikipedia.org/w/index.php?title=Wingsail&oldid=1177547961

[10] 'Kite rig', *Wikipedia*. Jun. 17, 2024. Accessed: Sep. 16, 2024. [Online]. Available: https://en.wikipedia.org/w/index.php?title=Kite_rig&oldid=1229592650

[11] 'DynaRig', *Wikipedia*. Feb. 18, 2024. Accessed: Sep. 16, 2024. [Online]. Available: https://en.wikipedia.org/w/index.php?title=DynaRig&oldid=1208597140

[12] S. Editor, 'New wing sail technology to be launched', SAFETY4SEA. Accessed: Sep. 16, 2024. [Online]. Available: https://safety4sea.com/new-wing-sail-technology-to-be-launched/

[13] G. Bordogna, 'Aerodynamics of Wind-Assisted Ships', 2020.

[14] V. Vigna and M. Figari, 'Wind-Assisted Ship Propulsion: Matching Flettner Rotors with Diesel Engines and Controllable Pitch Propellers', *J. Mar. Sci. Eng.*, vol. 11, no. 5, p. 1072, May 2023, doi: 10.3390/jmse11051072.

[15] Nikos Vasileiadis, 'DYNAMIC ANALYSIS OF HYDROFOILS AND FLETTNER ROTORS IMPLEMENTED ON A MARINE CLOUD BRIGHTENING SPRAY VESSEL', presented at the International Conference on Postgraduate Research in Maritime Technology, 2022, p. 17.

[16] R. Ma *et al.*, 'Evaluation Method for Energy Saving of Sail-Assisted Ship Based on Wind Resource Analysis of Typical Route', *J. Mar. Sci. Eng.*, vol. 11, no. 4, p. 789, Apr. 2023, doi: 10.3390/jmse11040789.

[17] N. R. Ammar and I. S. Seddiek, 'Wind assisted propulsion system onboard ships: case study Flettner rotors', *Ships Offshore Struct.*, vol. 17, no. 7, pp. 1616–1627, Jul. 2022, doi: 10.1080/17445302.2021.1937797.

[18] F. Tillig and J. W. Ringsberg, 'A 4 DOF simulation model developed for fuel consumption prediction of ships at sea', *Ships Offshore Struct.*, vol. 14, no. sup1, pp. 112–120, Oct. 2019, doi: 10.1080/17445302.2018.1559912.

[19] Gerasimos Politis, *Ship Resistance and Propulsion*, 5th ed. Athens, 2019.

[20] 'TOWING TANK MODEL TEST REPORT FOR A 82000DWT BULK CARRIER WITH PSV'.
[21] '232(65).pdf'. Accessed: Feb. 10, 2024. [Online]. Available: https://wwwcdn.imo.org/localresources/en/OurWork/Environment/Documents/232(65).pdf
[22] 'ABS_Energy_Efficiency_Advisory.pdf'. Accessed: Feb. 10, 2024. [Online]. Available: https://ww2.eagle.org/content/dam/eagle/advisories-and-debriefs/ABS_Energy_Efficiency_Advisory.pdf
[23] '75-04-01-011.pdf'. Accessed: Feb. 11, 2024. [Online]. Available: https://www.ittc.info/media/9874/75-04-01-011.pdf
[24] S. Liu, B. Shang, A. Papanikolaou, and V. Bolbot, 'Improved formula for estimating added resistance of ships in engineering applications', *J. Mar. Sci. Appl.*, vol. 15, no. 4, pp. 442–451, Dec. 2016, doi: 10.1007/s11804-016-1377-3.
[25] N. R. Ammar and I. S. Seddiek, 'Wind assisted propulsion system onboard ships: case study Flettner rotors', *Ships Offshore Struct.*, vol. 17, no. 7, pp. 1616–1627, Jul. 2022, doi: 10.1080/17445302.2021.1937797.
[26] D. Gkoufas, 'Examining the Effect of a Wind-Assisted Propulsion System (Flettner Rotors) on Ship's Energy Efficiency'.
[27] V. Vigna and M. Figari, 'Wind-Assisted Ship Propulsion: Matching Flettner Rotors with Diesel Engines and Controllable Pitch Propellers', *J. Mar. Sci. Eng.*, vol. 11, no. 5, Art. no. 5, May 2023, doi: 10.3390/jmse11051072.
[28] 'What are suction wings and how do they work? – IMO'. Accessed: May 09, 2024. [Online]. Available: https://futurefuels.imo.org/faq/what-are-suction-wings-and-how-do-they-work/
[29] R. Eggers, 'Operational performance of wind assisted ships', in *Proc. 10th Symposium on High-Performance Marine Vehicles (HIPER)*, 2016.
[30] F. Tillig and J. W. Ringsberg, 'A 4 DOF simulation model developed for fuel consumption prediction of ships at sea', *Ships Offshore Struct.*, vol. 14, no. sup1, pp. 112–120, Oct. 2019, doi: 10.1080/17445302.2018.1559912.
[31] D. E. Elger, M. Bentin, and M. Vahs, 'Comparison of different methods for predicting the drift angle and rudder resistance by wind propulsion systems on ships', *Ocean Eng.*, vol. 217, p. 108152, Dec. 2020, doi: 10.1016/j.oceaneng.2020.108152.
[32] J. He, Y. Hu, J. Tang, and S. Xue, 'Research on sail aerodynamics performance and sail-assisted ship stability', *J. Wind Eng. Ind. Aerodyn.*, vol. 146, pp. 81–89, Nov. 2015, doi: 10.1016/j.jweia.2015.08.005.
[33] M. Hirano, 'On Calculation Method of Ship Maneuvering Motion at Initial Design Phase', *J. Soc. Nav. Archit. Jpn.*, vol. 1980, no. 147, pp. 144–153, 1980, doi: 10.2534/jjasnaoe1968.1980.144.
[34] 'CEAS engine calculations', MAN Energy Solutions. Accessed: Dec. 14, 2023. [Online]. Available: https://www.man-es.com/marine/products/planning-tools-and-downloads/ceas-engine-calculations
[35] V. Shigunov, 'Numerical Prediction of Added Power in Seaway', *J. Offshore Mech. Arct. Eng.*, vol. 140, no. 5, p. 051102, Oct. 2018, doi: 10.1115/1.4039955.
[36] J. Seifert, 'A review of the Magnus effect in aeronautics', *Prog. Aerosp. Sci.*, vol. 55, pp. 17–45, Nov. 2012, doi: 10.1016/j.paerosci.2012.07.001.
[37] 'MAIN Engine SHOP TEST'.
[38] 'ΕΞΕΤΑΣΗ ΜΕΘΟΔΩΝ ΓΙΑ ΤΟΝ ΥΠΟΛΟΓΙΣΜΟ ΤΗΣ ΠΡΟΣΘΕΤΗΣ ΑΝΤΙΣΤΑΣΗΣ ΚΥΜΑΤΙΣΜΟΥ..pdf'. Accessed: Feb. 11, 2024. [Online]. Available: https://dspace.lib.ntua.gr/xmlui/bitstream/handle/123456789/58527/%ce%95%ce%9e%ce%95%ce%a4%ce%91%ce%a3%ce%97%20%ce%9c%ce%95%ce%98%ce%9f%ce%94%ce%a9%ce%9d%20%ce%93%ce%99%ce%91%20%ce%a4%ce%9f%ce%9d%20%ce%a5%ce%a0%ce%9f%ce%9b%ce%9f%ce%93%ce%99%ce%a3%ce%9c%ce%9f%20%ce%a4%ce%97%ce%a3%20%ce%a0%ce%a1%ce%9f%ce%a3%ce%98%ce%95%ce%a4%ce%97%ce%a3%20%ce%91%ce%9d%ce%a4%ce%99%ce%a3%ce%a4%ce%9

1%ce%a3%ce%97%ce%a3%20%ce%9a%ce%a5%ce%9c%ce%91%ce%a4%ce%99%
ce%a3%ce%9c%ce%9f%ce%a5..pdf?sequence=1&isAllowed=y

Appendix A: Ship data from towing tank test report

This appendix contains data from ship towing tank test report.

A.1 Modified propeller open water performance characteristics

Table 19: Open water performance characteristics of modified propeller

Modified propeller's open-water performance			
Particular	**Symbol**	**Unit**	**Value**
Diameter	D	m	6.95
J	**k_T**	**$10*k_Q$**	**η_0**
0.25	0.2731	0.3309	0.3284
0.2893	0.2566	0.3128	0.3777
0.3286	0.2398	0.2944	0.426
0.3679	0.2228	0.2757	0.473
0.4071	0.2055	0.2569	0.5184
0.4464	0.188	0.2377	0.5619
0.4857	0.1702	0.2182	0.6028
0.525	0.1549	0.2015	0.642
0.5643	0.1366	0.1816	0.6756
0.6036	0.118	0.1612	0.7029
0.6429	0.099	0.1405	0.7208
0.6821	0.0797	0.1195	0.7242
0.7214	0.0599	0.0979	0.7029
0.7607	0.0398	0.076	0.6348
0.8	0.0193	0.0536	0.4593

A.2 Effective power curves

Table 20: Effective calm water resistance with PSV [20, pp. 21–28]

	Scantling Draft (14.45m)
V (kn)	**R_{PSV} (kN)**
10	335.4
10.5	369.24

11	406.96
11.5	448.56
12	494.05
12.5	543.44
13	596.73
13.5	653.93
14	715.06
14.5	780.1
15	849.08
15.5	921.99

Corresponding curve plots appear in the following figure.

A.3 Self-propulsion factors

Table 21: Self-propulsion factors for scantling draft

Scantling Draft (14.45m)					
With PSV					
V (kn)	**t**	**w**	**η_r**	**C_P**	**C_N**
10	0.215	0.37	0.999	0.99	1
10.5	0.215	0.37	0.999		
11	0.215	0.37	0.999		
11.5	0.215	0.37	0.999		
12	0.216	0.362	1.001		
12.5	0.215	0.359	1.003		
13	0.215	0.359	1.005		
13.5	0.217	0.36	1.006		
14	0.215	0.358	1.006		
14.5	0.207	0.354	1.007		
15	0.214	0.359	1.005		
15.5	0.214	0.359	1.005		

Appendix B: Added resistances

B.1 Added wave and wind resistances

B.1.1 Added wind resistance – Fujiwara regression formula

For the wind resistance coefficient C_{DA}, the Fujiwara regression formula [23, p. 51] can be used. According to this formula:

$$C_{DA} = C_{LF} \cdot \cos\psi_{WR} + C_{XLI} \cdot \left(\sin\psi_{WR} - \frac{1}{2} \cdot \sin\psi_{WR} \cdot \cos^2\psi_{WR}\right) \cdot \sin\psi_{WR} \cdot \cos\psi_{WR} + C_{ALF} \cdot \sin\psi_{WR} \cdot \cos^3\psi_{WR}$$

With:

for $0 \leq \psi_{WR} < 90(deg.)$

$$C_{LF} = \beta_{10} + \beta_{11} \cdot \frac{A_{YV}}{L_{OA} \cdot B} + \beta_{12} \cdot \frac{C_{MC}}{L_{OA}}$$

$$C_{XLI} = \delta_{10} + \delta_{11} \cdot \frac{A_{YV}}{L_{OA} \cdot h_{BR}} + \delta_{12} \cdot \frac{A_{XV}}{B \cdot h_{BR}}$$

$$C_{ALF} = \varepsilon_{10} + \varepsilon_{11} \cdot \frac{A_{OD}}{A_{YV}} + \varepsilon_{12} \cdot \frac{B}{L_{OA}}$$

for $90 \leq \psi_{WR} < 180(deg.)$

$$C_{XLI} = \delta_{20} + \delta_{21} \cdot \frac{A_{YV}}{L_{OA} \cdot h_{BR}} + \delta_{22} \cdot \frac{A_{XV}}{A_{YV}} + \delta_{23} \cdot \frac{B}{L_{OA}} + \delta_{24} \cdot \frac{A_{XV}}{B \cdot h_{BR}}$$

$$C_{LF} = \beta_{20} + \beta_{21} \cdot \frac{B}{L_{OA}} + \beta_{22} \cdot \frac{h_C}{L_{OA}} + \beta_{23} \cdot \frac{A_{OD}}{{L_{OA}}^2} + \beta_{24} \cdot \frac{A_{XV}}{B^2}$$

$$C_{ALF} = \varepsilon_{20} + \varepsilon_{21} \cdot \frac{A_{OD}}{A_{YV}}$$

for $\psi_{WR} = 90(deg.)$

$$C_{DA}|_{\psi_{WR}=90(deg.)} = \frac{1}{2} \cdot \left(C_{DA}|_{\psi_{WR}=90(deg.)-\mu} + C_{DA}|_{\psi_{WR}=90(deg.)+\mu}\right)$$

Where:

A_{OD}: lateral projected area of superstructures etc. on deck,

A_{XV}: area of maximum transverse section exposed to the winds,

A_{YV}: projected lateral area above the waterline,

B: ship breadth,

C_{DA}: wind resistance coefficient,

C_{MC}: horizontal distance from midship section to centre of lateral projected area A_{YV},

h_{BR}: height of top of superstructure (bridge etc.),

h_C: height from waterline to centre of lateral projected area A_{YV},

L_{OA}: length overall,

μ: smoothing range; normally $10(deg.)$,

ψ_{WR}: smoothing range; normally $10(deg.)$,

Non-dimensional parameters β_{ij}, δ_{ij} and ε_{ij} are defined below.

Table 22: Non-dimensional parameters [23, Tbl. F-2]

	i	j				
		0	1	2	3	4
β_{ij}	1	0.922	-0.507	-1.162	-	-
	2	-0.018	5.091	-10.367	3.011	0.341
δ_{ij}	1	-0.458	-3.245	2.313	-	-
	2	1.901	-12.727	-24.407	40.310	5.481
ε_{ij}	1	0.585	0.906	-3.239	-	-
	2	0.314	1.117	-	-	-

The parameters that need to be inputted in regression formula by Fujiwara are portrayed in the following figure.

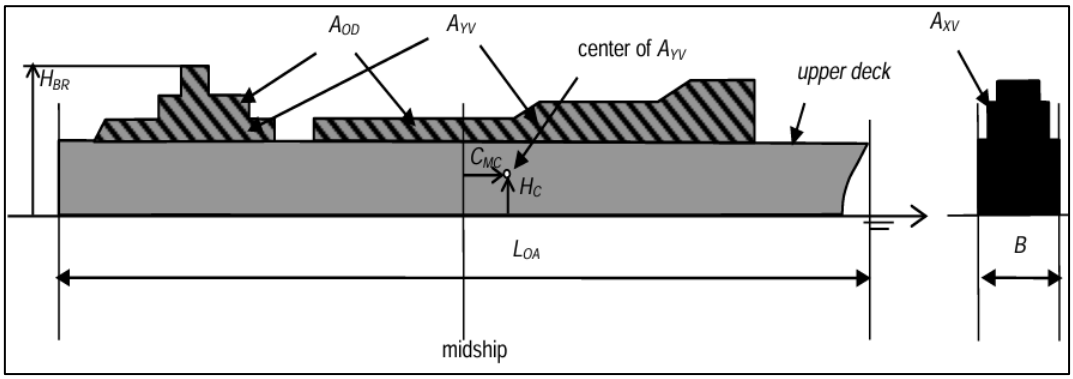

Figure 47: Input parameters for regression formula by Fujiwara

B.1.2 Added wave resistance

B.1.2.1 Wave reflection added resistance R_{AWR}

This part of the added wave resistance is computed using the sum:

$$R_{AWR} = \sum_{i=1}^{4} R_{AWR_i}$$

With:

- $R_{AWR_1} = \frac{2.25}{4} \cdot \rho \cdot g \cdot B \cdot \zeta_\alpha^2 \cdot a_T \cdot \left\{\sin^2(E_1 - a) + \frac{2 \cdot \omega_0 \cdot U}{g} \cdot [\cos E_1 \cdot \cos(E_1 - a) - \cos a]\right\} \cdot \left(\frac{0.87}{C_B}\right)^{1+4 \cdot \sqrt{Fr}}$
- $R_{AWR_2} = \frac{2.25}{4} \cdot \rho \cdot g \cdot B \cdot \zeta_\alpha^2 \cdot a_T \cdot \left\{\sin^2(E_1 + a) + \frac{2 \cdot \omega_0 \cdot U}{g} \cdot [\cos E_1 \cdot \cos(E_1 + a) - \cos a]\right\} \cdot \left(\frac{0.87}{C_B}\right)^{1+4 \cdot \sqrt{Fr}}$
- $R_{AWR_3} = -\frac{2.25}{4} \cdot \rho \cdot g \cdot B \cdot \zeta_\alpha^2 \cdot a_T \cdot \left\{\sin^2(E_2 + a) + \frac{2 \cdot \omega_0 \cdot U}{g} \cdot [\cos E_2 \cdot \cos(E_2 + a) - \cos a]\right\} \cdot \left(\frac{0.87}{C_B}\right)^{1+4 \cdot \sqrt{Fr}}$
- $R_{AWR_4} = -\frac{2.25}{4} \cdot \rho \cdot g \cdot B \cdot \zeta_\alpha^2 \cdot a_T \cdot \left\{\sin^2(E_2 - a) + \frac{2 \cdot \omega_0 \cdot U}{g} \cdot [\cos E_2 \cdot \cos(E_2 - a) - \cos a]\right\} \cdot \left(\frac{0.87}{C_B}\right)^{1+4 \cdot \sqrt{Fr}}$

Where:

- ρ: seawater density in $[kg/m^3]$
- g: acceleration due to gravity in $[m/s^2]$
- B: ship breadth in $[m]$
- ζ_α: wave amplitude $[m]$
- $a_T = \begin{cases} 1 - e^{-4 \cdot \pi \cdot \left(\frac{T^*}{\lambda} - \frac{T^*}{2.5 \cdot L_{pp}}\right)}, & \frac{\lambda}{L_{pp}} \leq 2.5 \\ 0, & \frac{\lambda}{L_{pp}} > 2.5 \end{cases}$
- λ: wave length in $[m]$
- For cases 1 and 2, $T^* = T_{max}$ but for cases 3 and 4, $T^* = \begin{cases} \frac{T_{max} \cdot \left(4 + \sqrt{|\cos a|}\right)}{5}, & for\ C_B \leq 0.75 \\ \frac{T_{max} \cdot \left(2 + \sqrt{|\cos a|}\right)}{5}, & for\ C_B > 0.75 \end{cases}$
- ω_0: angular velocity of wave in $[rad/s]$
- U: ship speed in $[m/s]$
- a: is the angle of the wave, in $[rad]$, with 0 being the following waves and π being the bow waves
- Fr: is the Froude number of the ship
- E_1, E_2: are the angles, in $[rad]$, shown in the picture below

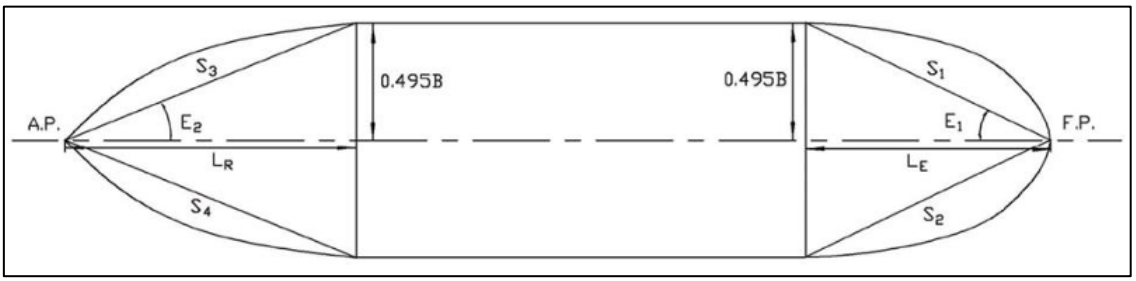

Figure 48: Lengths L_R, L_E and angles E_1, E_2 [38, Fig. 15]

B.1.2.2 Ship motion added resistance R_{AWM}

It can be calculated by the formula:

$$R_{AWM} = 4 \cdot \rho \cdot g \cdot \zeta_\alpha^2 \cdot \frac{B^2}{L_{pp}} \cdot a_1 \cdot a_2 \cdot a_3 \cdot \bar{\omega}^{b_1} \cdot e^{\frac{b_1 \cdot (1 - \bar{\omega}^{b_1})}{d_1}}$$

Where:

- $a_1 = \begin{cases} 60.3 \cdot C_B^{1.34} \cdot (4 \cdot k_{yy})^2 \cdot \left(\frac{0.87}{C_B}\right)^{-(1+Fr)\cdot\cos\alpha} \cdot \left(\ln\frac{B}{T_{max}}\right)^{-1} \cdot \frac{(1-2\cdot\cos\alpha)}{3}, & \frac{\pi}{2} \le \alpha \le \pi \\ linear\ interpolation\ between\ beam\ and\ following\ seas, & 0 \le \alpha \le \frac{\pi}{2} \\ f(U, V_g), & \alpha = 0 \end{cases}$
- $V_g = \frac{\sqrt{\frac{g \cdot \lambda}{2 \cdot \pi}}}{2}$, the wave group speed in $[m/s]$
- $a_2 = \begin{cases} 0.0072 + 0.1676 \cdot Fr, & Fr < 0.12 \\ Fr^{1.5} \cdot e^{-3.5 \cdot Fr}, & Fr \ge 0.12 \end{cases}$
- $a_3 = 1 + 28.7 \cdot \tanh^{-1} \frac{|T_a - T_f|}{L_{pp}}$
- T_a, T_f: draught at aft and fore respectively in $[m]$
- $\bar{\omega} = 2.142 \cdot \sqrt[3]{k_{yy}} \cdot \sqrt{\frac{L_{pp}}{\lambda}} \cdot \left[1 - \frac{0.111}{C_B} \cdot \left(\ln\frac{B}{T_{max}} - \ln 2.75\right)\right] \cdot \left(\frac{C_B}{0.65}\right)^{0.17} \cdot \left[(-1.377 \cdot Fr^2 + 1.157 \cdot Fr) \cdot |\cos\alpha| + \frac{0.618 \cdot (13 + \cos 2\alpha)}{14}\right]$
- k_{yy}: longitudinal mass radius of gyration (pitch)
- $b_1 = \begin{cases} 11, & \bar{\omega} < 1 \\ -8.5, & elsewhere \end{cases}$
- $d_1 = \begin{cases} 566 \cdot \left(\frac{L_{pp} \cdot C_B}{B}\right)^{-2.66}, & \bar{\omega} < 1 \\ -566 \cdot \left(\frac{L_{pp}}{B}\right)^{-2.66} \cdot \left(4 - \frac{125 \cdot \tan^{-1}|T_a - T_f|}{L_{pp}}\right), & elsewhere \end{cases}$

Appendix C: Side forces

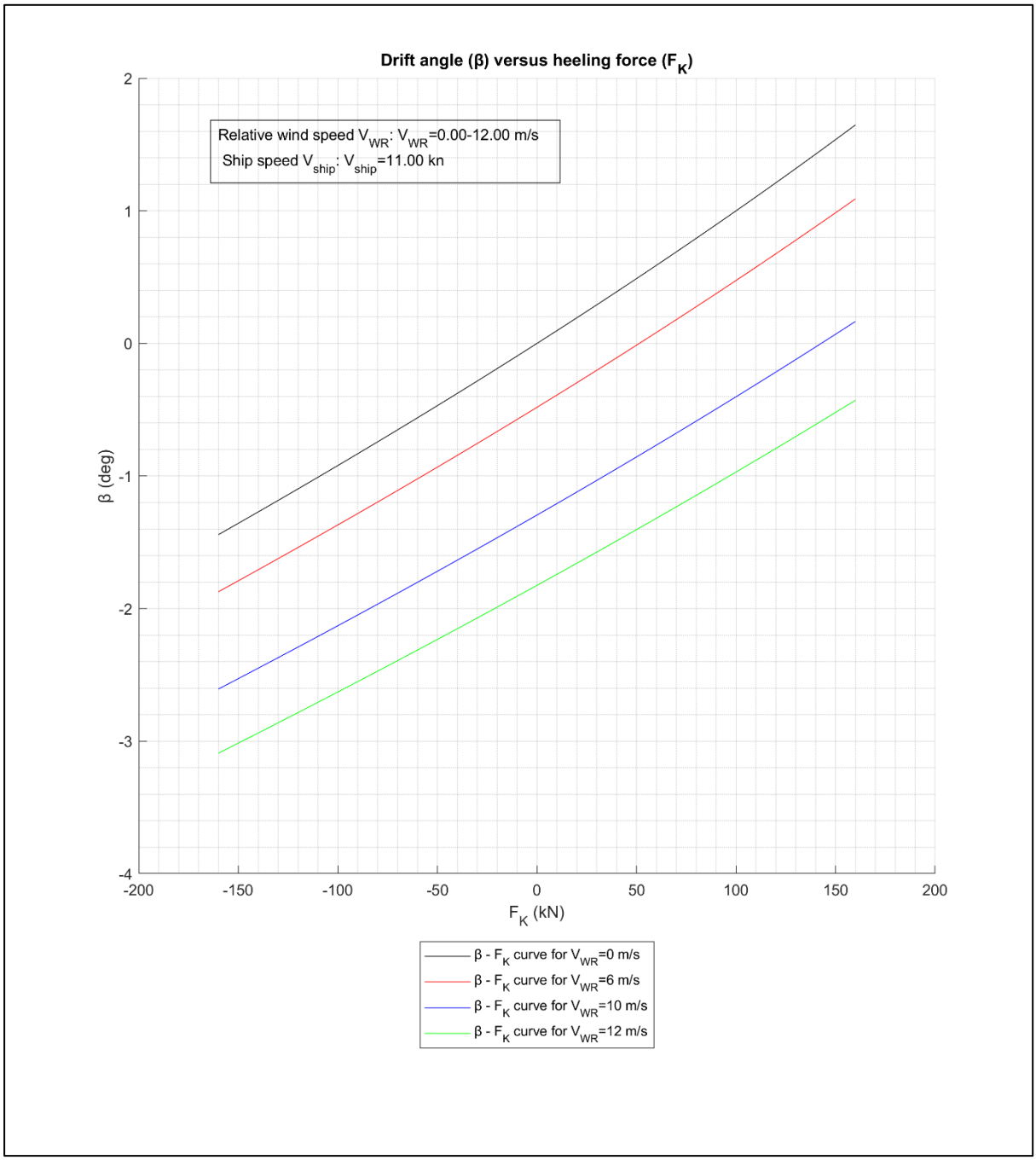

Figure 49: Drift angle (β) versus heeling force (F_K)

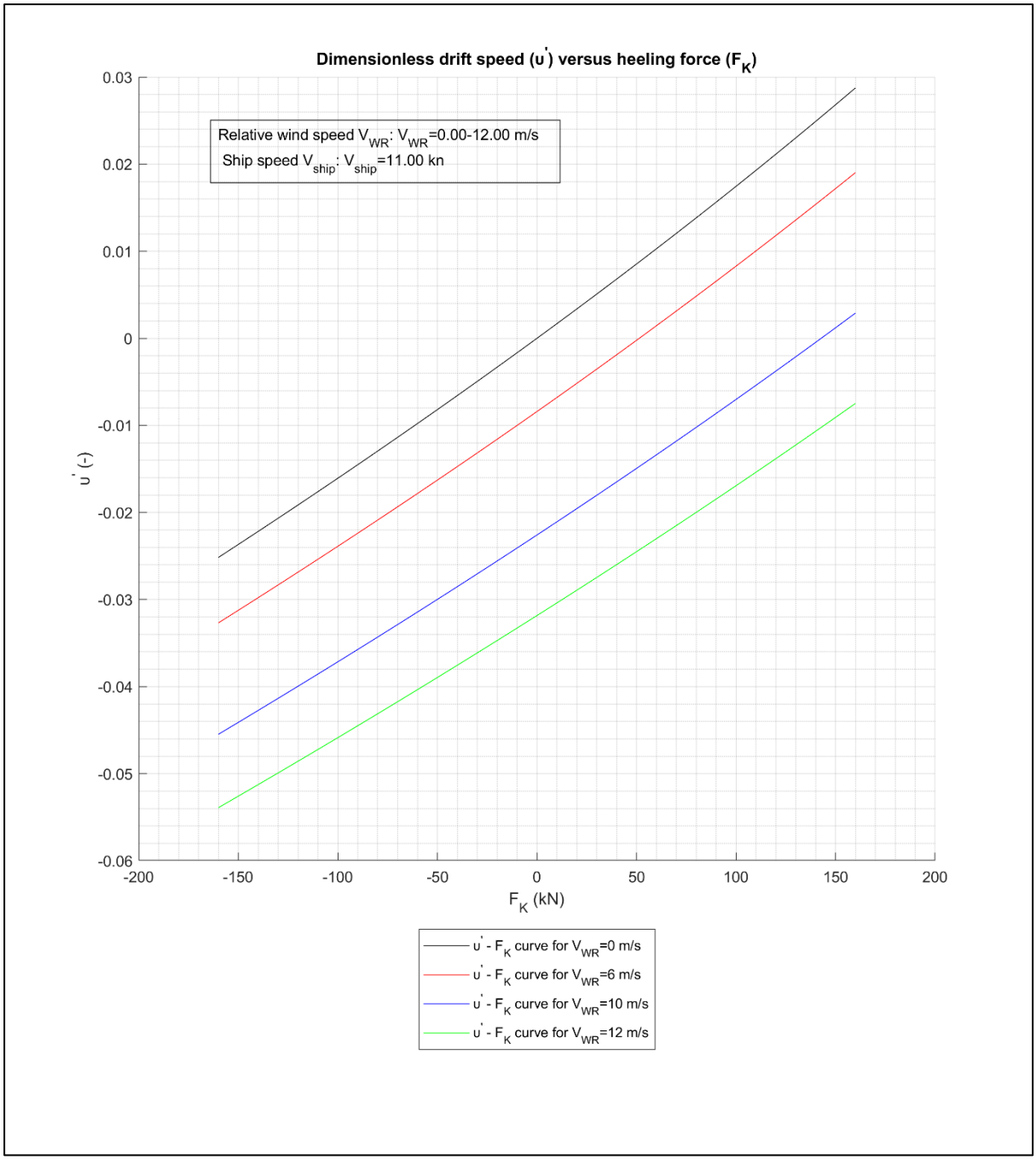

Figure 50: Dimensionless drift speed (υ') versus heeling force (F_K)

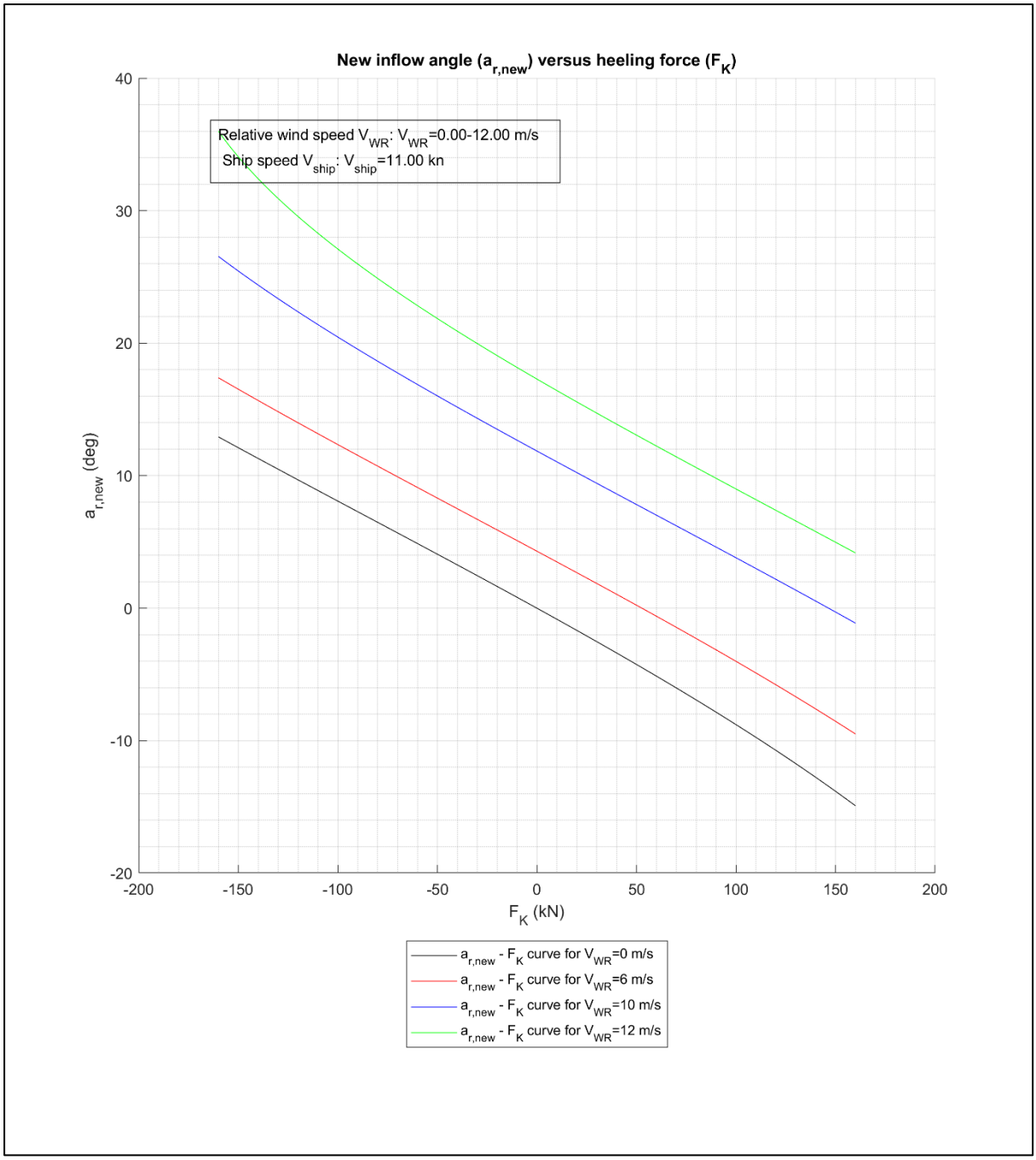

Figure 51: New inflow angle ($a_{r,new}$) versus heeling force (F_K)